

# CANADIAN THESES ON MICROFICHE

I.S.B.N.

## THESES CANADIENNES SUR MICROFICHE



National Library of Canada  
Collections Development Branch

Canadian Theses on  
Microfiche Service

Ottawa, Canada  
K1A 0N4

Bibliothèque nationale du Canada  
Direction du développement des collections

Service des thèses canadiennes  
sur microfiche

### NOTICE

The quality of this microfiche is heavily dependent upon the quality of the original thesis submitted for microfilming. Every effort has been made to ensure the highest quality of reproduction possible.

If pages are missing, contact the university which granted the degree.

Some pages may have indistinct print especially if the original pages were typed with a poor typewriter ribbon or if the university sent us a poor photocopy.

Previously copyrighted materials (journal articles, published tests, etc.) are not filmed.

Reproduction in full or in part of this film is governed by the Canadian Copyright Act, R.S.C. 1970, c. C-30. Please read the authorization forms which accompany this thesis.

**THIS DISSERTATION  
HAS BEEN MICROFILMED  
EXACTLY AS RECEIVED**

### AVIS

La qualité de cette microfiche dépend grandement de la qualité de la thèse soumise au microfilmage. Nous avons tout fait pour assurer une qualité supérieure de reproduction.

S'il manque des pages, veuillez communiquer avec l'université qui a conféré le grade.

La qualité d'impression de certaines pages peut laisser à désirer, surtout si les pages originales ont été dactylographiées à l'aide d'un ruban usé ou si l'université nous a fait parvenir une photocopie de mauvaise qualité.

Les documents qui font déjà l'objet d'un droit d'auteur (articles de revue, examens publiés, etc.) ne sont pas microfilmés.

La reproduction, même partielle, de ce microfilm est soumise à la Loi canadienne sur le droit d'auteur, SRC 1970, c. C-30. Veuillez prendre connaissance des formules d'autorisation qui accompagnent cette thèse.

**LA THÈSE A ÉTÉ  
MICROFILMÉE TELLE QUE  
NOUS L'AVONS REÇUE**



National Library of Canada

Bibliothèque nationale du Canada

Canadian Theses Division

Division des thèses canadiennes

Ottawa, Canada  
K1A 0N4

53855

0-315-05935-4

**PERMISSION TO MICROFILM — AUTORISATION DE MICROFILMER**

• Please print or type — Écrire en lettres moulées ou dactylographier

Full Name of Author — Nom complet de l'auteur

RONALD MALCOLM BELCHAMBER

Date of Birth — Date de naissance

9 / FEB / 1953

Country of Birth — Lieu de naissance

ENGLAND

Permanent Address — Résidence fixe

% 52<sup>A</sup> HARVEST ROAD  
ENGLEFIELD GREEN  
SURREY  
ENGLAND TW20 0QT

Title of Thesis — Titre de la thèse

NOISE CHARACTERIZATION OF AN INDUCTIVELY COUPLED  
PLASMA FOR ATOMIC EMISSION ANALYSIS

University — Université

UNIVERSITY OF ALBERTA

Degree for which thesis was presented — Grade pour lequel cette thèse fut présentée

Ph.D.

Year this degree conferred — Année d'obtention de ce grade

1981

Name of Supervisor — Nom du directeur de thèse

G. HORLICK

Permission is hereby granted to the NATIONAL LIBRARY OF CANADA to microfilm this thesis and to lend or sell copies of the film.

The author reserves other publication rights, and neither the thesis nor extensive extracts from it may be printed or otherwise reproduced without the author's written permission.

L'autorisation est, par la présente, accordée à la BIBLIOTHÈQUE NATIONALE DU CANADA de microfilmer cette thèse et de prêter ou de vendre des exemplaires du film.

L'auteur se réserve les autres droits de publication; ni la thèse ni de longs extraits de celle-ci ne doivent être imprimés ou autrement reproduits sans l'autorisation écrite de l'auteur.

Date

6 / AUG / 1981

Signature

THE UNIVERSITY OF ALBERTA

NOISE CHARACTERIZATION OF AN INDUCTIVELY COUPLED PLASMA  
FOR ATOMIC EMISSION ANALYSIS

by



RONALD M. BELCHAMBER

A THESIS

SUBMITTED TO THE FACULTY OF GRADUATE STUDIES AND RESEARCH  
IN PARTIAL FULFILMENT OF THE REQUIREMENTS FOR THE DEGREE  
OF DOCTOR OF PHILOSOPHY  
DEPARTMENT CHEMISTRY  
.....

EDMONTON, ALBERTA

FALL, 1981

T H E U N I V E R S I T Y O F A L B E R T A

RELEASE FORM

NAME OF AUTHOR Ronald M. Belchamber  
TITLE OF THESIS Noise Characterization of an Inductively  
Coupled Plasma for Atomic Emission  
Analysis.  
DEGREE FOR WHICH THESIS WAS PRESENTED Ph.D.  
YEAR THIS DEGREE GRANTED 1981

Permission is hereby granted to THE UNIVERSITY OF ALBERTA LIBRARY to reproduce single copies of this thesis and to lend or sell such copies for private, scholarly or scientific research purposes only.

The author reserves other publication rights, and neither the thesis nor extensive extracts from it may be printed or otherwise reproduced without the author's written permission.

(Signed)

*M. Belchamber*

PERMANENT ADDRESS

52<sup>A</sup> Harvest Road  
Englefield Green  
Surrey England TW20 0QT

DATED *Sept 1* 1981

THE UNIVERSITY OF ALBERTA  
FACULTY OF GRADUATE STUDIES AND RESEARCH

The undersigned certify that they have read, and recommend to the Faculty of Graduate Studies and Research, for acceptance, a thesis entitled NOISE CHARACTERIZATION OF AN INDUCTIVELY COUPLED PLASMA FOR ATOMIC EMISSION ANALYSIS submitted by RONALD M. BELCHAMBER in partial fulfilment of the requirements for the degree of Doctor of Philosophy in Analytical Chemistry.

*Gary Herlick*  
.....  
Gary Herlick, Supervisor

*B.S. Pons*  
.....  
B.S. Pons

*F.F. Cantwell*  
.....  
F.F. Cantwell

*E. R. Kanasevich*  
.....  
E. Kanasevich

*R. Browner*  
.....  
R. Browner, External Examiner

*K.R. Kopecky*  
.....  
K.R. Kopecky

Date *July 21/81*

DEDICATION

To my parents, my wife Sheila and Peter.

## ABSTRACT

The signal-to-noise performance of the ICP has been compared for several nebulization systems including a fixed tip cross-flow nebulizer, a concentric nebulizer and an ultrasonic nebulizer. The precision obtainable with these nebulizers has been ascertained for a range of integration times 10 msec - 30 sec. It was found that little improvement in precision is obtained with increasing integration time. In fact in the case of the ultrasonic nebulizer precision decreased with increasing integration time.

To clarify these results characteristic noise power spectra were obtained from the ICP operating with a variety of nebulizers. These noise power spectra were obtained by Fourier analysis of analyte emission signals.

Below 5 Hz the noise power spectra show a marked dependence on the type of nebulizer used. While a strict  $1/f$  character was not observed, the spectra were clearly dominated by low frequency components. Above 5 Hz the noise power spectra were, broadly speaking, independent of the nebulizer used. Distinct peaks were observed in the noise power spectra in the 200 Hz to 400 Hz region. The position and intensity were dependent on rf power and coolant gas flow rate. In addition, the intensity of these

peaks correspond exactly to similar peaks found in the acoustic noise power spectrum of the ICP. The cause of these peaks is believed to result from rotation of the plasma.

Correlation studies have been carried out between noise in the emission signal and various plasma parameters such as incident rf power, reflected rf power and nebulizer spray chamber pressure. No correlation was observed between fluctuations in either the incident or reflected power levels and the emission signal. Correlation was however, observed between fluctuations in the spray chamber pressure and the emission signal. These pressure fluctuations were caused by the flow of liquid droplets in the drain hose from the spray chamber. This problem was eliminated by the use of a "soak-away" spray chamber arrangement.

The use of internal standards for improving ICP precision is investigated. Good correlation is observed between analyte and a variety of internal standard elements. When these internal standards are used, factors of approximately two improvement in precision are noted.



## ACKNOWLEDGEMENTS

My thanks to Professor, Gary Horlick for his invaluable help and imaginative direction.

My thanks to fellow graduate students who made carrying out this work a pleasure.

My thanks to Annabelle Wiseman for her patient typing and correction of this thesis.

TABLE OF CONTENTS

CHAPTER		PAGE
I	Noise in Inductively Coupled Plasma Emission Spectrometry .....	1
	A. Introduction to the ICP.....	1
	B. Characterization of Emission Noise.....	2
	1. Signal-to-Noise Ratio.....	2
	2. Noise Power Spectra.....	3
	C. Noise Sources in Atomic Emission Spectrometry.....	5
	1. Introduction.....	5
	2. Shot Noise.....	10
	3. Source Flicker Noise.....	13
	i) The Transfer Function and Meas- urement Effects on Flicker Noise.....	16
	4. Systematic Source Noise.....	21
	D. The Combined Effects of Noise on the Signal.....	23
	1. The Combination of Noises.....	23
	2. Multiplicative and Additive Noise...	24
	E. Inductively Coupled Plasma Noise Studies	25

CHAPTER		PAGE
II	A. ICP Instrumentation and Modifications ..	31
	1. The ICP Source.....	31
	2. Plasma Torch.....	31
	3. Analyte Delivery System.....	36
	4. Pneumatic Nebulizers.....	37
	5. Ultrasonic Nebulizer.....	37
	6. Modifications to the Gas Supply Controls.....	41
	7. Ignition and Running Conditions of the ICP.....	42
	B. The Optical System.....	42
	C. Data Acquisition System.....	45
	1. Measurement Electronics.....	45
	2. Minicomputer System.....	48
	3. Dual Channel Data Acquisition.....	50
III	The Effect of Integration Period on Measurement Precision in Inductively Coupled Plasma Emission Spectrometry and Related Studies.....	52
	A. Introduction.....	52
	B. Experimental.....	53
	C. Discussion of Results.....	62
	D. Conclusions.....	64

CHAPTER	PAGE	
IV	Noise Power Spectra of Optical and Acoustic Emission Signals from the Inductively Coupl- ed Plasma.....	65
	A. Introduction.....	65
	B. Experimental.....	66
	1. ICP Operating Conditions.....	66
	2. Data Acquisition and Bandwidth Control.....	66
	3. Computer Calculation of Noise Power Spectra.....	69
	C. Low Frequency Noise Power Spectra (0-5 Hz).....	71
	D. High Frequency Noise Power Spectra (0-500 Hz).....	77
	E. Acoustic Emission Signals.....	86
	F. Simultaneous Dual Channel Measurement.....	91
	G. Conclusions.....	98
V	Correlation of Spray Chamber Pressure Fluc- tuations with Noise in the Emission Signal..	100
	A. Introduction.....	100
	B. Experimental Measurement of Spray Chamber Pressure.....	102

CHAPTER	PAGE
C. The Effect of Plasma Operating Conditions on the Spray Chamber Pressure.....	102
D. Correlation Studies.....	110
1. Experimental.....	110
2. Calculation of the Correlation Function.....	110
3. Results from the Scott Spray Chamber.....	112
4. "Soak-Away" Spray Chamber.....	115
5. Results from the "Soak-Away" Spray Chamber.....	115
E. Conclusions from Spray Chamber Pressure Measurements.....	119
 VI Correlation of Noise in the Incident and Re- flected Power Circuits with Noise in the Emission Signal.....	 120
A. Introduction.....	120
B. Experimental Monitoring of Incident and Reflected Power Levels.....	120
C. Discussion of Results.....	123
 VII The Use of Internal Standards with the ICP...	 131

CHAPTER	PAGE
A. The Internal Standard Principle.....	131
B. Some Statistics Associated with the Use of an Internal Standard.....	134
C. Experimental.....	138
D. Results from the Use of an Internal Standard.....	139
E. Conclusions.....	153
VIII Summary.....	154
Bibliography.....	157
Appendix A - Use of Added Random Noise to Improve Bit Resolution in Digital Signal Averaging..	165
Bibliography - Appendix A.....	174
Appendix B - Data Logging System Based on the Intel 8748 Single Chip Microcomputer.....	175
Bibliography - Appendix B.....	187
Appendix C - Software Developed for Data Acquisition and Processing.....	188

## LIST OF TABLES

<u>Table</u>	<u>Description</u>	<u>Page</u>
I	ICP System Specifications.	32
II	Ultrasonic Transducer Specifications.	40
III	Typical Operating Conditions of the ICP.	43
IV	Monochromator Specifications.	46
V	Comparison of Mercury Vapor Introduction System and a Meinhard Nebulizer Aspirating 100 ppm Mercury Solution.	61
VI	Signal-to-Noise Ratios for CaII 393.3 nm (1 ppm).	72
VII	Spectral Lines and Concentrations Used for Internal Standard Study.	140
VIII	Internal Standard Study.	149
AI	Bit Resolution of ADC Measurements.	170
BI	Summary of 8748 Features.	176
BII	"8048" Family - Single Component Micro-computers.	179

## LIST OF FIGURES

<u>Figure</u>	<u>Description</u>	<u>Page</u>
1	Noise sources in atomic emission spectro- metry.	6
2	Noise power spectra (a) white noise, (b) 1/f noise.	14
3	Transfer function of first order low pass filter (a) RC = 1 s, (b) RC = 0.1 s, (c) RC = 0.01 s.	18
4	Transfer function of integrator (a) t = 1 s, (b) t = 0.3 s, (c) t = 0.1 s.	19
5	ICP source schematic.	33
6	Spray chamber and torch assembly.	34
7	(a) Regular torch, (b) Tall torch. All dimensions in mm. All dimensions id- entical except where indicated.	35
8	Pneumatic nebulizers (a) variable tip cross-flow, (b) fixed tip cross-flow, (c) Meinhard concentric.	38
9	Ultrasonic nebulizer.	39
10	Optical arrangement of spectrometer.	44
11	Measurement electronics.	47
12	Dual sample and hold amplifiers.	51
13	Log-log plot of SNR vs integration time for CaII 393.3 nm (1 ppm) using a Meinhard nebulizer.	55
14	Log-log plot of SNR vs integration time for CaII 393.3 nm using a cross-flow nebulizer.	56
15	Log-log plot of SNR vs integration time for CdII 214.4 nm (50 ppm) using a Mein- hard nebulizer.	57



<u>Figure</u>	<u>Description</u>	<u>Page</u>
16	Log-log plot of SNR vs integration time for CdII 214.4 nm (1 ppm) using an ultrasonic nebulizer.	58
17	Log-log plot of SNR vs integration time for ArI 415.8 nm.	59
18	Bandwidth control and sampling frequency required in order to minimise aliasing in the 0-500 Hz region.	68
19	Flow chart for the calculation of noise power spectra.	70
20	Low frequency (0-5 Hz) noise power spectra of the CaII 393.3 nm (1 ppm) optical emission signal using four different nebulizers.	74
21	Effect of analyte concentration (CaII, 393.3 nm) on the 0-5 Hz region noise power spectrum using a Meinhard nebulizer.	76
22	Noise power spectrum (0-500 Hz) of the CaII 393.3 nm optical emission signal. Meinhard nebulizer.	79
23	Effect of plasma power (1 kw-1.9 kw) on the noise power spectrum of the CaII 393.3 nm optical emission signal.	81
24	Plot of noise feature frequency as a function of power.	82
25	Plot of noise feature frequency as a function of coolant gas flow rate.	83
26	Typical ICP noise power spectra in the 0-500 Hz bandwidth. Meinhard nebulizer.	84
27	The effect of lens lateral position on noise power spectra. (b) central vertical axis, (a) 4 mm left displacement and (c) 4 mm right displacement. NO band head.	87
28	The effect of lens focal position on noise power spectra. (b) sharp visual focus, (a) 4 mm displacement towards plasma and (c) 4 mm displacement towards monochromator. CaII 393.3 nm (1 ppm).	88

<u>Figure</u>	<u>Description</u>	<u>Page</u>
29	Microphone circuit used for acoustic measurements.	89.
30	Acoustic noise power spectra of the ICP discharge. (a) regular torch, (b) tall torch.	90
31	Simultaneous dual channel data acquisition system.	92
32	Optical configuration for simultaneous dual channel measurement of plasma emission signals.	94
33	Noise peak. Isolated by means of electronic high and low pass filters.	95
34	Simultaneously digitised noise signal for CaII 393.3 nm from monochromator A (solid line) and monochromator B (dashed line), showing 90° phase shift.	96
35	Simultaneously digitised noise signal for CaII 393.3 nm from monochromator A split and fed through electronic channels A and B. Showing no measurement phase shift.	97
36	Pressure transducer for spray chamber pressure measurement (a) connections to spray chamber, (b) electrical connections.	103
37	Plot of spray chamber pressure as a function of nebulizer gas flow rate.	105
38	Plot of spray chamber pressure as a function of auxiliary gas flow rate.	106
39	Plot of spray chamber pressure as a function of plasma gas flow rate.	107
40	Plot of spray chamber pressure as a function of input rf power.	108
41	Correlation of CdII 214.4 nm (50 ppm) emission with spray chamber pressure fluctuations. Scott spray chamber.	113

<u>Figure</u>	<u>Description</u>	<u>Page</u>
42	Correlation of ArI 415.9 nm emission with spray chamber pressure fluctuations. Scott spray chamber.	114
43	"Soak-away" spray chamber.	116
44	Correlation of CdII 214.4 nm (50 ppm) emission with spray chamber pressure fluctuations. Soak-away spray chamber.	117
45	Correlation of ArI 415.9 nm emission with spray chamber pressure fluctuations. Soak-away spray chamber.	118
46	Circuit for monitoring incident and reflected power fluctuations.	122
47	Noise power spectrum of incident rf power.	124
48	Noise power spectrum of reflected rf power.	125
49	Correlation of CaII emission signal with incident power.	126
50	Correlation of ArI emission signal with incident power.	127
51	Correlation of CaII emission signal with reflected power.	128
52	Correlation of ArI emission signal with reflected power.	129
53	Correlation of CaII emission signals from dual monochromator system.	141
54	Correlation of CaII and ArI emission signals.	142
55	Correlation of CaII and SrII emission signals.	143
56	Correlation of CaII and ScII emission signals.	144

<u>Figure</u>	<u>Description</u>	<u>Page</u>
57	Correlation of CaII and InI emission signals.	145
58	Correlation of CaI emission signals from dual monochromator systems.	146
59	Correlation of CaI and ArI emission signals.	147
60	Correlation of CaI and InI emission signals.	148
A1	Bit resolution improvement of 8 bit ADC to 12 bits by signal averaging and added random noise.	171
B1	Block diagram 8748.	178
B2	Schematic diagram of data acquisition system.	181
B3	Schematic diagram of 8748 - teletype interface.	182

## CHAPTER I

### NOISE IN INDUCTIVELY COUPLED PLASMA EMISSION SPECTROMETRY

#### A. Introduction to the ICP

The inductively coupled plasma (ICP) as a source for atomic emission analysis was first described by Greenfield et al. (1) in 1964. A year later Wendt and Fassel (2) published the results of the ICP work that they had been concurrently pursuing. The design of the ICP torch used in both of these studies was based on the earlier design of Reed (3,4) who had an ICP system for growing refractory crystals.

The ICP has found widespread use in analytical laboratories throughout the world. The rapidly growing usage of the ICP has spurred the publication of many general review articles, which may be consulted for an overview of the technique (5-12).

The factors that make the ICP attractive as a spectroscopic source include high sensitivity, wide linear dynamic range and relative freedom from chemical interferences. These advantages, coupled with the ability of the ICP to excite a much wider variety of elements than flames, make the ICP uniquely suited for simultaneous analysis by atomic emission spectrometry.

Many fundamental studies have been carried out into the characteristics of the ICP. While much interest has been focussed on excitation mechanisms and source temperature, comparatively little fundamental work has been carried out on ICP noise. The purpose of this work is to study some of the types, causes and characteristics of ICP noise. In addition a number of techniques for improving ICP precision will be investigated. However, before entering into the discussion of ICP noise a general review of noise in atomic emission spectrometry will be presented.

## B. Characterization of Emission Noise

### 1. Signal-to-Noise Ratio

Noise may be defined as any *unwanted* fluctuation present in a signal. In the case of atomic emission analysis these are unwanted variations in the *measured* emission intensity of the source. The amplitude of the fluctuations is usually expressed as either the r.m.s. noise current or voltage, or more often, by the standard deviation of a number of repeated measurements of the signal. If the number of measurements is reasonably large then the standard deviation approximates the r.m.s. noise (13).

Usually, in atomic spectroscopy the standard deviation ( $\sigma$ ) is referenced to the signal intensity ( $S$ ) to give a measure of the relative noise or signal-to-noise ratio (SNR).

$$\text{SNR} = S/\sigma \quad (1)$$

The other approach to expressing the relative noise is the percent relative standard deviation (RSD).

$$\text{RSD} = (\sigma/S) \times 100 \quad (2)$$

Either way, these two quantities are useful in expressing the precision that can be obtained from the emission source with *given* instrumentation and under *given* conditions.

The use of the SNR or RSD does *not* however give any information as to the effects on the precision if the instrumentation or *any* of the conditions are changed. To characterize completely the noise in the system, it is necessary to have the knowledge of its frequency distribution. A representation of this frequency distribution is a plot of noise power density as a function of frequency, which is known as the noise power spectrum.

## 2. Noise Power Spectra

As was previously mentioned the noise power spectrum

is a plot of noise power density vs frequency. These plots are most useful as they enable the prediction of how instrumentation and measurement parameters will affect the precision.

Two methods are commonly used to obtain the noise power spectra of a source. The first makes use of a frequency analyzer. In this approach the emission signal obtained by means of a suitable detector such as a photomultiplier tube is fed to the frequency analyser. Essentially this is a narrow band tuned amplifier whose band pass is swept over the frequency range of interest. The signal power from the amplifier is then plotted as a function of frequency to give the noise power spectrum. The alternative approach is to use a Fourier transformation to convert noise in the time domain to noise power density in the frequency domain. In practice this is accomplished by sampling and recording the noise (after certain bandwidth limitations, see Chapter IV) as a function of time. A discrete Fourier transformation process is then carried out to produce the noise power spectrum.

With either of these techniques the noise power spectrum is a plot of noise power density, the units of which can be watts/Hz, volts<sup>2</sup>/Hz or amps<sup>2</sup>/Hz. Noise power density results, in the case of the frequency analyser,



because all the noise within the band-pass of the amplifier is simultaneously measured. -With the discrete Fourier transformation method similar considerations must be made with respect to the resolution of the transformation (14).

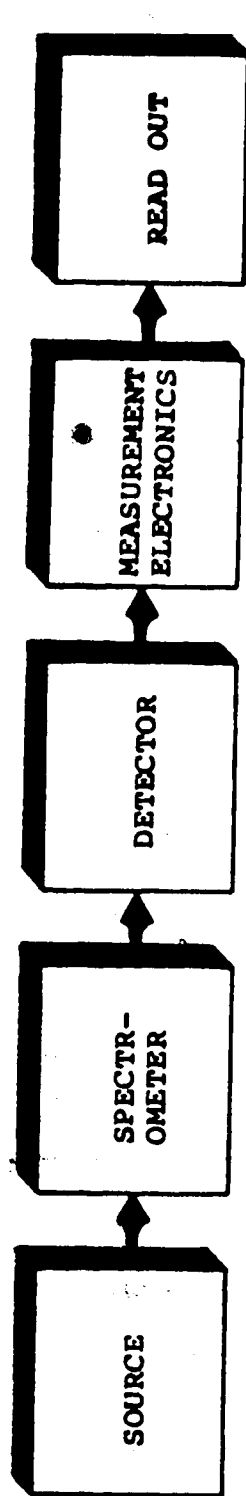
Noise power spectra will be extensively utilized in the following discussions of noise types and in the main body of the text for the interpretation of ICP noise.

### C. Noise Sources in Atomic Emission Spectrometry

#### 1. Introduction

The various components that comprise a typical ICP atomic emission spectrometer system are illustrated in Figure 1. While this configuration is typical for an ICP spectrometer most other emission techniques employ a similar arrangement of components. For this reason most of the following discussion, while directed principally at the ICP, will also be applicable to other emission techniques. All of the illustrated components are capable of introducing noise into the system. Because of this the spectrometer system shown in Figure 1 will be briefly discussed before a more detailed discussion of the more important noise sources and types.

In most light sources photons are emitted randomly,



- |                                 |                   |                       |                        |                     |
|---------------------------------|-------------------|-----------------------|------------------------|---------------------|
| 1) Photon noise<br>(shot noise) | 1) Thermal drifts | 1) Shot noise         | 1) Johnson noise       | 1) Quantizing noise |
| 2) Source flicker noise         |                   | 2) Dark current noise | 2) Semiconductor noise |                     |
| 3) Systematic source noise      |                   |                       | 3) RF interference     |                     |

Figure 1. Noise sources in atomic emission spectrometry.

which gives rise to a fundamental noise known as photon noise. The degree of photon noise is related to the photon flux reaching the detector. Because of this, photon noise is dependent on a number of factors including the intensity of the source, the collection efficiency of the imaging optics and the throughput of the monochromator. This dependence of shot noise on the rate of photons reaching the detector makes it more convenient to include photon noise under the more general heading of detector shot noise.

Source flicker noise is a "non-fundamental" noise present in the emission of most sources. It may be due to a combination of many factors including in the case of the ICP, fluctuations in nebuliser efficiency, power output, from the rf generator, support gas flow rates and turbulences within the source. Source flicker is the dominant noise source in the ICP when working with concentrations well above the detection limits for most emitting species. Because of the importance of flicker noise special attention will be given to its properties and characteristics later in this discussion.

Systematic noise may be present in the emission signals of some spectral sources. These signal fluctuations are non-random and are observed as a distinct periodic fluctuation in the emission intensity, often observed at

Finally, the act of converting the signal to a numerical value introduces a noise component known as quantising noise. It has been shown (22) that the variance due to quantising has a value of  $q^2/12$  if the total rms noise present on the signal is greater than  $q/2$ , where  $q$  is the quantising interval. If the rms noise present is less than  $q/2$  it may actually be desirable to introduce noise into the system, such that the  $q/2$  limit is just reached. This will ensure that the least significant bit of the analog-to-digital converter is randomised. This allows signal averaging to be carried out which results in improvement of the measurement precision. Digitization noise and the technique of noise addition is more fully discussed in Appendix A.

The more important noise sources encountered in atomic spectroscopy, that is shot noise, source flicker noise and systematic source noise, will now be discussed in somewhat more detail.

## 2. Shot Noise

The discussion of shot noise in this section will be explicitly for photoemissive devices such as phototubes and photomultiplier tubes. However, due to the photon noise component of shot noise similar conclusions may be drawn

for solid state detectors.

As was previously pointed out there are two contributing factors to shot noise; these are photon noise and photoelectron noise. In the case of photomultipliers an additional factor is also present caused by the amplification process in the dynode chain. Detailed discussions of shot noise can be found in the articles by Fried (23), Sharpe (24) and in the general literature (see for instance Van der Ziel (20,21)).

In a phototube, due to the random arrival of photons at the photocathode and the subsequent random emission of photoelectrons, the arrival of photoelectrons at the anode is random and obeys a Poisson distribution (7). Therefore the number of electrons ( $N$ ) arriving in time ( $t$ ) will do so with a standard deviation equal to  $N^{1/2}$ . This will result in an average signal current ( $i_a$ ) which is simply related to  $N$ , the charge on the electron ( $e$ ) and the measurement time.

$$i_a = Ne/t \quad (3)$$

The average root-mean-square noise current ( $i_{s,rms}$ ) will then be given by:

$$i_{s,rms} = N^{1/2}e/t \quad (4)$$

From Equations (3) and (4) the noise current can be expressed as a function of the signal and the measurement period.

$$i_{s\text{rms}} = i_a^{1/2} e^{1/2} / t^{1/2} \quad (5)$$

If one is now interested not in the average noise current but in the standard deviation of an integrated signal ( $\sigma_s$ ) the rms noise current is integrated over the entire measurement period.

$$\sigma_s = i_a^{1/2} e^{1/2} t^{1/2} \quad (6)$$

The expression for the signal-to-noise ratio becomes:

$$\text{SNR} = i_a^{1/2} t^{1/2} / e^{1/2} \quad (7)$$

Equation (7) shows the important conclusion that in the case of shot noise it is possible to gain a square root improvement in the signal-to-noise ratio simply by extending the measurement period (integration time). Also Equation (7) reveals a square root dependence of the signal-to-noise ratio on the signal intensity. Thus it is possible to reduce the effects of shot noise simply by increasing the photon flux reaching the detector.

The same conclusions also apply to the photomultiplier tube with respect to the effects of integration time and

photon flux. The amplification process does not alter the fundamental shot noise component. However, statistical variations in the number of secondary electrons emitted by the dynodes for each impinging primary electron adds an additional noise factor. The overall equation for the rms noise current becomes:

$$i_{s\text{ rms}} = a g^{1/2} e^{1/2} i_a^{1/2} / t^{1/2} \quad (8)$$

where  $a$  is the noise enhancement factor for the dynode chain induced noise and  $g$  is the gain of the photomultiplier tube. Typical values for  $a$  are in the region of 1.2 and the gain is in the order of  $10^5$  (24).

The noise power spectrum of shot noise is white, that is, the noise power density  $P(f)$  is independent of frequency (see Figure 2a). For a phototube an estimate of the noise power density  $P(f)$  may be given by:

$$P(f) = 2e i_a \quad (9)$$

For a photomultiplier tube additional factors for the gain and the dynode noise factor must be included (20):

$$P(f) = 2a g e i_a \quad (10)$$

### 3. Source Flicker Noise

Source flicker noise is a *non-fundamental* noise

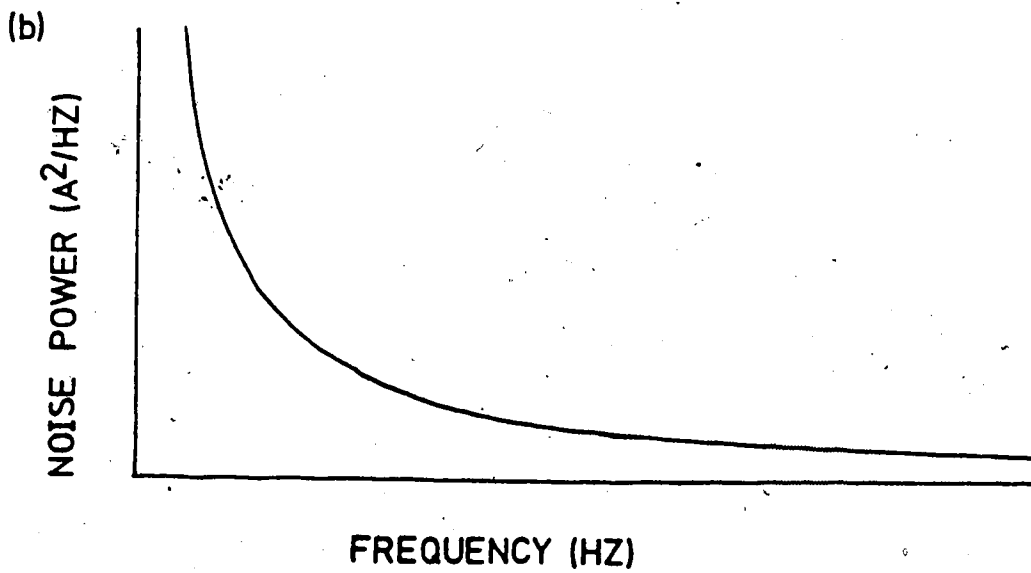
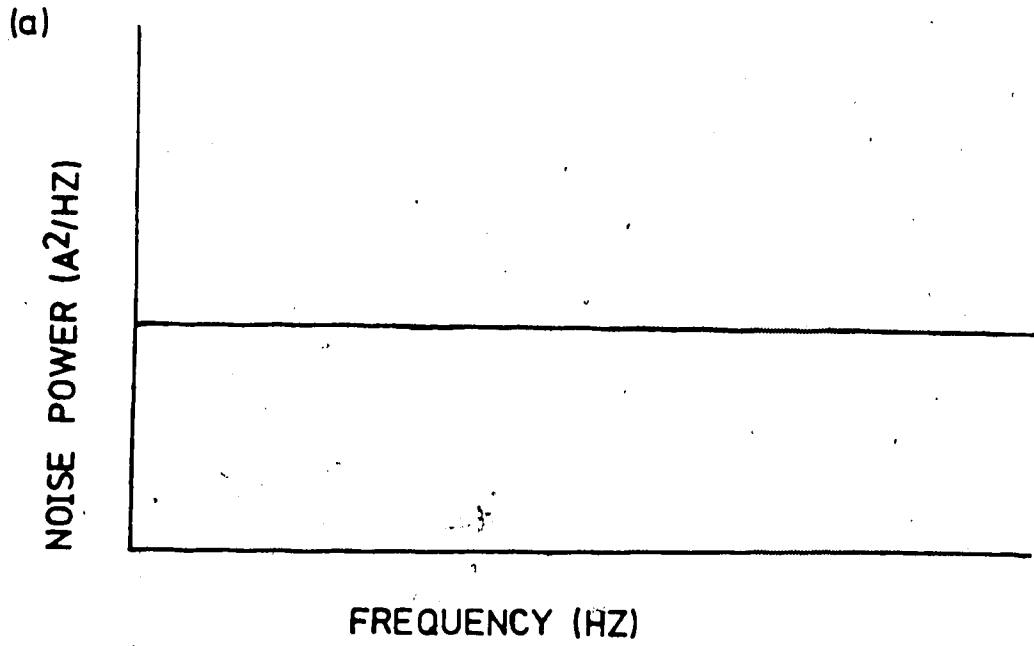


Figure 2. Noise power spectra (a) white noise, (b)  $1/f$  noise.



associated directly with the spectral source. It is synonymously known as analyte flicker, fluctuation and  $1/f$  noise. The main characteristics of source flicker noise are the proportionality of the noise to the signal and a noise power spectrum with approximately a  $1/f$  functionality.

Flicker noise is not unique to atomic spectroscopy. It is encountered in many physical systems including electrical noise in carbon films, semiconductors and zener diodes, and also with quartz oscillators, in the rotation of the earth and in the flow of highway traffic (17). While the sources of flicker noise in atomic spectroscopy are not well understood the causes of flicker noise in many electronic systems are well known and appear to be fundamental in nature and are associated with queuing phenomena (17).

In flame atomic absorption spectrometry Bower and Ingle (25) have stated that they believe source flicker is caused, to a large extent, by variations in the rate of analyte delivery to the flame by the nebulizer. As will be demonstrated later in this thesis the nebulizer also appears to be a major source of noise in the ICP system.

Winefordner et al. (26,27) used an empirical expression, that was previously shown to be applicable to certain electronic tubes, to describe source flicker noise

in atomic emission spectrometry. They assumed it applied equally well to evaluate the noise power density function of spectral source flicker noise:

$$P(f) = k i_a^\alpha / f^\eta \quad (11)$$

where  $i_a$  is the signal,  $f$  is the frequency and  $k$  is a dimensionless constant for a particular system. This constant expresses the ratio of flicker noise power to signal power upon which the flicker noise is carried.  $\alpha$  and  $\eta$  are also constants and take on values close to 2 and 1.

#### i) The Transfer Function and Measurement Effects on Flicker Noise

It was possible in the case of shot noise to calculate on a statistical basis the effect of integration time on the signal-to-noise ratio. Due to the *non-fundamental* nature of source flicker noise a similar calculation is not possible. However from a knowledge of the flicker noise power spectrum and the transfer function of the measurement system it is possible to predict the effect of changing the integration time.

The transfer function ( $H(f)$ ) may be used to characterize totally the frequency response of a system. It can

be defined as the ratio of signal amplitude at the input of a device ( $v_i$ ) to the amplitude at the output ( $v_o$ ), expressed as a function of frequency:

$$H(f) = v_o/v_i \quad (12)$$

in terms of power the transfer function becomes:

$$H(f)^2 = P_o/P_i \quad (13)$$

For example the transfer function of a first order RC low pass filter is (13):

$$H(f) = 1/[(2\pi fRC)^2 + 1]^{1/2} \quad (14)$$

The transfer function of this type of filter is shown in Figure 3 for a number of RC time constants. In any integrated measurement the transfer function resulting from the integration time itself must be considered. The transfer function associated with an integration time ( $t$ ) is given by (13):

$$H(f)^2 = \frac{\sin^2 \pi ft}{(\pi ft)^2} \quad (15)$$

The effective transfer function for several integration times is illustrated in Figure 4. For multicomponent systems the transfer function of the system is simply the

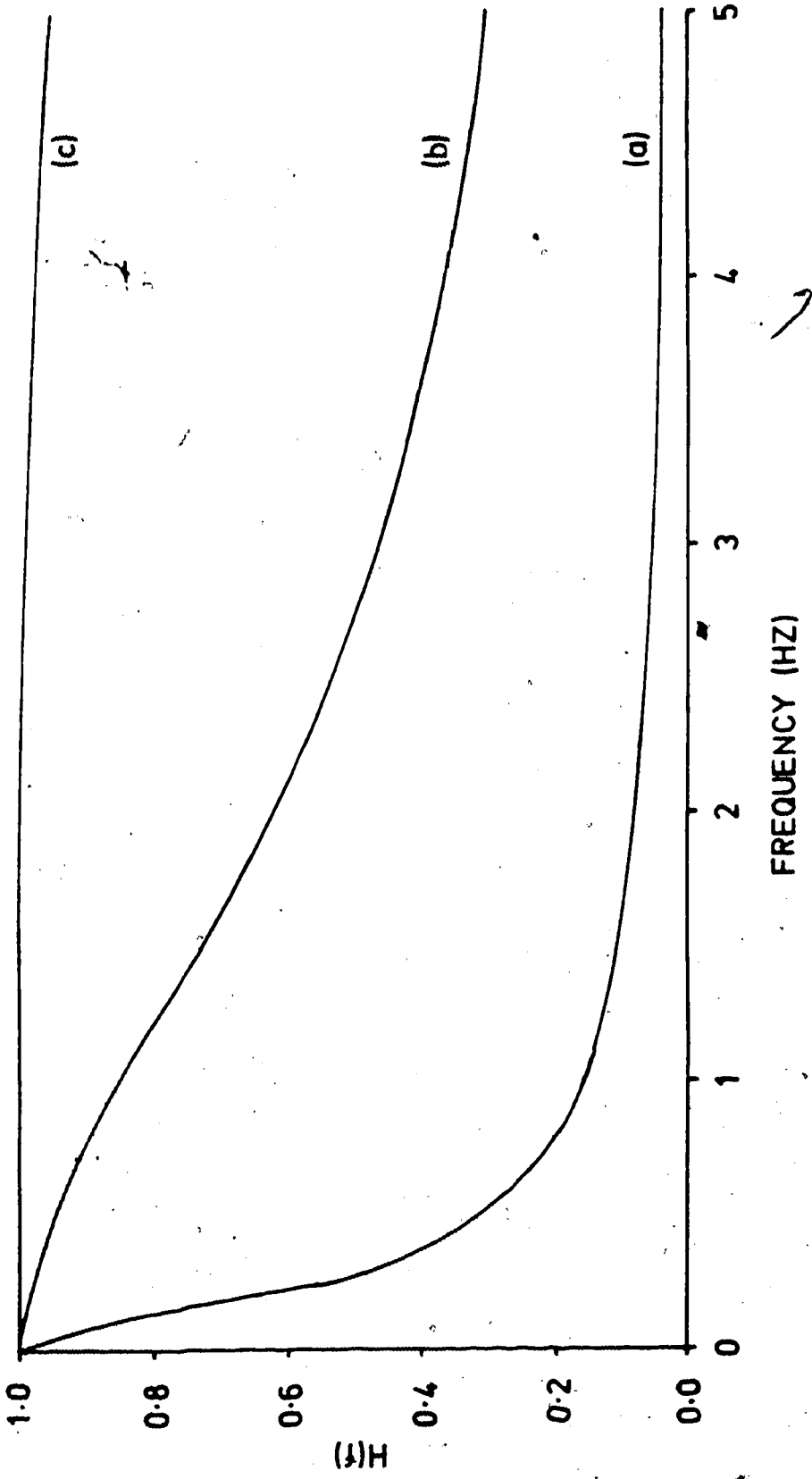


**Figure 3.** Transfer function of first order low pass filter (a)  $RC = 1$  s,  
 (b)  $RC = 0.1$  s, (c)  $RC = 0.01$  s.

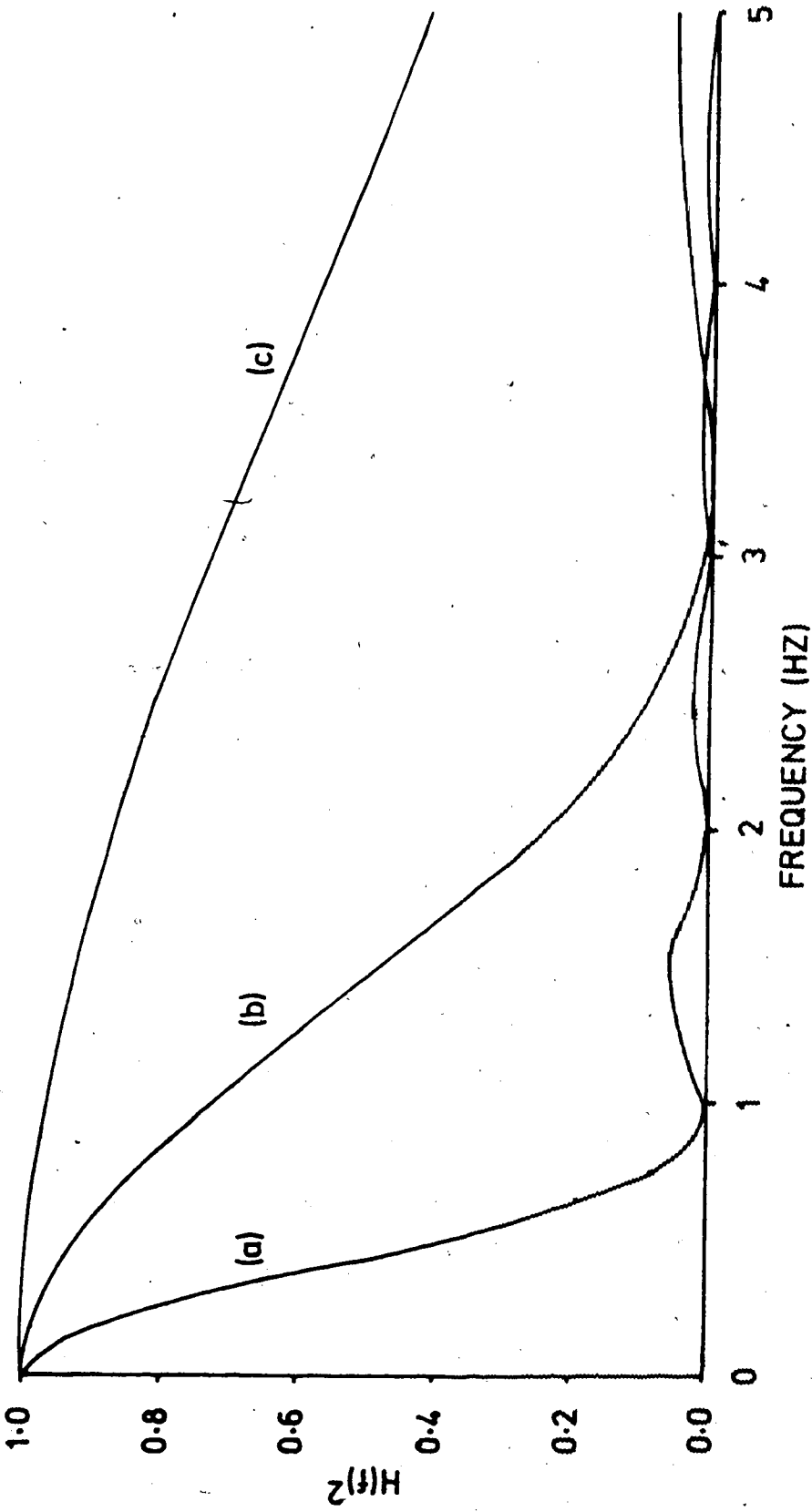


Figure 4. Transfer function of integrator (a)  $t = 1$  s, (b)  $t = 0.3$  s, (c)  $t = 0.1$  s.

product of the transfer function of its components:

$$H(f) = H(f)_1 H(f)_2 \dots H(f)_n \quad (16)$$

Now armed with the knowledge of the transfer function of the measurement system and the noise power spectrum of the source it is possible to calculate the effect of integration time on flicker noise. This is done by combining the noise power spectrum and the transfer function of the integrator and integrating over all frequencies (25):

$$i_f \text{ rms} = \left[ \int_0^\infty P(f) H(f)^2 df \right]^{1/2} \quad (17)$$

If one assumes a noise power spectrum that is described by Winefordner's empirical equation (Equation 11), setting  $\alpha = 2$  and  $\eta = 1$ , and substitutes this expression together with the transfer function of the integrator into Equation (17) an expression for the average flicker noise current ( $i_f \text{ rms}$ ) can be derived:

$$i_f^2 \text{ rms} = 4(\ln 2) k^2 i_a^2 \quad (18)$$

This equation is more commonly written in the form:

$$i_f \text{ rms} = \xi i_a \quad (19)$$

where  $\xi$  replaces the constant terms in Equation (18) and

is known as the flicker factor. If the flicker noise is now integrated for a finite period of time ( $t$ ) the standard deviation of these measurements ( $\sigma_f$ ) will be:

$$\sigma_f = \xi i_a t \quad (20)$$

In terms of the signal-to-noise ratio the expression becomes:

$$\text{SNR} = 1/\xi \quad (21)$$

This result should be compared with the equation obtained for shot noise (Equation (7)). The important consequences of Equation (21) are that unlike shot noise the signal-to-noise ratio is now independent of the integration time and the photon flux. Thus, no improvement in precision can be obtained by increasing the integration time or the signal intensity. Using this type of analysis it is also possible to show that for a system in which the low frequency components are greater than that predicted by a  $1/f$  relationship increasing the integration time will actually decrease the precision.

#### 4. Systematic Source Noise

In the noise power spectra of certain emission sources distinct peaks are observed. These peaks are due to noise

which is not random but systematic in nature.

Alkemade et al. (28) observed the presence of systematic noise in the emission of a premixed  $H_2-O_2-N_2$  flame.

Hieftje and Bystroff (29) also observed similar peaks in the noise power spectra of sheathed air-acetylene flames. Hieftje attributed the origin of these peaks to "the swirl effect of eddy currents in the flame". It is known (30) that flames may become unstable under certain conditions and oscillate at high frequencies. Presumably, this could lead to similar systematic noise in flames when they are operated under the appropriate conditions.

Noise of this type has been observed in ICP emission signals. Walden et al. (14) observed peaks in the noise power spectrum of the ICP but was unable to explain their origin. Belchamber and Horlick (31) observed similar peaks in the noise power spectrum of the ICP in the 200 to 400 Hz region. They explained their origin in the rotation of an assymmetric plasma body. The work leading to this conclusion is detailed in Chapter IV.

Because of the high frequency of these systematic noises it is possible to eliminate effectively their influence by the use of extremely short ingetration times. However, systematic noise of this nature may be a severe problem when monitoring transient emission signals or



when using the plasma as an atom or ion cell for atomic absorption or fluorescence studies. These noise components also pose a problem when a Fourier transform spectrometer is used as part of the measurement system (32).

#### D. The Combined Effects of Noise on the Signal

##### 1. The Combination of Noises

The total noise present at the output of the spectrometer is a combination of all noise components introduced by the system. For independent noise sources the total variance ( $\sigma_T^2$ ) is the sum of the variances of the individual noises:

$$\sigma_T^2 = \sigma_{\text{FLICK.}}^2 + \sigma_{\text{SHOT}}^2 + \sigma_{\text{ELECTRON.}}^2 \dots \quad (22)$$

Care must be taken however to ensure that the noise sources are independent, if they are not then an additional factor the correlation coefficient ( $r$ ) must be introduced (27,33):

$$\sigma_T^2 = \sigma_A^2 + \sigma_B^2 + 2r\sigma_A\sigma_B \quad (23)$$

The value of the correlation coefficient lies in the interval -1 to +1 and expresses the degree of linear relationship between the two noises. In most cases the noises encountered in atomic spectrometry are independent and

Equation (22) may be used to combine them. One major exception exists. This is encountered when combining flicker noise in the emission signal and flicker noise in the background emission. In this case it is reasonable to expect some degree of correlation to exist between the two noises. This calculation may be necessary under conditions of low signal-to-background ratio where background fluctuations become the dominant source of noise (34).

## 2. Multiplicative and Additive Noise

Noise from spectroscopic emission sources can either be additive or multiplicative in its effects on the signal (29,35). One example of additive noise is variations in the emission intensity of the background. In this case the noise is merely superimposed upon the signal. Multiplicative noise is a modulation in the intensity of the emission signal. This modulation may be brought about by a number of factors including variations in the analyte transport rate to the source or changes in the excitation conditions.

Additive noise originating in the background emission is obviously more of a problem under low signal-to-background ratios. Salin and Horlick (34) showed that in the ICP by altering the rf power level they could bring about changes in the signal-to-background ratios of emission

lines with accompanying changes in their signal-to-noise ratios. For SrII emission at a signal-to-background ratio of 22 the signal-to-noise ratio was 430. Decreasing the signal-to-background ratio to 5 decreased the signal-to-noise ratio to 290 as the additive background noise became more important.

When operating at low radiant fluxes the limiting noise may be due to additive dark current flicker. This was shown to be true for the ICP by Greenfield and Thorburn-Burns (36). Under these conditions the use of source modulation will result in a gain in signal-to-noise ratio (37).

Multiplicative noise may be dealt with by the use of the internal standard technique. This technique involves ratioing the emission intensity of the analyte to either the emission intensity of another element or some other parameter whose amplitude is modulated by similar multiplicative noise. If the dominant noise is not multiplicative but additive then it is obvious that no gain in precision can be expected by the use of an internal standard, indeed the precision may be degraded.

#### E. Inductively Coupled Plasma Noise Studies

While few fundamental studies have been carried out

specifically on ICP noise, information of this nature is of critical importance if the technique is to reach its full potential. Meddings et al. (38) pointed out the great financial burden often placed on the precision of ICP analysis. While most studies into ICP noise have focussed on the detection limit relatively little attention has been paid to the precision of measurements of concentrations considerably in excess of the detection limit. The signal-to-background ratio has been used as a figure of merit (39,40). Salin and Horlick (34) showed that this ratio is only significant when the limiting noise present in the system is related to the plasma background emission.

Boumans (41,42) stated that for his system there was a constant standard deviation of approximately 1% in his signal and also a 1% standard deviation in the background emission over the entire spectral range. Later Boumans (9) concluded that the increase in relative standard deviation with decreasing concentration was in keeping with a system in which background carried fluctuation noise dominates. Greenfield (43) stated emphatically that noise in his ICP was directly proportional to the signal.

Salin and Horlick (34) studied the signal-to-noise

ratio performance of the ICP using a photodiode array spectrometer. Their conclusions were that well above the detection limit analyte flicker is the dominant noise. As the concentration is decreased a gradual transition takes place until at very low concentrations detector noise becomes limiting. A similar result was shown by Greenfield and Thorburn-Burns (36): under certain conditions of low radiant fluxes the principal component of the background signal with photomultiplier tube was dark current.

Ediger et al. (44) in a study on the selection of ICP instrumental properties noted that for arsenic, manganese and uranium emitting species little improvement in the precision of analysis was to be gained by the use of long integration times.

From these studies it seems safe to conclude that at concentrations largely in excess of the detection limit the limiting ICP noise is source flicker. As the detection limit is approached background flicker noise becomes dominant and under some conditions this background noise is not due to the plasma but is detector dark current noise.

The causes of source flicker are not well understood. However, the nebulisation step plays an important role.

Greenfield (45) compared ten nebulizers for use with the ICP and found considerable differences in their precision. Salin and Horlick (34) stated that in their opinion the most probable sources of source flicker lie in the nebulizer-sample delivery and gas flow systems of the ICP. This point of view manifests itself in the fact that attempts to improve the precision of the ICP have largely concentrated on nebulizer and sample transport system design.

The first design of a nebulizer specifically for use with the ICP was a variable tip cross-flow nebulizer operating at low gas flow rates described by Knisely et al. (46) in 1974. Myers et al. (47) pointed out the very considerable effects of tip alignment with this type of cross-flow nebulizer, on the signal-to-noise ratio. Meddings et al. (38,48) concluded that in terms of short term precision cross-flow nebulizers gave the best results though in terms of long term stability the rigid tube alignment present in concentric nebulizers helped give better reproducibility. They then described a fixed tip cross-flow nebulizer operated at a pressure of 200 psi. This nebuliser when used in conjunction with electronic mass flow controllers to control delivery of argon to the ICP, gave a precision of  $<0.5\%$  RSD in routine analysis. A fixed tip cross-flow nebulizer used with an impact ball

has also been described by Novak et al. (49) for use with the ICP. The detection limits obtained with this nebulizer are comparable to those obtained with others. No data is, however, available on its precision.

Schutyser and Janssens (50) evaluated a number of spray chamber designs for ICP use. These spray chambers were modifications to the original design of Scott et al. (51). Relative standard deviations using these spray chambers with the same Meinhard concentric nebulizer for  $LiI$  (670.8 nm) and  $CdII$  (226.5 nm) were in the range of 0.4% for the best case to 2.6% for the worst.

It is the intent of the work contained in this thesis to expand on, and explore more fully some of the origins of source flicker and other noises associated with the ICP. It is also the intent to investigate procedures such as internal standardisation in their effectiveness in removing the affects of source flicker noise in ICP emission analysis.

To help characterize the noise from the ICP a study of the effect of integration period on precision was carried out for a number of nebulizers. To characterize the emission noise more completely noise power spectra of the ICP were obtained, with a number of nebulizers and under different running conditions.

In addition, correlation studies have been carried

out between noise in the emission signal and fluctuations in ICP parameters including spray chamber pressure, incident power and reflected power. Correlation studies have also been carried out to investigate the effectiveness of a number of internal standard elements. Before entering into these studies, the ICP system, its modifications and the measurement equipment used to carry out this work will be described.



## CHAPTER II

### A. ICP Instrumentation and Modifications

#### 1. The ICP Source

The ICP system used for this work was a Plasma-Therm ICP 5000 (Plasma-Therm, Inc., Kresson N.J.). The specifications for this system are listed in Table I. Power from the radio frequency generator is coupled via an automatic impedance matching and tuning network to the ICP source (Figure 5). This matching network allows efficient power transfer to the plasma, under a wide range of operating conditions. A four turn load coil surrounds the top of the plasma torch and serves to couple RF power to the plasma itself (Figure 6).

#### 2. Plasma Torch

Two basic designs of torch were used. The internal dimensions were close to those suggested by Fassel and Kniseley (6). The difference between the two designs were in the length of the outer quartz tube (Figure 7). The shorter of the two torches was used for the major part of this work; the tall torch being mainly used for comparison purposes in Chapter IV.

The torches consist of three concentric quartz tubes.

TABLE I

## ICP System Specifications

R.F. Generator frequency	27.12 MHz (crystal controlled)
Rated output power	5 kW
Envelope ripple	<5%
Generator, output impedance	50 $\Omega$
Matching network, input impedance	50 $\Omega$
Matching network, output impedance	wide range
Load coil	4 turn

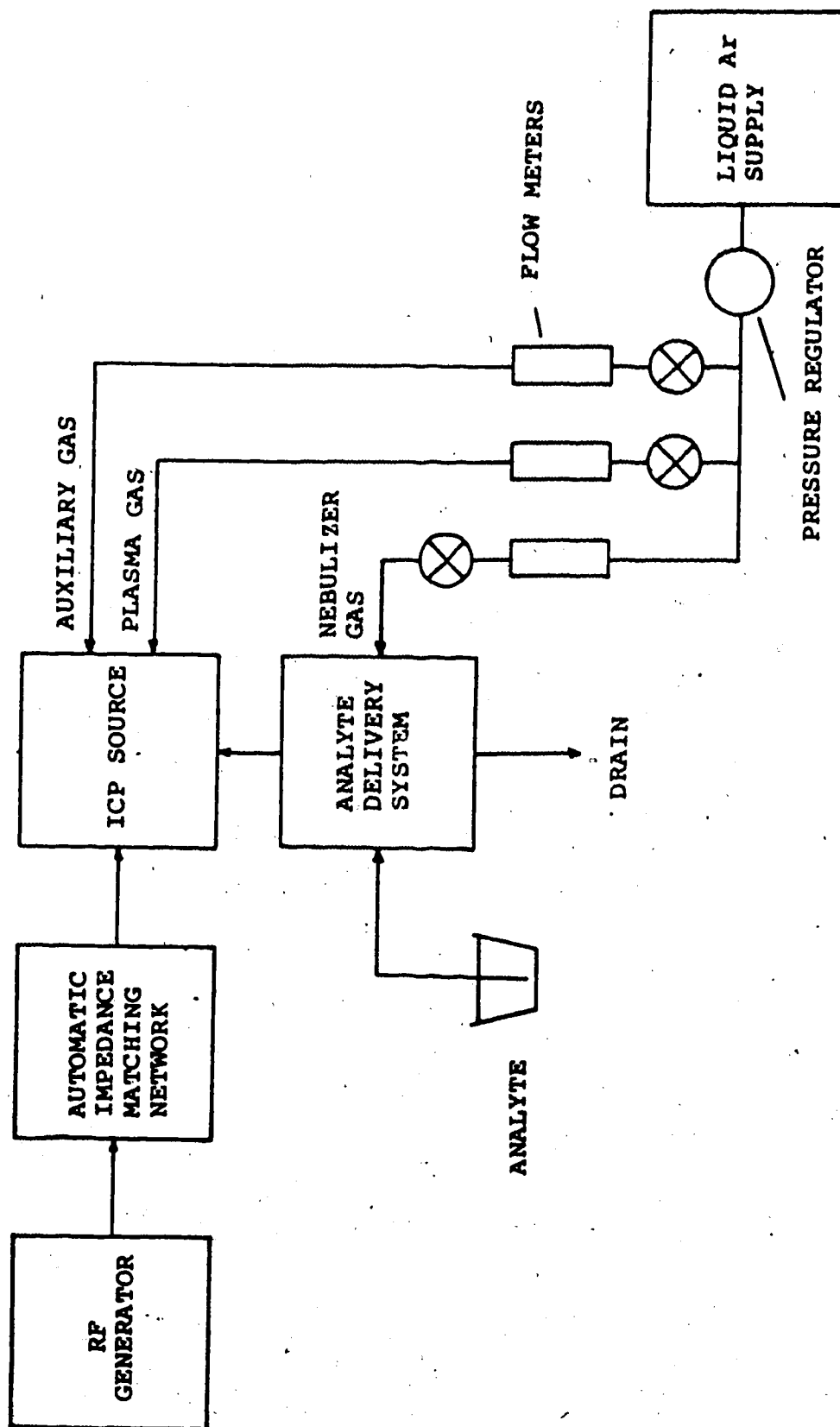


Figure 5. ICP source schematic.

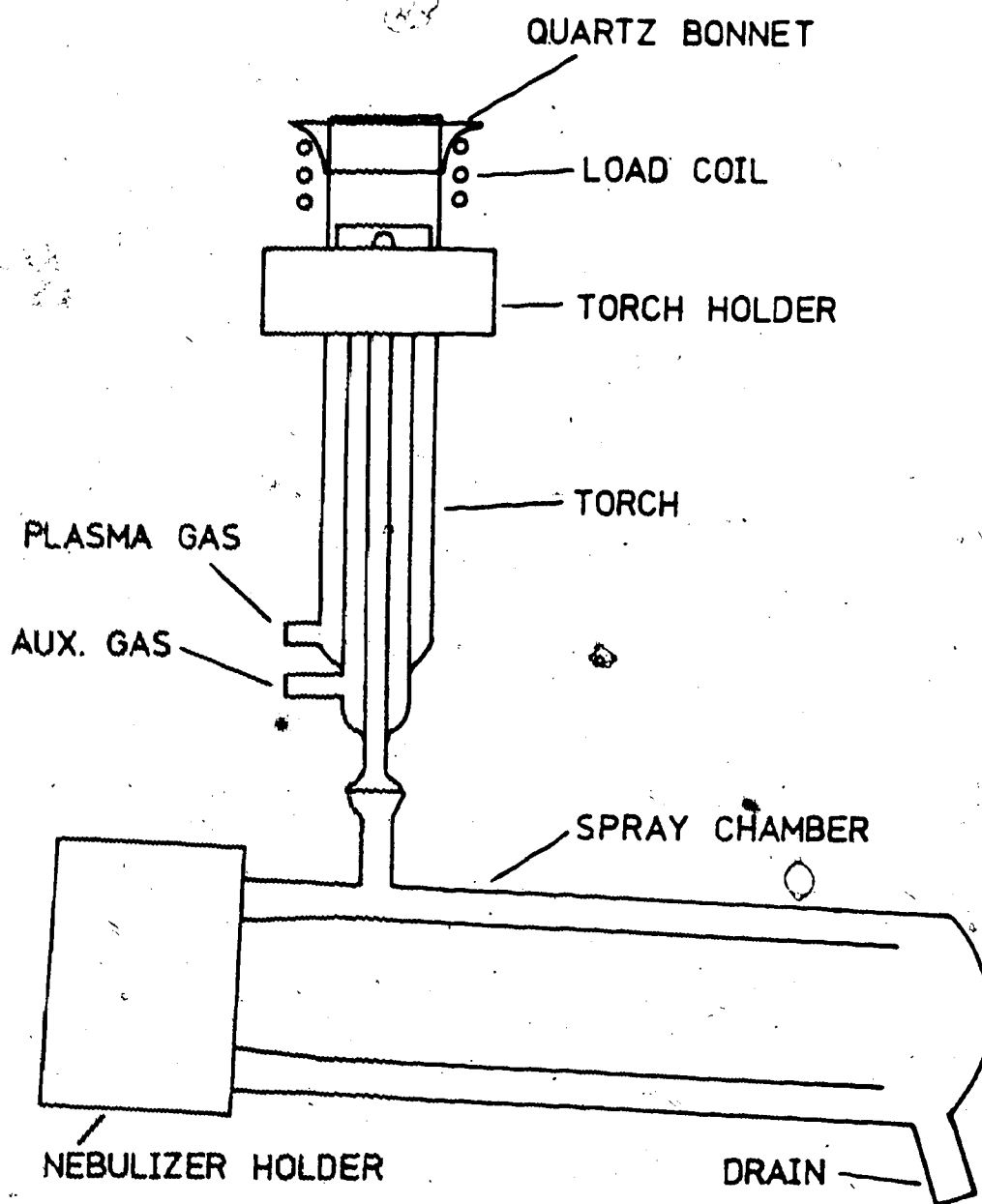


Figure 6. Spray chamber and torch assembly.

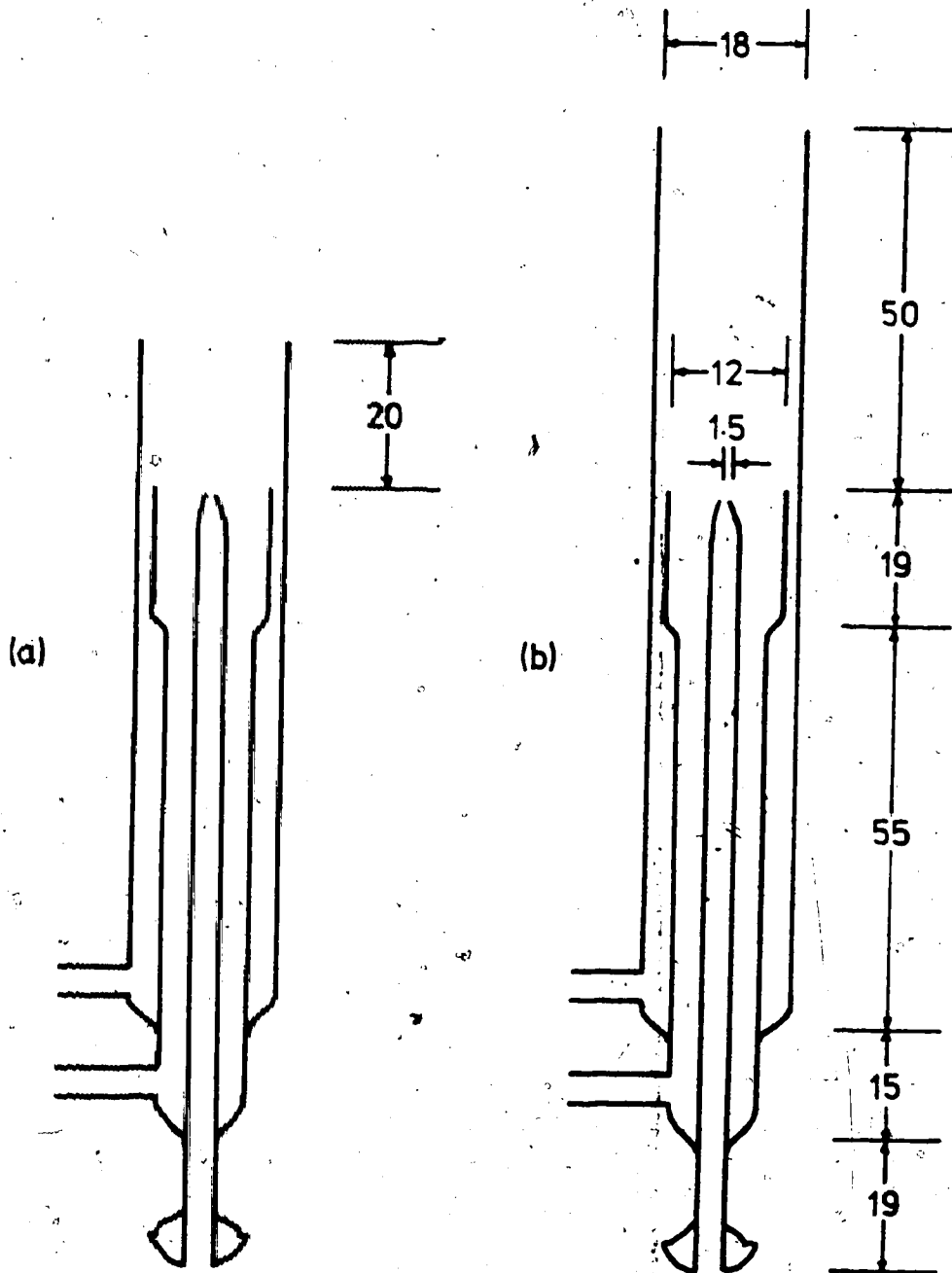


Figure 7. (a) Regular torch, (b) Tall torch. All dimensions in mm. All dimensions identical except where indicated.

The central tube is the injector tube used to feed the analyte aerosol stream into the centre of the plasma. The intermediate tube is the auxiliary gas tube. This provides a low flow rate of argon which serves to lift the plasma slightly and prevent the injector tube tip from melting. The main support or plasma gas is tangentially injected into the base of the outer tube. This gas supply serves not only to support the plasma but is judiciously adjusted to maintain a stable plasma discharge and prevent the outer quartz tube from melting.

Around the top of the torch and over the load coils a quartz bonnet is placed. This prevents arcing from the plasma body to the coils during the ignition procedure.

### 3. Analyte Delivery System

The analyte delivery system, essentially, consists of two parts, the nebulizer and the spray chamber. The nebulizer converts the analyte solution into a fine mist. It is mounted inside the spray chamber. The main function of the spray chamber is to allow via impingement and gravitational settling only the smaller aerosol droplets to reach the plasma. Typically, less than 10% of the nebulised liquid actually reaches the plasma, the majority settling out in the spray chamber. The spray chamber used

for the major part of this work was of the Scott design (51) and is illustrated in Figure 6.

#### 4. Pneumatic Nebulizers

The three pneumatic nebulizers used are illustrated in Figure 8. The glass concentric nebulizer was a model TR-30-A1 supplied by J.E. Meinhard Associates, Santa Ana, California. This nebulizer had a liquid uptake rate of 0.8 ml/min at a gas throughput of 1 l/min, at a -5 cm liquid head. The variable tip cross-flow nebulizer was supplied by Plasma-Therm Inc., Kresson, N.J. The fixed tip cross-flow nebulizer was of a design by Blades (52). Both designs of the cross-flow nebulizer had higher fluid uptake rates than the concentric nebulizer.

All the pneumatic nebulizers were operated, for convenience, under conditions of natural uptake.

#### 5. Ultrasonic Nebulizer

The ultrasonic nebulizer, constructed in this laboratory, was of the batch type and is illustrated in Figure 9. It consists of a glass tube about 4 cm in diameter and about 24 cm in length. At the bottom of the tube an ultrasonic transducer is mounted in a Teflon block. The details of this transducer are provided in Table II.

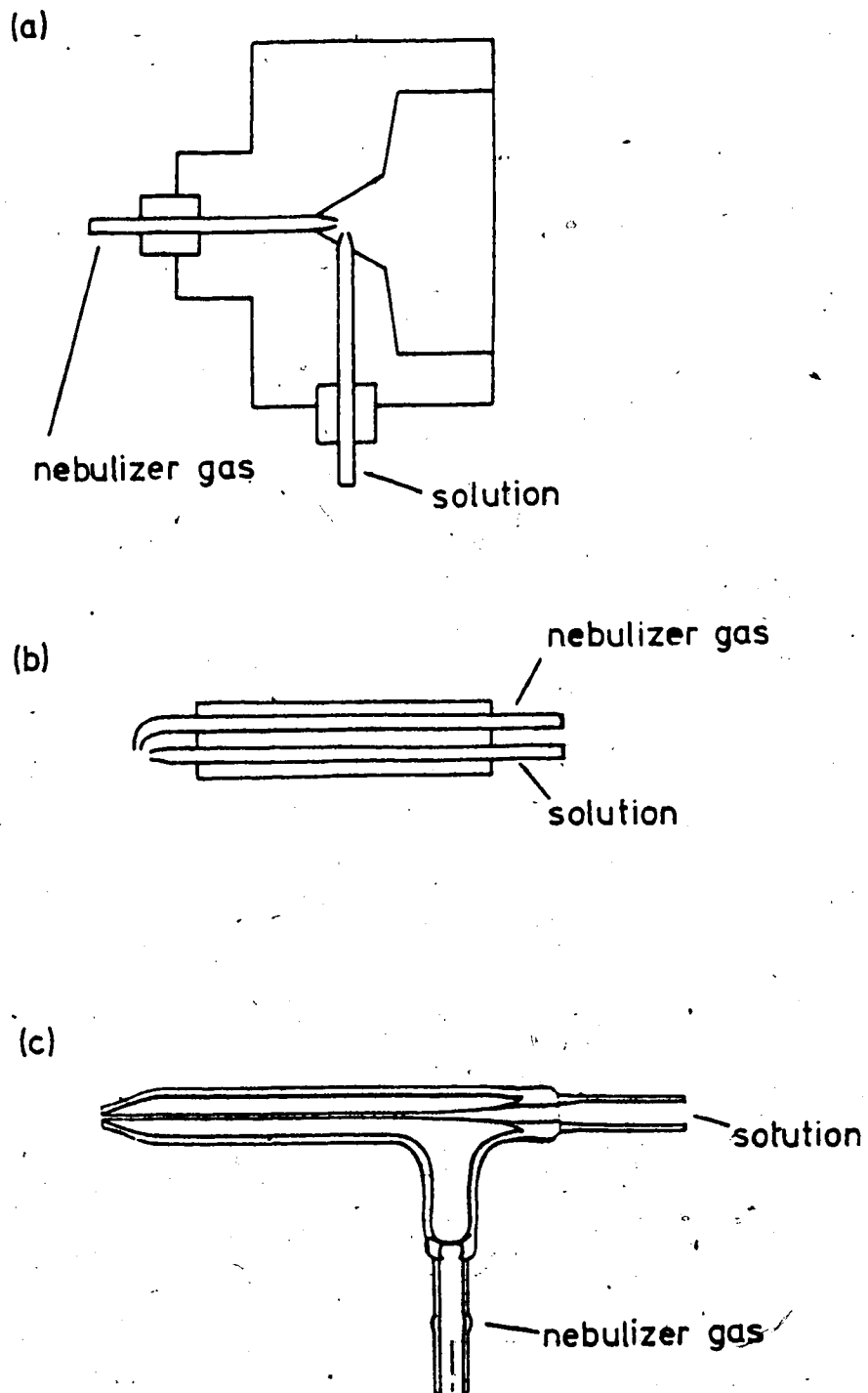


**Figure 8.** Pneumatic nebulizers (a) variable tip cross-flow, (b) fixed tip cross-flow, (c) Meinhard concentric.



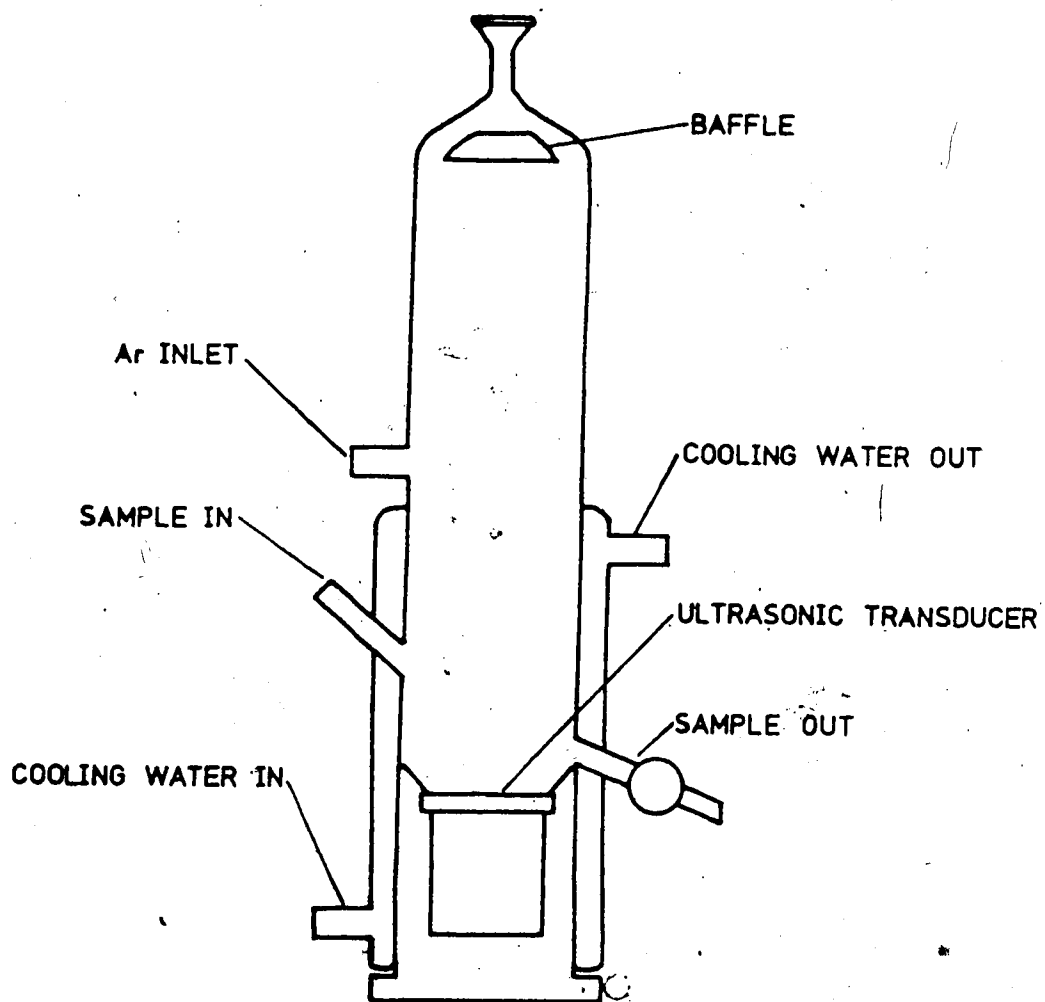


Figure 9. Ultrasonic nebulizer.

TABLE II

## Ultrasonic Transducer Specifications

Manufacturer	Channel Products Inc.
Model	CPMT
Nominal Frequency	1.4 MHz
Drive Voltage (Max.)	50 V (rms)
Drive Current (Max.)	1 A (rms)
Dimensions	1 1/16" dia. × 0.135" thick
Output Mist (Min.)	5 cc/min at 20 W

About 15 ml of analyte are placed in the nebulizer chamber and the inlet side arm is closed with a stopper. Radio frequency power is then applied to the transducer. A fountain of analyte rises above the transducer and a fine mist of analyte droplets is produced. This mist is then swept out of the chamber by a tangential flow of argon carrier gas. The carrier gas enters through a side arm about halfway up the chamber.

The long path length from the transducer to the exit of the chamber and the baffle also ensure that to some degree the larger droplets settle out before the analyte aerosol leaves the chamber.

The transducer was powered by a radio frequency generator (model UNPS-1, Plasma-Therm, Inc.). A forward power of 15 watts was typically used. The generator could be tuned about its nominal frequency of 1.4 MHz, by a fine frequency control. This was adjusted for minimum reflected power, meaning that the frequency of the output power matched exactly the resonant frequency of the transducer.

## 6. Modifications to the Gas Supply Controls

Modifications to the original Plasma-Therm gas flow controls were made to enable accurate measurement of all the gas flow rates.

The auxiliary gas supply was re-routed through the flowmeter originally provided for the nebulizer gas. The nebulizer gas was then controlled using a Matheson 7600 series flowmeter equipped with a 603 tube (0.1 to 4.8 l/min). The needle valve on this flowmeter was positioned at the top (exit) of the rotameter. This arrangement allows accurate flow rate measurements to be made for any nebulizer back-pressure, provided the pressure of the gas fed to the meter is kept constant at its calibration pressure, (50 psi). The configuration of these gas flow controls is shown in Figure 5.

#### 7. Ignition and Running Conditions of the ICP

The ICP discharge is initiated by a momentary high voltage spark, generated by a tesla coil connected to the base of the torch. The operating conditions of the ICP are listed in Table III. These conditions provide a stable and reproducible discharge, with ion line emission intensity peaking at about 17-18 mm above the load coil.

#### B. The Optical System

The ICP source, imaging optics and monochromator were mounted on an optical rail system (Figure 10). The use of this rail system provided precise and accurate imaging of

TABLE III

## Typical Operating Conditions of the ICP

R.F. Power (Incident)	1.5 kW
R.F. Power (Reflected)	<0.03 kW
Plasma gas flow rate	16 l/min
Auxiliary gas flow rate	0.7 l/min
Nebulizer gas flow rate	dependent on nebulizer; optimised for maximum signal intensity (0.7 - 1.5 l/min)

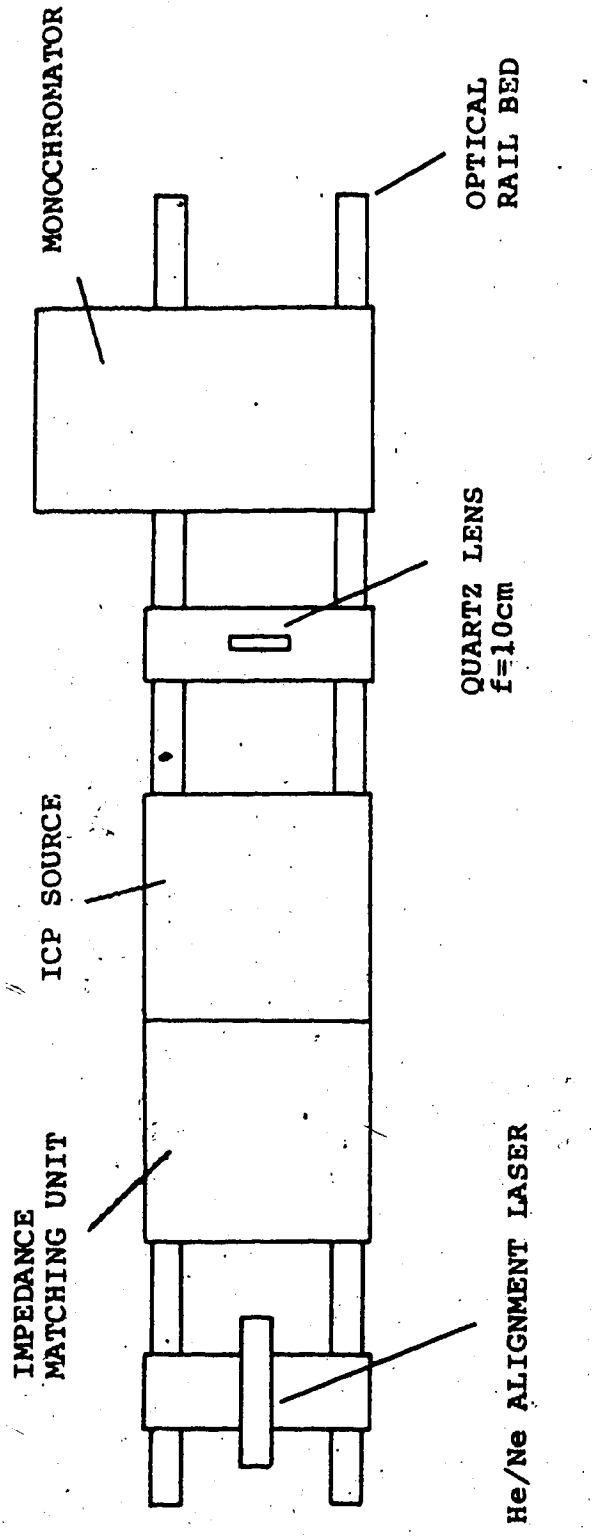


Figure 10. Optical arrangement of spectrometer.

the plasma. For dual monochromator experiments (Chapters IV and VII) a rail bed consisting of four parallel rails was used.

A 2:1 inverted image of the plasma was focussed on the entrance slit of the monochromator by a 10 cm focal length quartz lens. An aperture (3 mm) was placed in front of the entrance slit, thus a 6 mm slice of the plasma was observed.

The monochromators used were exclusively Heath/GCA McPherson EU-270 0.35 m monochromators, the specifications of which are listed in Table IV. The detectors were photomultiplier tubes (RCA, type 1P28) operated at 600 V. The high voltage power supplies for these photomultiplier tubes were model 244 High Voltage Supply, Keithley Instruments Inc. or a model EU-701-30 Heath Photomultiplier Module.

Accurate alignment of the entire optical system was achieved by means of a helium-neon laser also mounted on the optical rail bed.

## C. Data Acquisition System

### 1. Measurement Electronics

The measurement electronics available are illustrated in Figure 11. This arrangement of components was typical for most of the experiments carried out. Where differences

TABLE IV

## Monochromator Specifications

Model	GCA McPherson EU 270
Type	Czerny-Turner
Focal length	0.35 m
Grating	Plane grating 1180 lines per mm, blazed at 250 nm
Reciprocal linear dispersion	Approximately 2.0 nm per mm
Available slit width	Continuously variable between 5 and 2000 micrometers
Typical slit width	10 to 20 micrometers
Available slit height	12 mm
Typical slit height	3 mm (aperture)



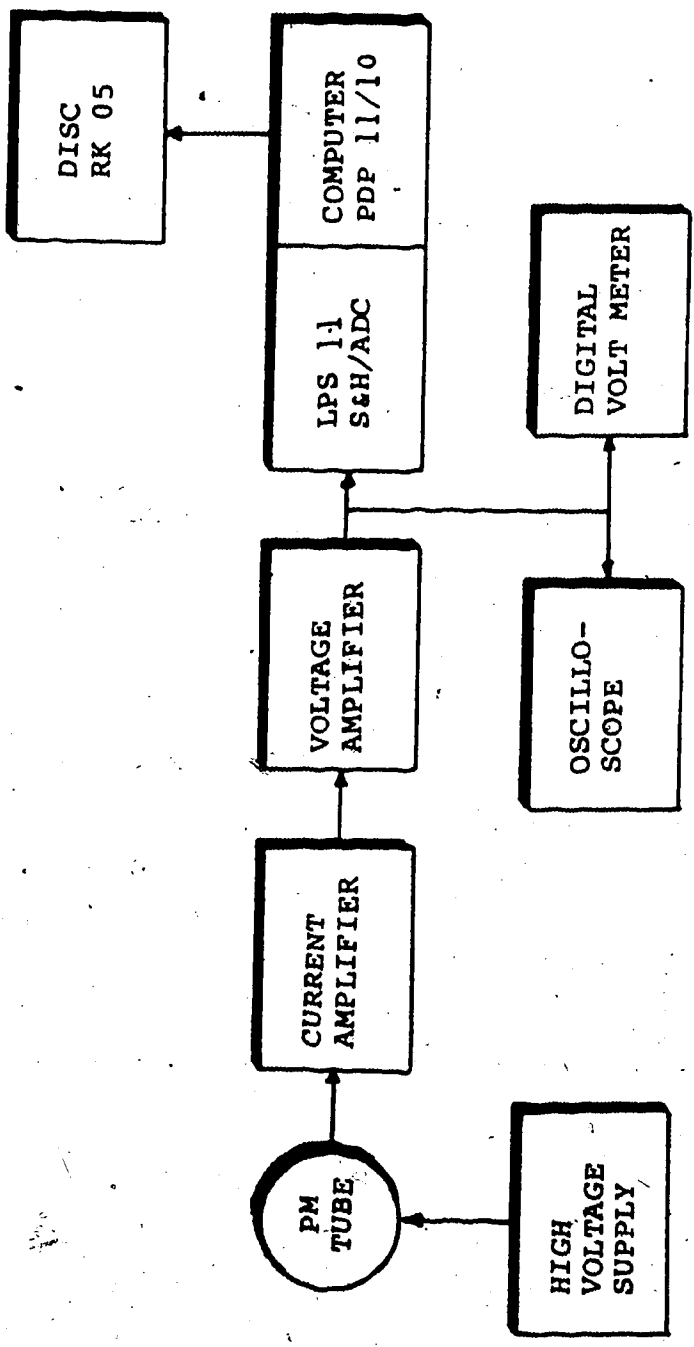


Figure 11. Measurement electronics.

occur these will be pointed out in the separate experimental sections.

The signal from the photomultiplier tube is first amplified by a high speed current amplifier (model 427, Keithly Instruments Inc., Cleveland, Ohio). An additional amplifier (model AM502, Tektronix Inc., Beaverton, Oregon) is used for two purposes: firstly, to convert the 0 to 10 V unipolar output of the current to a  $\pm 5$  V bipolar signal suitable for the analog-to-digital converter of the data acquisition system, secondly, the amplifier provided additional gain and band pass control when required.

The signal, in addition to being acquired by the computer, could simultaneously be monitored by an oscilloscope (model SC502, Tektronix Inc.) and a digital voltmeter (model DM501, Tektronix Inc.). These two monitors prove particularly useful when setting up the initial plasma conditions and when changing the wavelength setting of the monochromator.

## 2. Minicomputer System

The data acquisition system was based on a PDP 11/10 minicomputer system (Digital Equipment Comp., Maynard, Mass.). This computer was equipped with a 16k byte memory core. This core size was sufficient for data acquisition routines

but was inadequate for the larger Fourier transformation programs used to produce the noise power spectra and cross correlation functions. These programs were run on a similar computer system but having a larger, 32k byte core.

The data acquisition computer is equipped with a laboratory peripheral interface (model LPS 11, Digital Equipment Corp.). This unit contains a sample and hold amplifier and a 12 bit successive approximation analog-to-digital converter (ADC). This ADC system can be made to sequentially read any of eight analog input channels. In addition this unit provides the digital I/O ports that were used to control the external sample and hold amplifiers used in experiments requiring the simultaneous monitoring of two channels.

After signal acquisition, data was usually stored on a 1 M byte hard disc storage system (model RK05, Digital Equipment Corp.): Further work up and plotting of these data were carried out on the larger computer system. Plotting of these data, noise power spectra and cross correlation functions were carried out on an incremental plotter (model 130, Zeta Research Inc., Lafayette, California).

### 3. Dual Channel Data Acquisition

For cross-correlation experiments it is necessary to acquire two signals simultaneously. However, the computer data acquisition system even though equipped with a number of analog input channels, can only read them sequentially. This problem was circumvented by the use of two additional external sample and hold amplifiers. These sample and hold amplifiers (model AD582, Analog Devices, Norwood, Mass.) were connected in parallel (Figure 12). Sample or hold signals were provided from bit 0 of the digital output port of the LPS 11 unit. This allowed data to be acquired simultaneously with the two sample and hold amplifiers and then to sequentially read their outputs. The software for controlling and reading the sample and hold amplifiers was written in Macro assembler language and is listed in Appendix C.

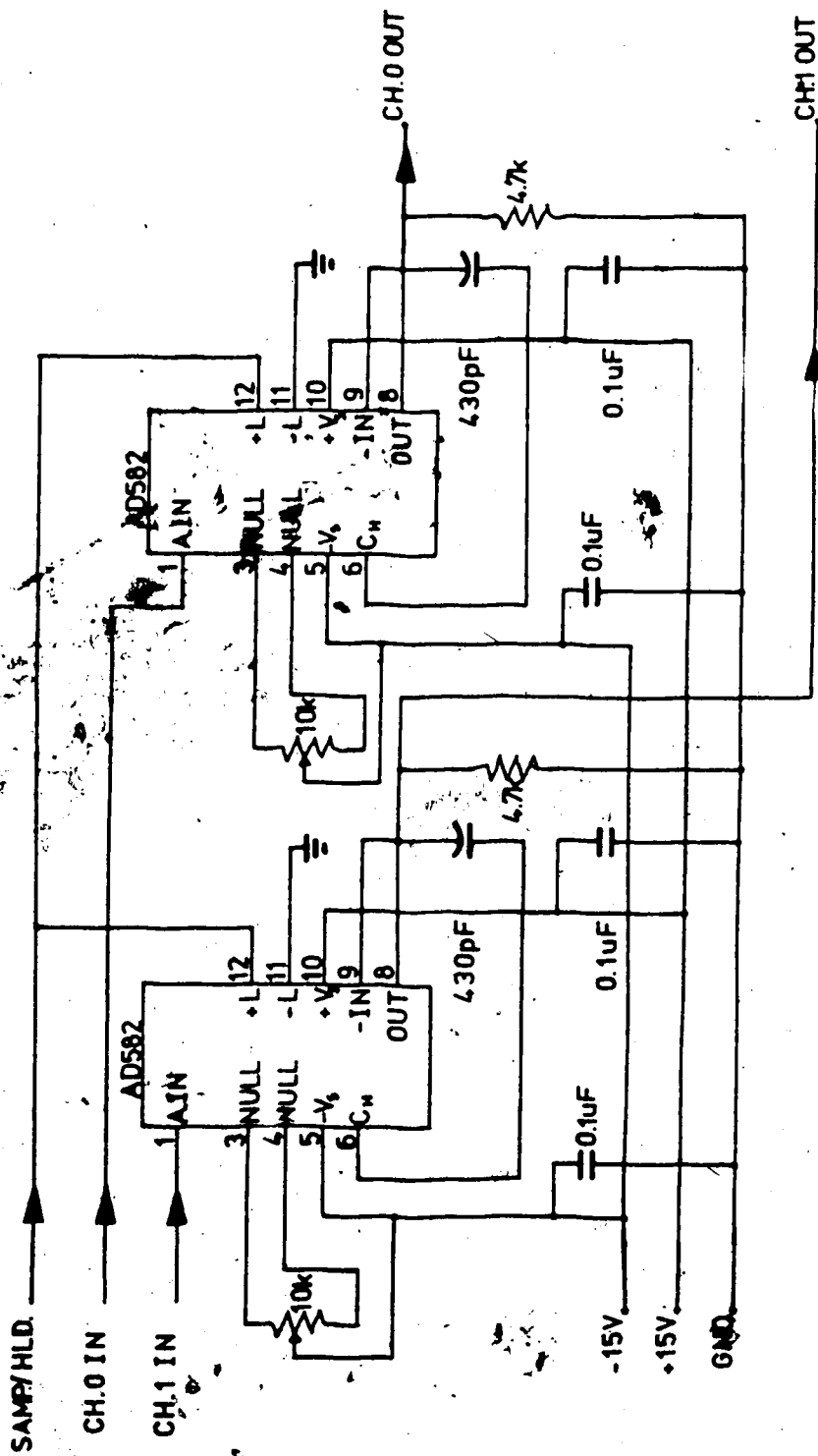


Figure 12. Dual sample and hold amplifiers.

## CHAPTER III

### THE EFFECT OF SAMPLE INTEGRATION PERIOD ON MEASUREMENT PRECISION IN INDUCTIVELY COUPLED PLASMA EMISSION SPECTROMETRY AND RELATED STUDIES

#### A. Introduction

It is often assumed, almost intuitively, that the precision of a measurement can be improved by the increasing signal integration period. However, as was shown in Chapter I, the improvement that can be achieved is dependent on the exact nature of the limiting noise in the system.

The signal-to-noise ratios will improve to the square root of the integration time when the limiting noise possesses a "white" noise power spectrum; such would be the case in a shot noise limited system. If, as in the case of flicker noise domination, the noise power spectrum is  $1/f$  in nature, measurement precision cannot be improved by increasing the signal integration period.

The effect of increasing the integration period from 10 msec to 30 seconds for ICP emission signals of several species will be discussed. The signals studied include CaII (393.3 nm), CdII (214.4 nm) and ArI (415.8 nm) emissions.

Nebulizer type and design have proven critical in determining the precision of ICP analysis. The precision performance of a glass concentric (Meinhard), a variable tip cross-flow and an ultrasonic nebulizer were evaluated as a function of integration time. To assess the role of the nebulizer in determining the precision of ICP emission signals the ArI emission signal was also monitored as a function of integration time. The emission intensity of this line if the nebulizer gas was not flowing would be independent then of the nebulization process. In addition to this experiment an experiment was conducted in which mercury vapor was introduced independently of the nebulizer into the carrier gas stream and the precision of the mercury emission signal measured.

#### B. Experimental

The Plasma-Therm ICP 5000 system, monochromator, photomultiplier tube and electronic measurement system, as described in Chapter II, was used for these experiments.

The amplified signal from the photomultiplier tube was digitised and acquired by the computer data acquisition system. The 12 bit high speed ADC (successive approximation) was clocked at 1 kHz. Precise integration periods ranging from 10 msec to 30 seconds were achieved by summing the

appropriate number of successive conversions. The software for controlling the integrator was written in Macro assembly language and the calling program which also automatically computed the signal-to-noise ratios was written in Fortran IV. These programs are listed in Appendix C. The noise bandwidth of the system, in addition to being controlled by the integration time, was limited by means of the first order low pass filter of the Tektronix amplifiers in all cases the -3dB point was set at 1 kHz.

The signal-to-noise ratios were calculated by dividing the mean of 32 background subtracted signal measurements by their standard deviation. The background signals were obtained by aspirating distilled water and taking the mean of 32 measurements. The background was measured prior to the study of each integration time; the intensity was assumed to remain constant throughout the time of the 32 signal intensity measurements.

The results of these experiments are presented as plots of log signal-to-noise ratio vs log integration time. Figures 13, 14, 15, 16, 17 show the results from a 1 ppm solution of calcium with the concentric nebulizer, variable tip cross-flow and ultrasonic nebulizers, a 50 ppm cadmium solution with the concentric nebulizer, and argon



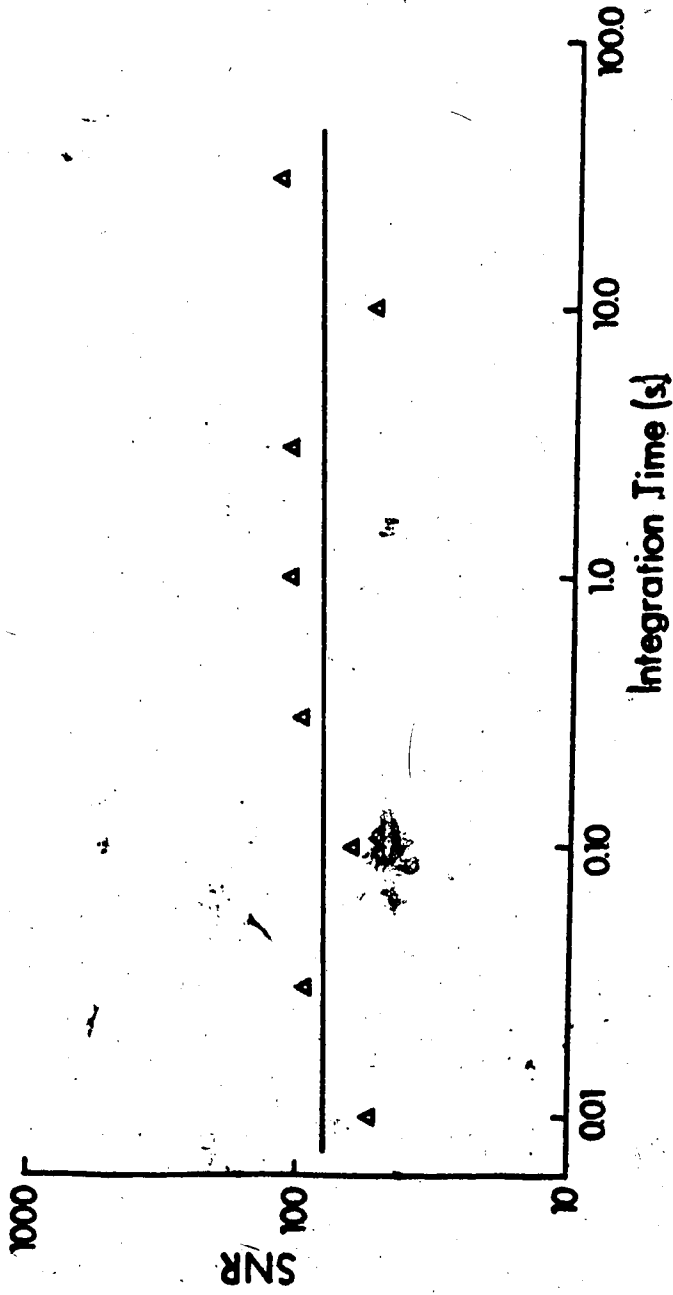


**Figure 13.** Log-log plot of SNR vs integration time for CaII 393.3 nm (1 ppm) using a Meinhard nebulizer.

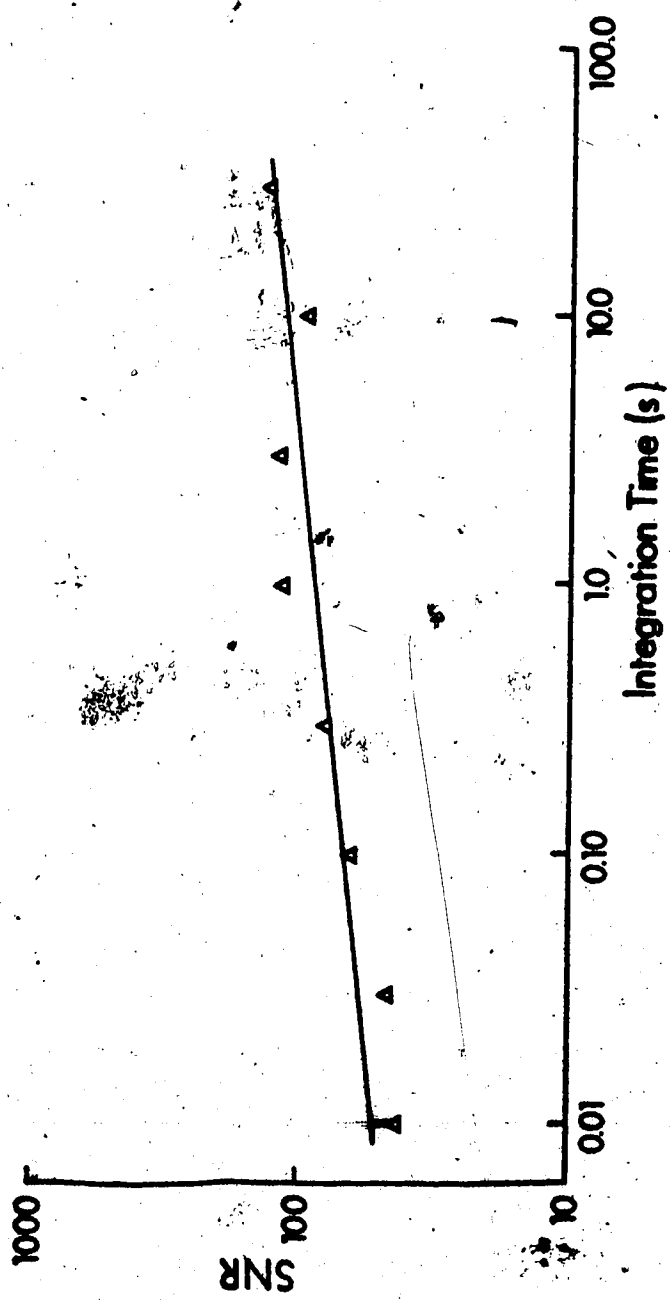


Figure 14. Log-log plot of SNR vs integration time for CaII 393.3 nm using a cross-flow nebulizer.

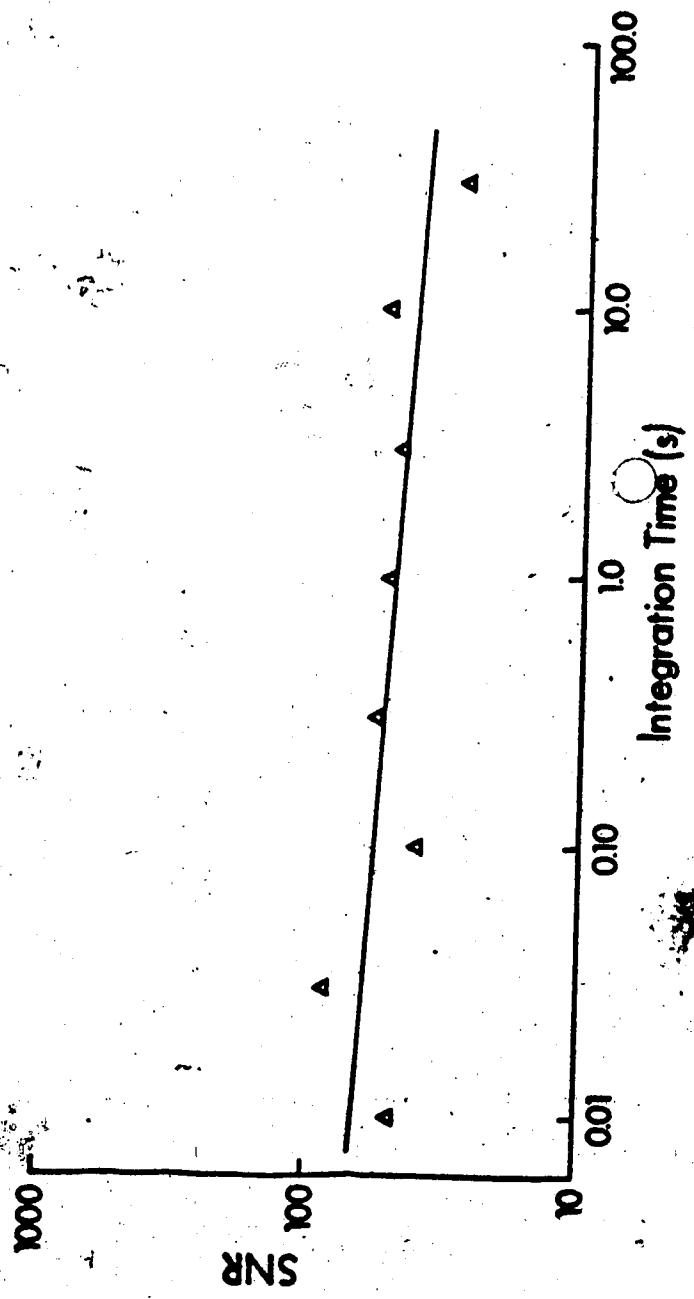
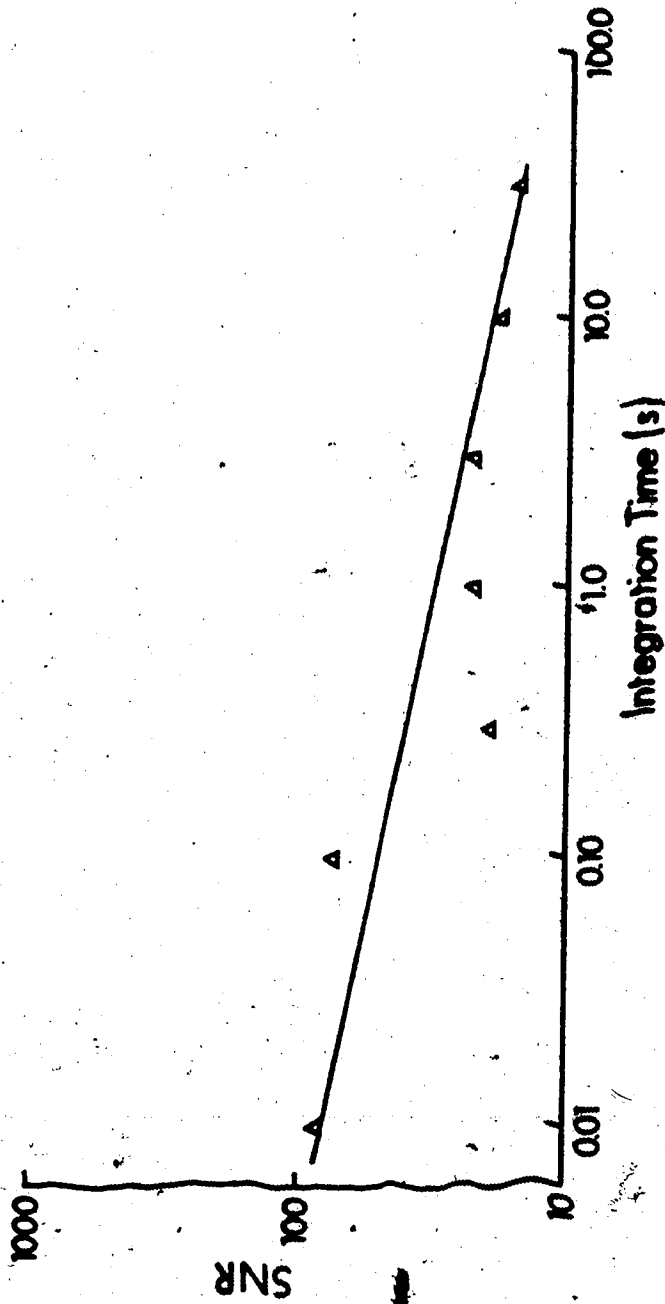


Figure 15. Log-log plot of SNR vs integration time for CdII 214.4 nm (50 ppm) using a Meinhard nebulizer.



**Figure 16.** Log-log plot of SNR vs integration time for CaII 393.3 nm (1 ppm) using an ultrasonic nebulizer.

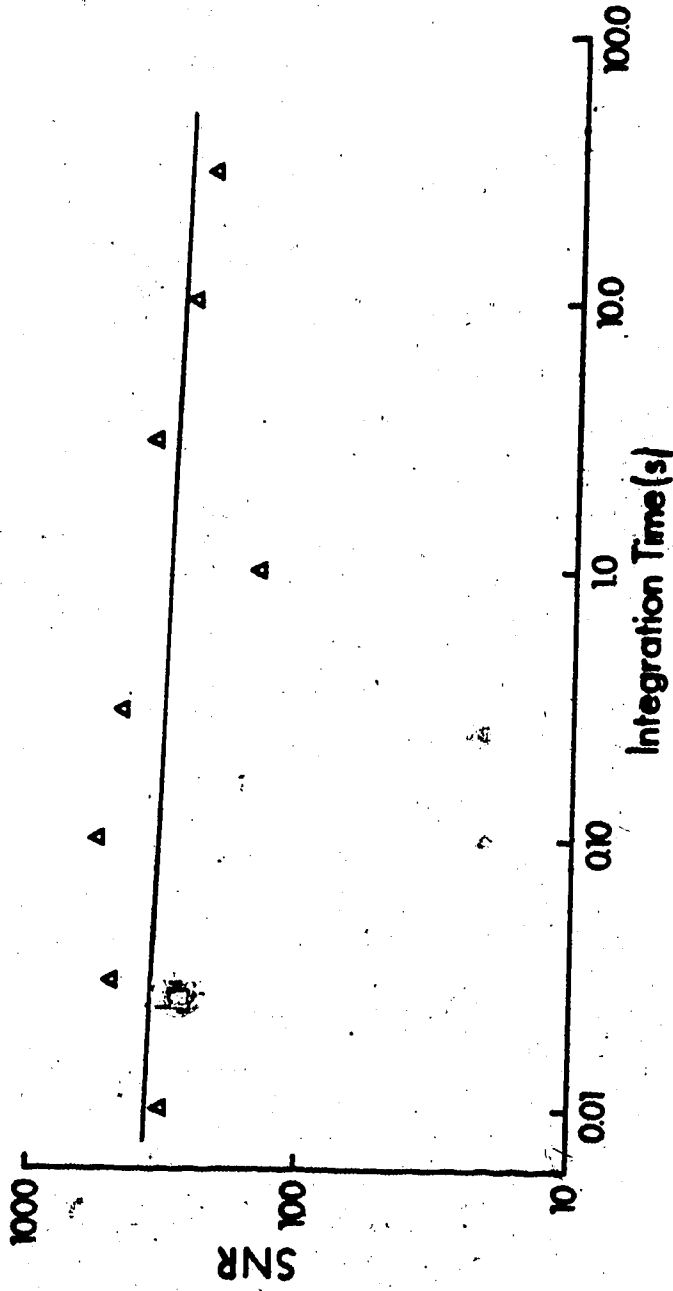



Figure 17. Log-log plot of SNR vs integration time for ArI 415.8 nm.



emission obtained as distilled water was aspirated with the concentric nebuliser.

In attempt to elucidate the relative importance of the nebulisation/transport step in determining the precision, an additional experiment was devised. A device was constructed that allowed mercury vapor to be efficiently mixed with the carrier gas stream, without the use of a nebuliser. This device consisted simply of a coil of glass tubing 1 m in length and 2 cm in diameter. This was packed with glass wool and beads of metallic mercury. Carrier gas flowed through the coil and then directly via the injector tube to the plasma. It was necessary to place the coil in a large beaker of water for thermal stability.

The emission intensity of the HgI (253.7 nm) line when this device was in operation, corresponded closely to that obtained when a 100 ppm solution of mercury was aspirated with the concentric nebuliser. The precision of the results obtained with mercury vapor introduction device and the concentric nebuliser were compared. An integration time of 1 second was used. The signal-to-noise ratios were, again, calculated on the basis of 32 background subtracted measurements. In addition each experiment was repeated, typically ten times, and the results pooled to provide a more reliable result. These results are reproduced in Table V.

TABLE V

Comparison of Mercury Vapor Introduction System and a  
Meinhard Nebulizer Aspirating 100 ppm Mercury Solution

	Mercury Vapor	Meinhard Nebulizer
Signal	$0.1143 \times 10^7$	$0.1107 \times 10^7$
Std. Deviation	$0.217 \times 10^4$	$0.151 \times 10^5$
Background Signal	$0.7461 \times 10^5$	$0.6812 \times 10^5$
Background Std. Deviation	$0.223 \times 10^3$	$0.361 \times 10^3$
SNR	543	75.9

### C. Discussion of Results

The log-log plots of signal-to-noise ratio vs signal integration period for CaII (393.3 nm, 1 ppm) is shown in Figure 13 for the concentric (Meinhard) nebuliser and in Figure 14 for the variable tip cross-flow. For both the concentric and cross-flow nebulisers little, if any, improvement in signal-to-noise ratio is realised in increasing the signal integration period from 10 msec to 30 seconds (3.5 orders). This clearly shows that the emission signal from these two nebulisers possesses a  $1/f^\eta$  noise power spectrum, where  $\eta = 1$ . Similar results were obtained for a number of other species, for instance, the effect of integration time on the signal-to-noise ratio of CdII emission (214.4 nm, 50 ppm) is shown in Figure 15. All these features being clear indication that for signals well removed from the detection limits the dominant noise is source flicker.

In the case of the ultrasonic nebuliser (Figure 16) the trend was for a decrease in signal-to-noise ratio as the integration time was increased. This implies that a severe flicker noise problem exists with this nebuliser and that the low frequency components of the noise are greater than predicted by a  $1/f$  relationship.



The signal-to-noise ratio of the argon emission line (Figure 17) was little affected by increasing the integration time. The indications of this are that while a flicker noise component is associated with the nebulization/aerosol transportation step an additional flicker noise component is associated with the plasma itself. The cause of this is uncertain but may lie in fluctuations in the flow rates of the support gases.

The signal-to-noise ratios obtained from monitoring this argon emission line are in the range 400 to 600, values approximately five times greater than those obtained from nebulized species. These signal-to-noise ratios correspond closely with those obtained in the mercury vapor introduction experiment (see Table V). These values of signal-to-noise ratio reveal the baseline nebulizer independent noise of the ICP system. They represent the maximum signal-to-noise ratios that can be expected from this ICP regardless of what type of nebulizer is being used.

#### D. Conclusions

Several important conclusions can be drawn from these results. Clearly, little is to be gained in ICP emission spectrometry by using long signal integration times and in

fact quite short integration times ( $<1$  sec) may actually be desirable. All these results strongly imply that source flicker noise with approximately a  $1/f$  noise power spectrum limits measurement precision.

It is also apparent that the majority of the flicker noise originates in the nebulization/aerosol transportation steps, although a flicker noise component is also associated with the plasma itself.

True characterization of these noise components requires the measurement of noise power spectra. Such measurements have been carried out and will be described in Chapter IV.

## CHAPTER IV

### NOISE POWER SPECTRA OF OPTICAL AND ACOUSTIC EMISSION SIGNALS FROM THE INDUCTIVELY COUPLED PLASMA

#### A. Introduction

In order to clarify some of the effects noted in Chapter III, noise power spectra of the ICP were measured under different operating conditions and with a variety of nebulizers.

Noise power spectra have proven useful in the characterization of noise encountered in the emission of a number of analytical sources (53-55) and specific studies towards both flame emission (28, 29, 56, 57) and atomic absorption spectrometry (25) have been reported. Noise power spectra may allow identification of noise types, identification of noise sources, and, of course, frequency composition characterization. Intelligent choices of measurement conditions such as signal integration periods or possible modulation frequencies may also be made. Knowledge of noise power spectra may provide sound rationale for future system improvement and the noise power spectra can provide a monitor of effectiveness of such improvements. Finally, noise power spectra can reveal important physical characteristics of a spectral source that may otherwise

go unnoticed.

In this study noise power spectra of optical emission signals from an ICP have been measured. It will be seen that low frequency spectra (0-5 Hz) are very useful for the characterization of nebulizer performance and analyte noise. High frequency spectra (0-500 Hz) reveal structure characteristics of plasma spatial dynamics. Noise power spectra of acoustic emission signals and two channel correlation measurements were also carried out in order to clarify plasma noise characteristics. Our measurements and observations in the 0-500 Hz region expand on those recently reported on by Walden et al. (14).

## B. Experimental

### 1. ICP Operating Conditions

The plasma system was the Plasma-Therm ICP system detailed in Chapter II. The operating conditions are listed in Table III unless otherwise stated. All gas flows are argon.

### 2. Data Acquisition and Bandwidth Control

The optical emission signals after detection by the photomultiplier tube were amplified by means of a current amplifier and an additional voltage amplifier (see Chapter

II).

After amplification the bandwidth of the signal was limited by a low pass filter (model 3343, Krohn-Hite Corporation, Avon, Mass.). This unit has two filters with 8th order Butterworth response. When these filters are cascaded together the combined effect is a filter whose roll-off above the combined -6 dB point is -96 dB/octave.

This high degree of bandwidth control is crucial to obtaining unaliased, and hence, meaningful noise power spectra.

The data was then acquired using the PDP 11/10 data acquisition system. For the 0-500 Hz spectra the sampling rate was 1.4 kHz and the -6 dB point of the Krohn-Hite filter was set at 700 Hz which is also the Nyquist frequency. Without the use of this filter, frequencies higher than the Nyquist frequency would be aliased (folded)

back into the 0-500 Hz region giving spuriously high power information. As shown in Figure 18 the use of the filter reduces aliasing in the 0-500 Hz region to negligible levels. For the 0-5 Hz spectra data were sampled at a rate of 14 Hz and the -6 dB point of the Krohn-Hite filter was set at 7 Hz. The response curve (transfer function) of the filter over this range was similar in shape to that for the 0-500 Hz region.

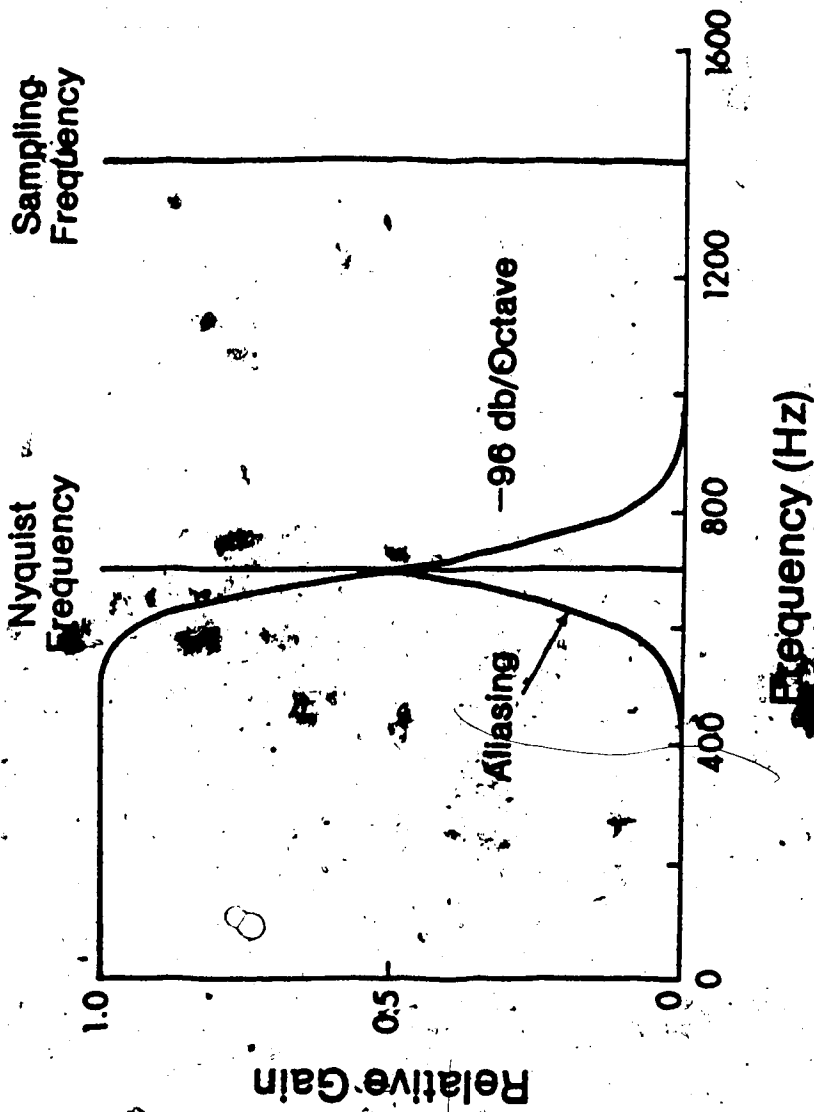


**Figure 18.** Bandwidth control and sampling frequency required in order to minimise aliasing in the 0-500 Hz region.

### 3. Computer Calculation of Noise Power Spectra

For processing, the data were transferred to a larger PDP 11/10 computer system equipped with a 32k byte core.

The steps in the processing of this data to obtain the noise power spectrum are shown in Figure 19. The programs used to acquire the data and produce the noise power spectra are listed in Appendix C. The first step in processing was d.c. level subtraction, to allow efficient Fourier transformation. Apodization (windowing) of the data was carried out to prevent the generation of unwanted side lobes in the transformed data. These side lobes are caused by the convolution of the rectangular data window with the data itself. Apodization consists of multiplying the data with a mathematical function that reduces the effect of the rectangular data window. In this case, the apodization was accomplished using a Gaussian function (factor 10). For more details of this apodization process consult Yuen (58). After apodization the d.c. level was again subtracted to remove any small level introduced. Fourier transformation was then carried out to convert the noise information from the time to the frequency domain. To accomplish this the Fast Fourier Transform algorithm (FFT) was used. Finally, signal averaging was carried out

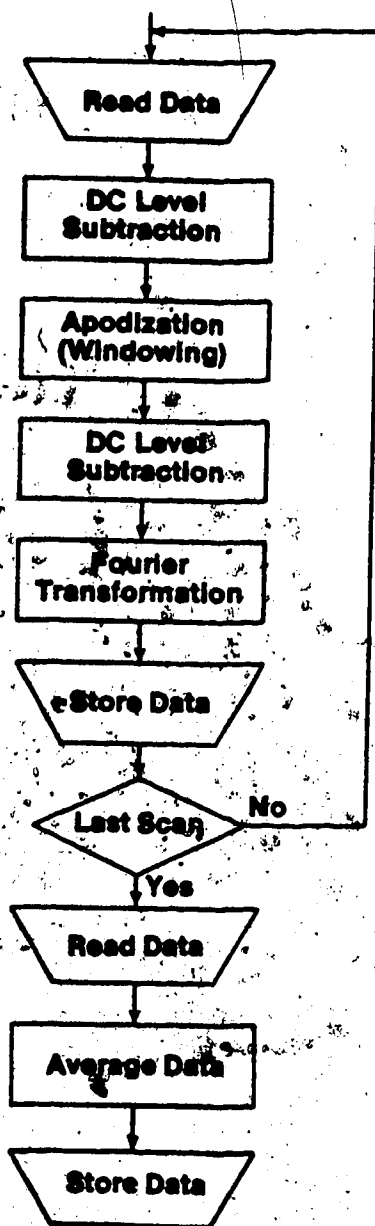


Figure 19. Flow-chart for the calculation of noise power spectra.



in the frequency domain to produce the final noise power data. In every case ten individual sets of transformed data were averaged to provide a more accurate estimate of noise power density. The noise power spectra were then plotted. No attempt was made to calibrate the noise power density axis, as only information of a relative nature was required. However, the units are proportional to  $\text{amps}^2/\text{Hz}$  or  $\text{volts}^2/\text{Hz}$ .

#### C. Low Frequency Noise Power Spectra (0-5 Hz)

It is well established that nebulizer type, adjustment, and running conditions can have a marked effect on overall system performance. The signal levels, standard deviations, and signal-to-noise ratios for CaII 393.3 (1 ppm) obtained using four different nebulisers, at the time when the noise power spectra were obtained, are listed in Table VI. In each case the integration time was 1 sec and the standard deviations are based on 32 replicate measurements. In order of best signal-to-noise ratio performance the nebulizers rank glass concentric first followed by the fixed tip cross-flow, variable tip cross-flow with the ultrasonic last. However, other than this fact, the signal-to-noise ratio provides no real guide to the source of the different behaviour or dir-

TABLE VI

Signal-to-Noise Ratios for CaII 393.3 nm (1 ppm)

<u>Nebulizer</u>	<u>Signal</u>	<u><math>\sigma</math></u>	<u>S/<math>\sigma</math></u>
Glass Concentric	14.9	0.11	134
Fixed Tip Cross-Flow	21.8	0.25	90
Variable Tip Cross-Flow	22.9	0.34	72
Ultrasonic	30.3	1.06	30

actions for improvement.

Noise power spectra (0-5 Hz) for these same nebulizers are shown in Figure 20. In each case the signal monitored was CaII 393.3 (1 ppm). All ordinates have the same scale. Interesting and significant differences between these nebulizers can be assessed by referring to these noise power spectra. The two cross-flows have generally similar spectra, with noise power increasing approximately linearly as one moves from 5 Hz towards 0 Hz with a strong increase near 0 Hz. However, the fixed tip cross flow clearly has generally reduced noise level at all frequencies when compared to the variable tip cross-flow. The fixed tip cross-flow was constructed in this laboratory and consists of two glass capillary tubes epoxied in a fixed cross-flow configuration (Figure 8). This provides a more stable arrangement than the adjustable cross-flow. The adjustable cross-flow was the Plasma Therm unit based on the original design of Kniseley et al: (46) (also illustrated in Figure 8). Thus the fixed tip arrangement for a cross-flow nebulizer seems to be an improvement and several workers are developing cross-flow nebulizers with very rigid tip alignment (48,49).

The glass concentric nebulizer (Meinhard) has a very clean noise power spectrum with only a weak (relative to

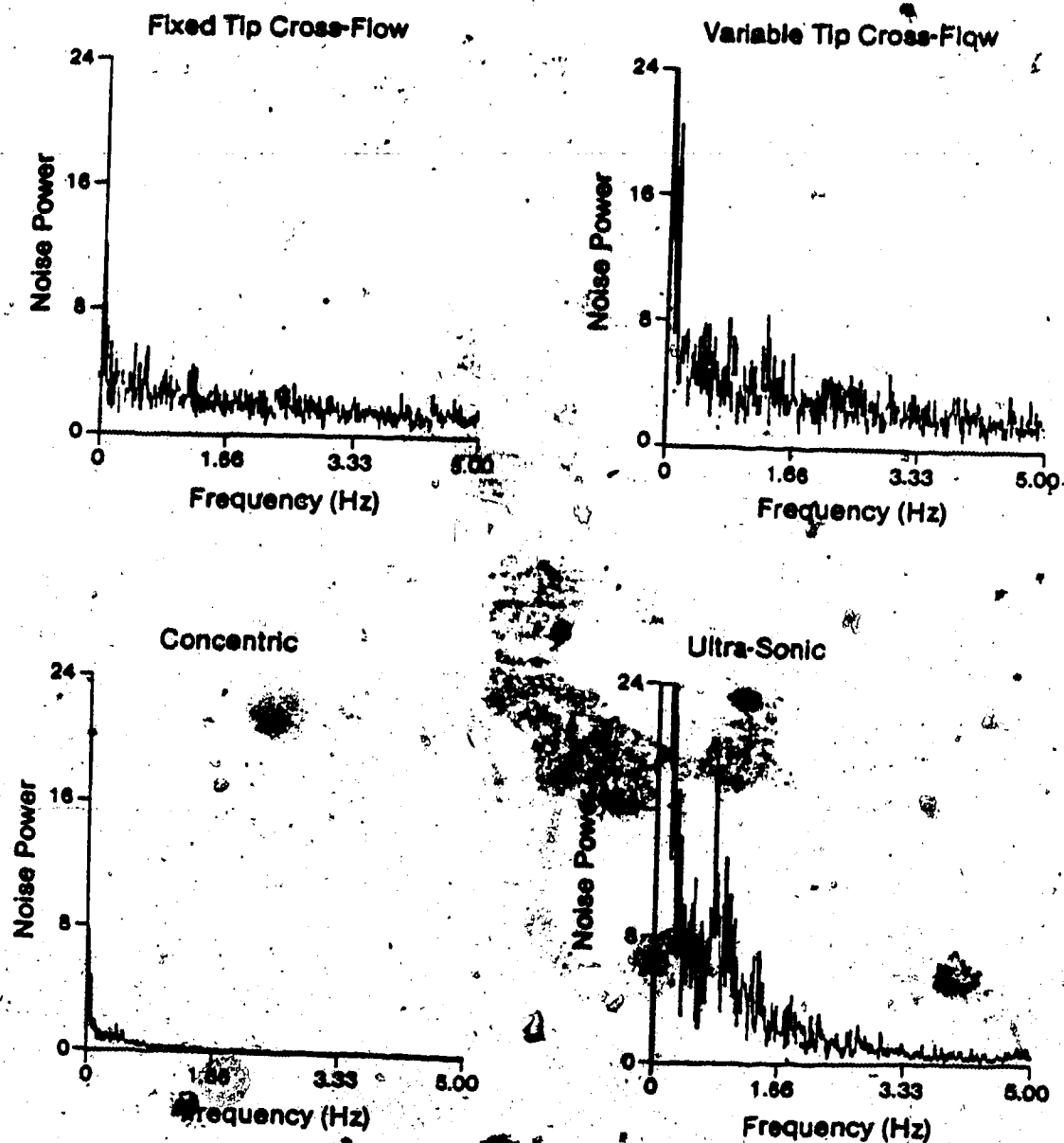


Figure 20. Low frequency (0-5 Hz) noise power spectra of the CaII 393.3 nm (1 ppm) optical emission signal using four different nebulizers.

the other nebulizers)  $1/f$  component below about 1 Hz. The ultrasonic nebulizer, on the other hand, has a complex and relative intense noise power spectrum. The ultrasonic nebulizer was the vertical design of our own construction (Figure 9) and used without desolvation. For this ultrasonic nebulizer the low frequency components in the noise power spectrum are intense and a strong  $1/f$  dependence is observed. In addition a peak in the noise power spectrum occurs at about 1 Hz and it is felt that it results from the rise and collapse of the fountain of analyte above the transducer, which was observed to occur at about this frequency. It is interesting to note that the ultrasonic nebulizer actually exhibits lower noise power levels in the 2.5 to 5 Hz region than either of the cross flow nebulisers. If a unit designed to control or eliminate excessive solution turbulence was employed, its signal-to-noise ratio performance might well be improved over that of the cross-flows.

The effect of analyte concentration on the low frequency noise power spectrum is illustrated in Figure 21. The overall intensity of the noise power spectrum depends on analyte concentration (i.e. signal level) and an order of magnitude increase in concentration is accompanied by approximately a two order magnitude increase in noise

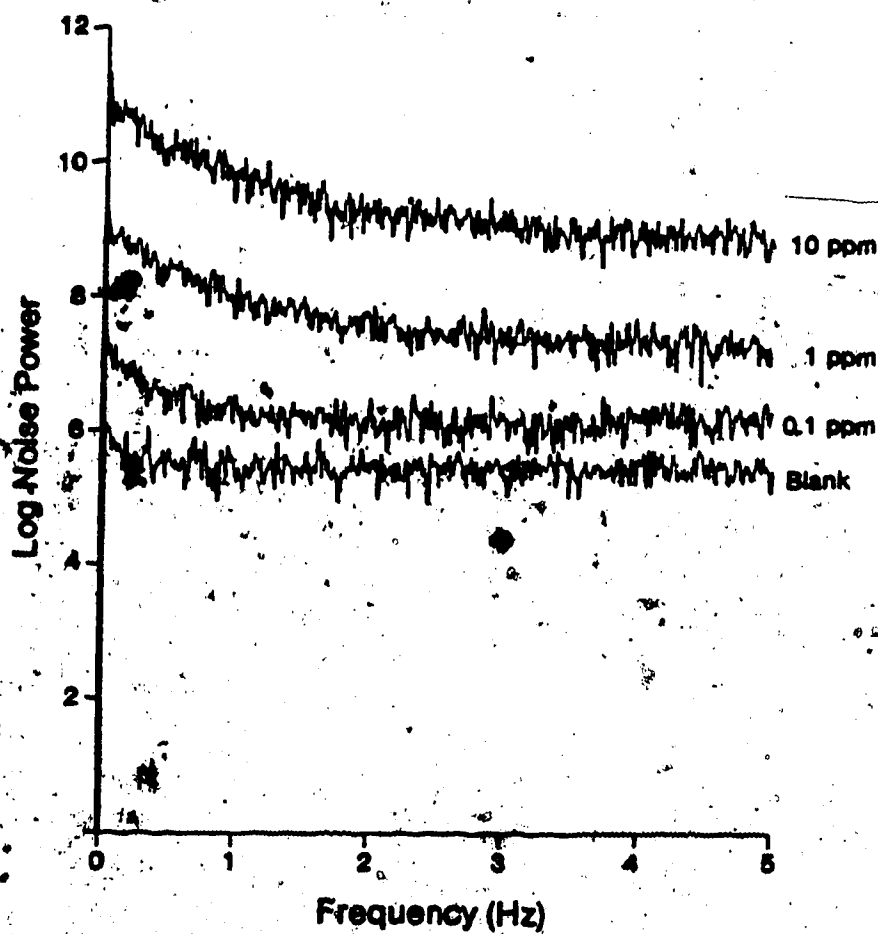


Figure 21. Effect of analyte concentration (CaII, 393.3 nm) on the 0-5 Hz region noise power spectrum using a Meinhard nebulizer.

power (i.e. one order of magnitude in noise amplitude). Note also the rather strong increase in the relative importance of noise frequencies below about 2 Hz as the concentration of analyte increases, all consistent with the conclusion that analyte flicker is the dominant noise. It is interesting to note that Figure 21 is generally similar to Figure 4 of Bower and Ingle (25) which was obtained for atomic absorption measurements. Likewise, their conclusion, based on the nature of these noise power spectra, that there is little merit in integrating such signals for longer than about 10 sec is also valid for ICP signals and in fact, data presented in Chapter III illustrates that integration periods of 1 second or less will normally result in as good signal-to-noise ratio as can be expected.

#### D. High Frequency Noise Power Spectra (0-500 Hz)

For the most part, ICP emission signals have not been observed with wide bandwidth measurement systems. With normal solution sample introduction using standard nebulizers signals are typically integrated for 1 to 30 sec. However, certain ICP measurements require wide bandwidth measurement systems. In this laboratory several sample introduction systems based on direct sample insertion

(59), laser vaporization (60) and electrothermal vaporization (61) all generate transient signal plumes which, for basic investigation, must be time resolved and hence observed with measurement electronics considerably faster than the standard integration systems. In other laboratories, atomic fluorescence measurements (62,63) have been carried out using ICP's and the choice of a modulation frequency requires a knowledge of the ICP noise features at higher frequencies. Finally, in this laboratory work has been carried out in coupling an ICP source to a UV-VIS Fourier transform spectrometer (64) and this system requires that the ICP emission signals be observed with measurement system bandwidths ranging from 0 to 20 kHz. Thus, from these points of view and also from fundamental interest a study was carried out of the noise power spectra of the ICP at higher frequencies than might normally be thought of as important or of interest.

One of our first noise power spectra in the region 0-500 Hz is shown in Figure 22. The signal observed was CaII 393.3 nm (1 ppm). In addition to the power line features which are always present to varying degrees, a somewhat broad but prominent noise feature is seen at about 325 Hz in an otherwise relatively flat noise power spectrum. This feature was also observed by Walden et al. (14) but



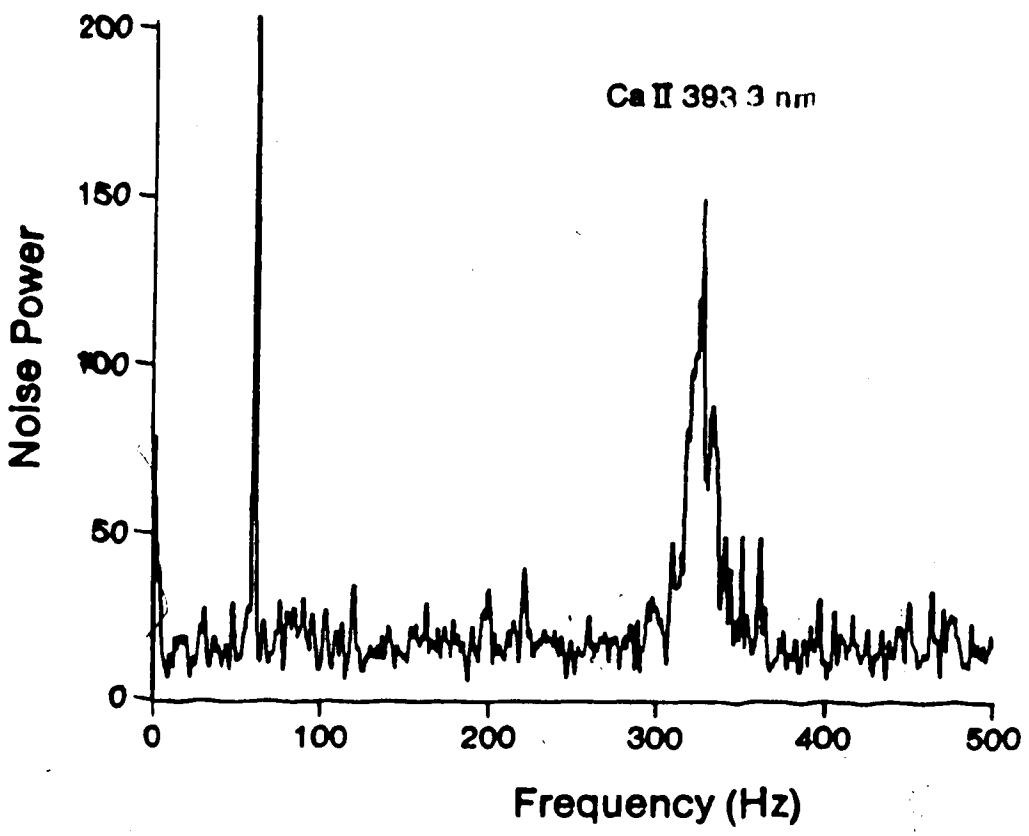


Figure 22. Noise power spectrum (0-500 Hz) of the CaII 393.3 nm optical emission signal. Meinhard nebulizer.

few details were presented about its nature. Preliminary investigation of the noise power spectra at bandwidths up to 2.5 kHz (5 kHz sampling rate) did not reveal any other interesting features and efforts were concentrated on clarification of the 0-500 Hz region.

The effect of power on the frequency and intensity of this noise feature is shown in Figure 23. The frequency position of the noise peak is almost linearly dependent on power as shown in Figure 24. The effect of coolant flow rate on peak frequency is shown in Figure 25.

Increasing the coolant flow rate from 15 to 25 L/min at first causes the peak to shift to higher frequencies, pass through a maximum frequency position and then shift to lower frequencies as the coolant flow rate is further increased.

Over the course of several weeks of experiments two characteristic peaks were often observed in the 0-500 Hz region. A typical spectrum is shown in Figure 26a. The upper peak was always twice the frequency of the lower peak. Similar noise power spectra were observed for other emitting species such as CdII 214.6 nm (Figure 26b) and ArI 415.9 nm (Figure 26c). Also, overall, the absolute and relative intensities of these peaks in the noise power spectra were not particularly reproducible from experiment

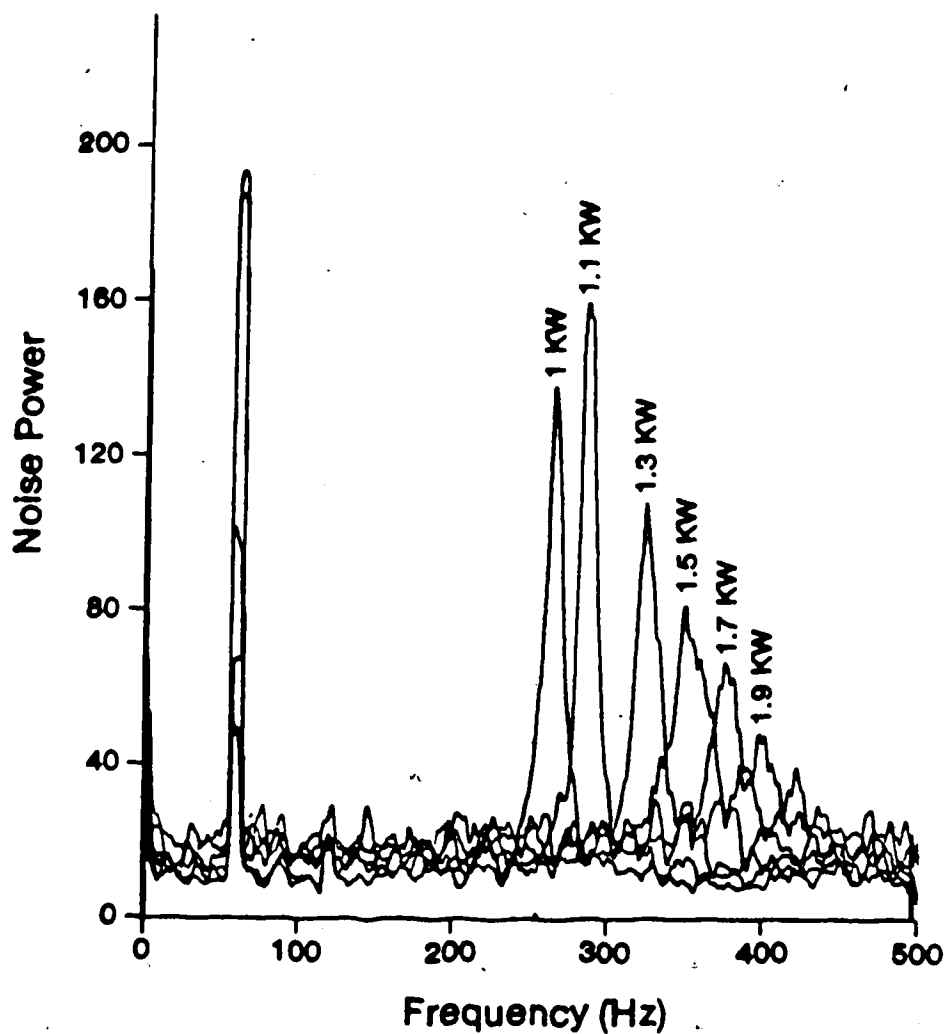


Figure 23. Effect of plasma power (1 kw - 1.9 kw) on the noise power spectrum of the CaII 393.3 nm optical emission signal. Meinhard nebulizer.

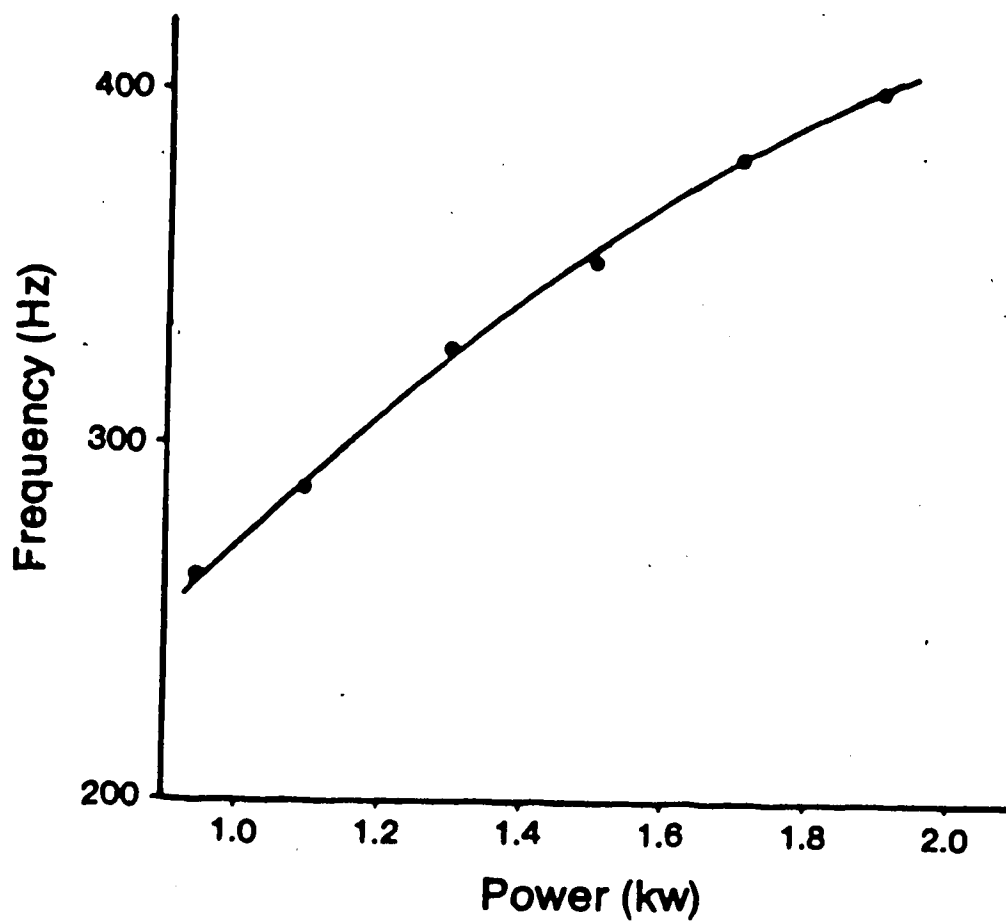


Figure 24. Plot of noise feature frequency as a function of power.

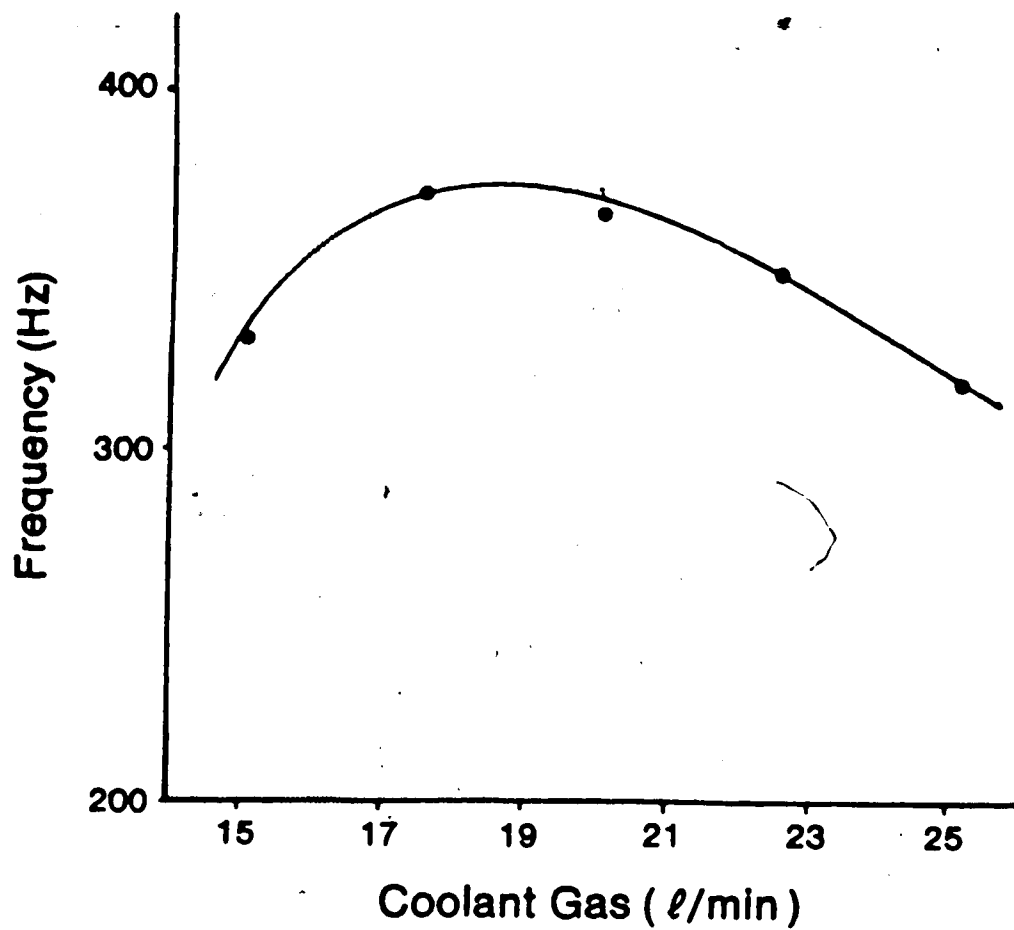


Figure 25. Plot of noise feature frequency as a function of coolant gas flow rate.

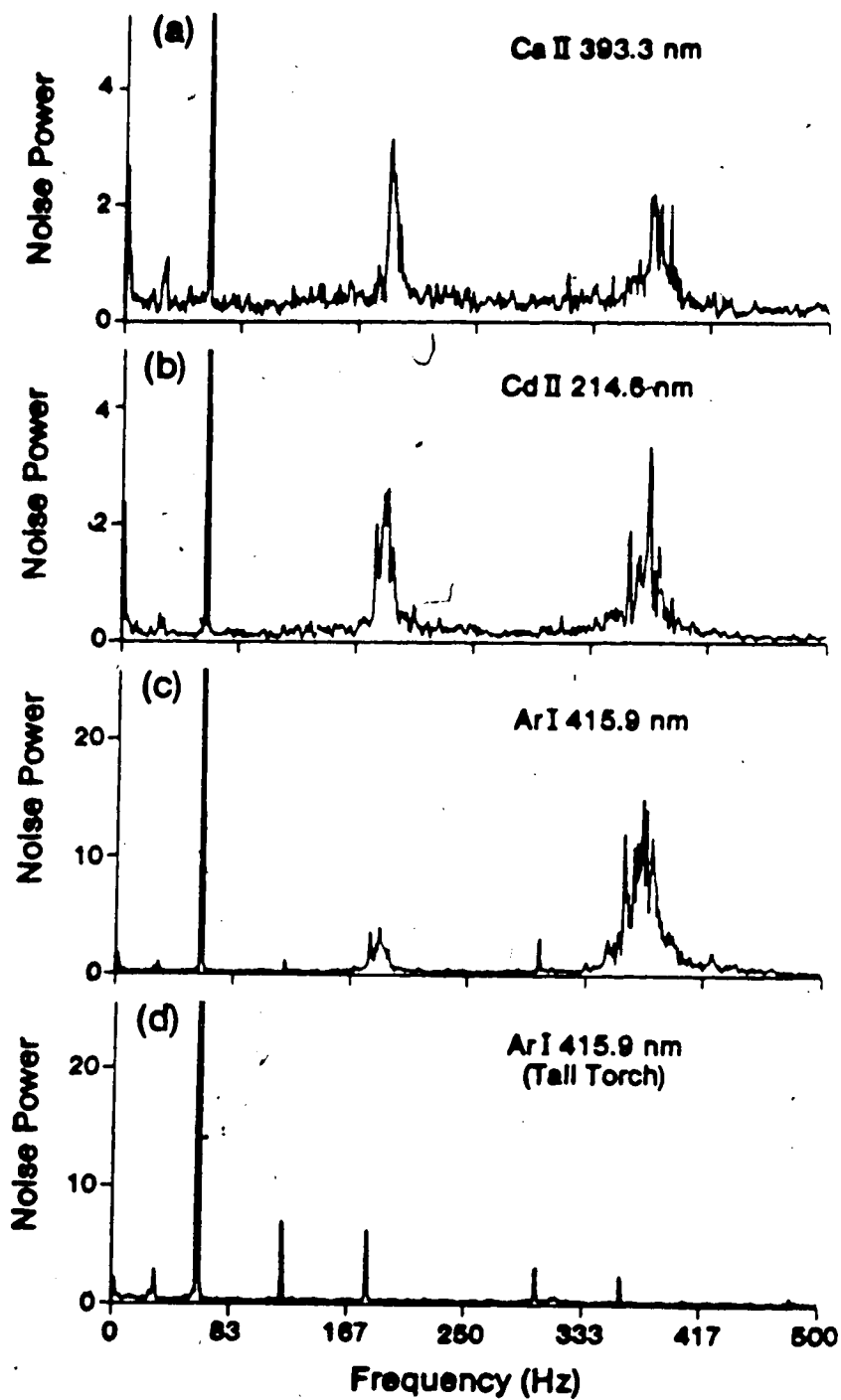


Figure 26. Typical ICP noise power spectra in the 0-500 Hz bandwidth. Meinhard nebulizer.

to experiment. These peaks were present irrespective of the nebulisation system used. Finally, an important observation was the complete disappearance of these features when a tall torch (see Figure 7) was used and emission observed, at normal heights, through the extended tube (Figure 26d).

It was felt at this point that some aspect of plasma gas dynamics was responsible for these noise power spectrum features and characteristics. The most reasonable explanation centered on rotation of a slightly asymmetric plasma discharge and that the asymmetry was primarily induced by air entrainment as indicated by the "tall torch" experiment. The lower frequency was that due to the fundamental frequency of plasma rotation (about 200 Hz in Figure 26). Since the central vertical axis of the plasma discharge is imaged on the monochromator any asymmetry in the discharge would also have a strong second harmonic component as the discharge rotates, the asymmetry being viewed twice for each rotation of the discharge. This also leads one to conclude that the absolute and relative intensities of these features in the noise power spectrum will be highly dependent on the spatial region of the plasma actually observed. Thus, lens focal position, depth of discharge viewed, wavelength of observation

(chromatic aberation) and lateral viewing position will all affect, to some extent the nature of the noise power spectrum. This is shown in Figures 27 and 28 for lens focal position and lens lateral position. Thus great care should be exercised in making any particular conclusions about the intensities of these features.

One other possible explanation of the presence of these peaks may have been acoustic resonances in the torch. Calculations based on the well-known organ pipe formula reveal that the very lowest frequency that gas could resonate in a torch, of the dimensions used, would be about 800 Hz. These calculations agree with those of Walden (14) who also rejected the possibility that acoustic resonances are responsible for the peaks.

#### E. Acoustic Emission Signals

The plasma discharge is a good acoustic transducer and power modulated plasma discharges have actually been used as loudspeakers. Thus it was felt that the acoustic emission signal from the ICP discharge should be studied for noise features. Using a simple electret microphone (Archer 270/092A) (see Figure 29) the noise power spectrum of the acoustic signal emitted by the ICP was measured and is shown in Figure 30a. Now only a single peak is observed



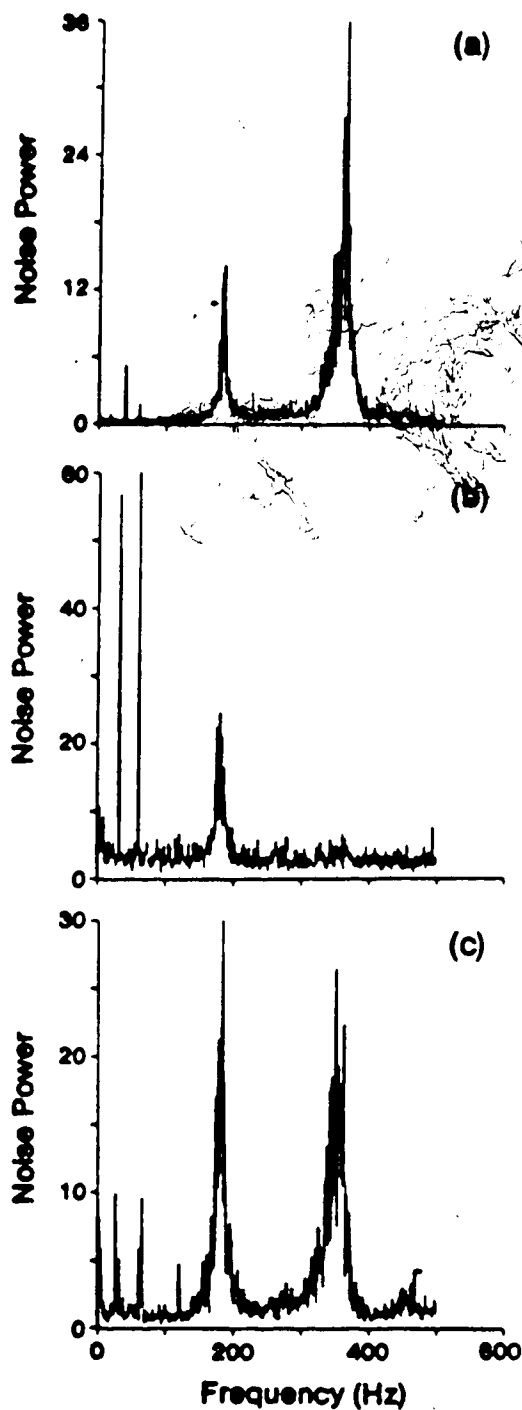


Figure 27. The effect of lens lateral position on noise power spectra. (b) central vertical axis, (a) 4 mm left displacement and (c) 4 mm right displacement. NO band head.

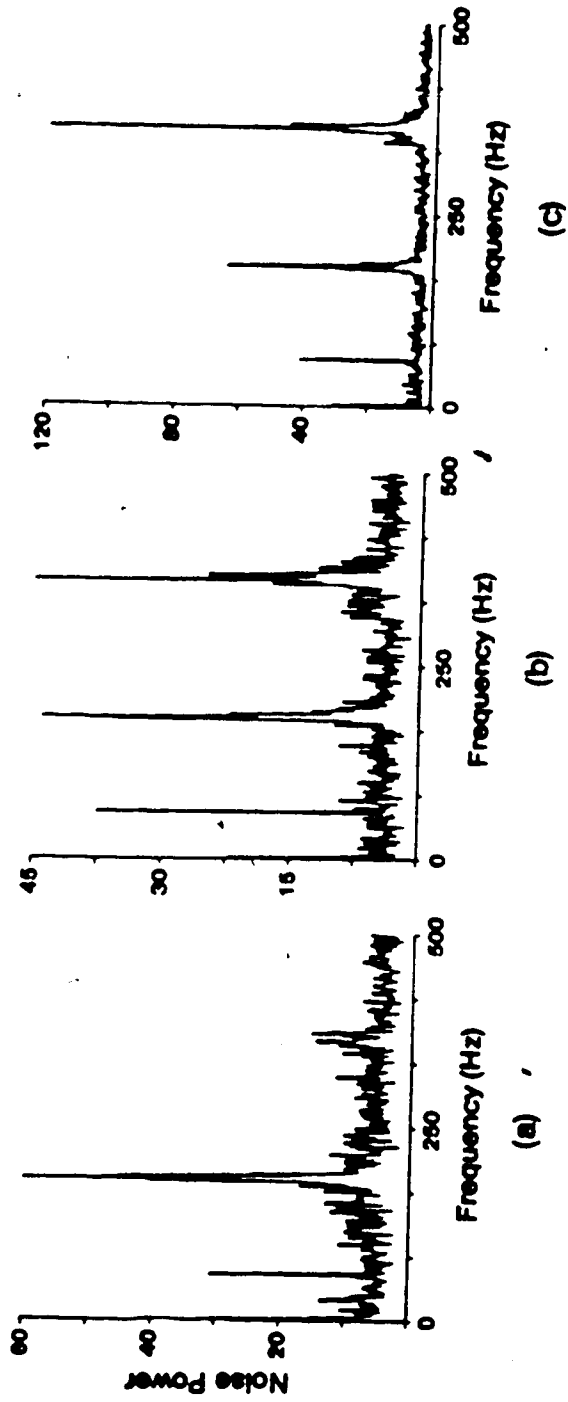


Figure 28. The effect of lens focal position on noise power spectra. (b) sharp visual focus, (a) 4 mm displacement towards plasma and (c) 4 mm displacement towards monochromator. CaII 393.3 nm (1 ppm).

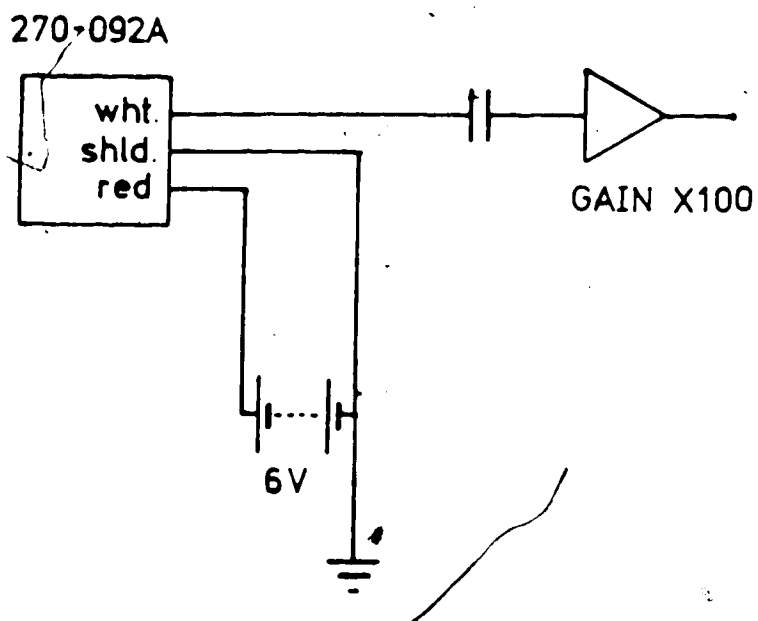


Figure 29. Microphone circuit used for acoustic measurements.

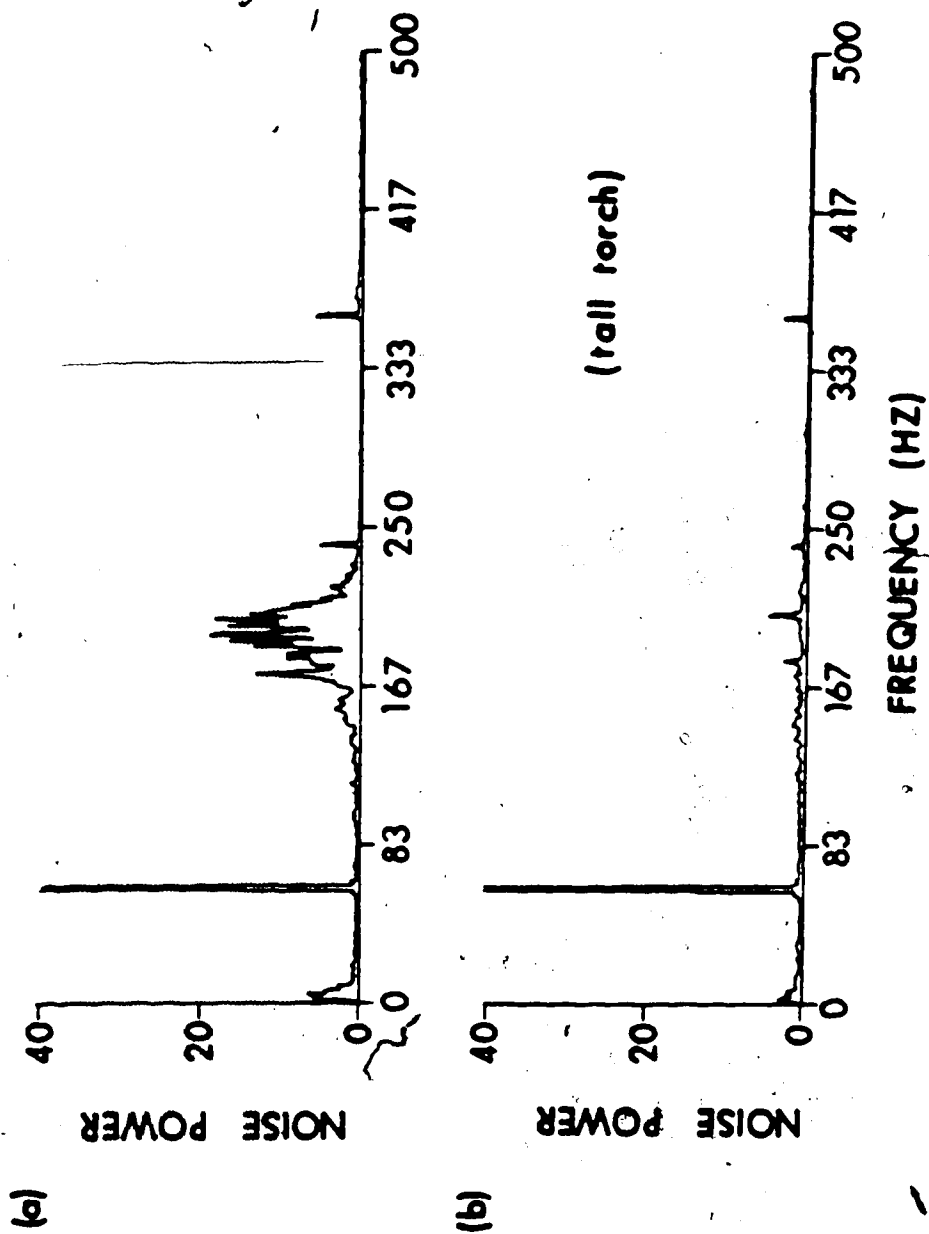


Figure 30. Acoustic noise power spectra of the ICP discharge. (a) regular torch, (b) tall torch.

in the noise power spectrum at a frequency corresponding to the lower frequency observed in the case of the optical emission signals, i.e., at the frequency of plasma rotation. This is further evidence that the upper frequency observed in the optical emission experiments is a result of spatial observation effects which, of course, will not affect the acoustic measurements. It is interesting to note that the peak in the acoustic noise power spectrum also disappears when a tall torch is utilized (Figure 30b). Thus there seems to be a general acoustic emission signal from the ICP at a frequency corresponding to the discharge rotation frequency and caused by the same mechanism.

#### F. Simultaneous Dual Channel Measurements

The evidence presented so far with respect to the rotation noise is still somewhat indirect. An experiment was designed that would allow direct observation of the rotation of the plasma. Two completely identical, parallel measurement systems were assembled each consisting of a monochromator and its associated measurement electronics, see Figure 31. The dual sample and hold amplifier (Figure 12) was used to allow time simultaneous monitoring of the signals from both measurement channels by the computer data acquisition system (see Chapter II). The optical system

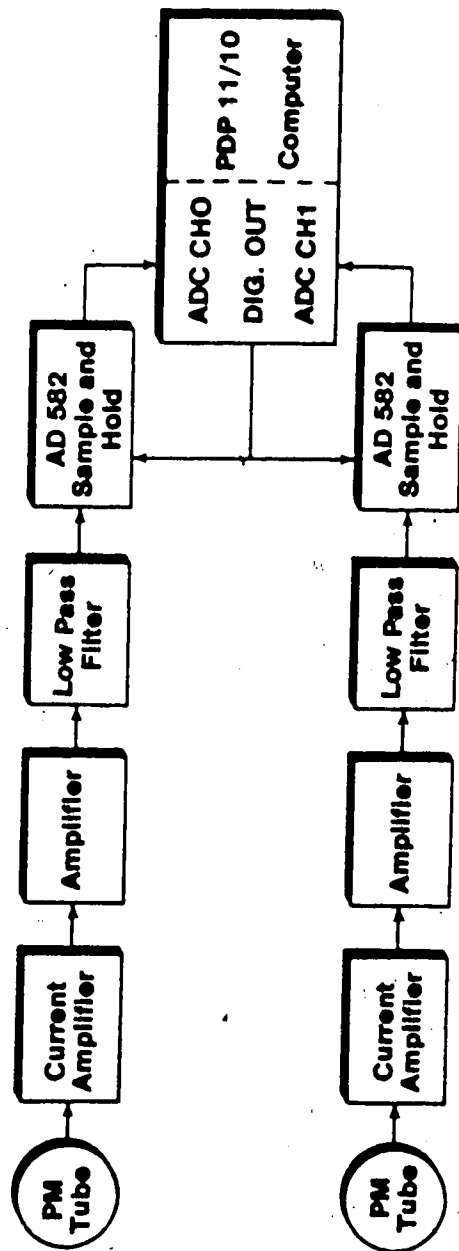
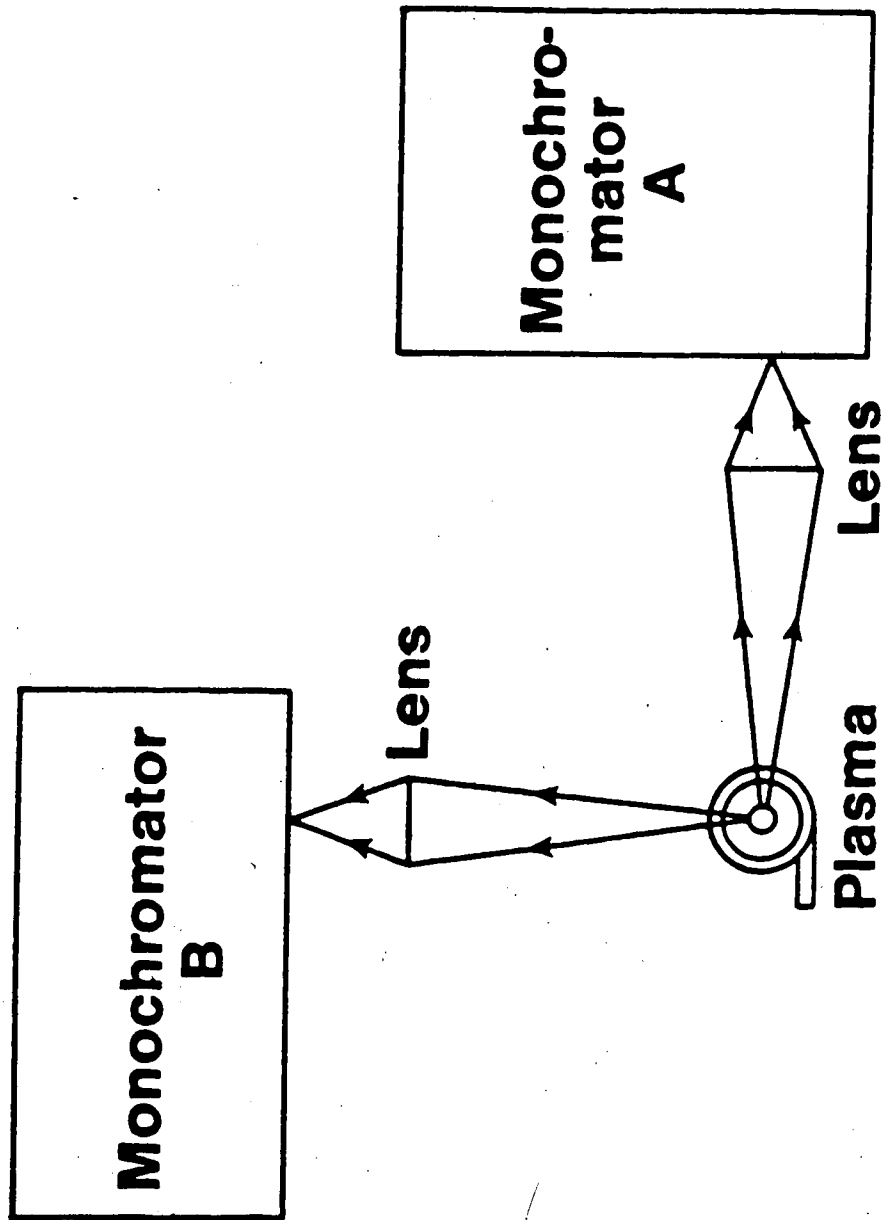


Figure 31. Simultaneous dual channel data acquisition system.

was arranged such that the plasma was observed simultaneously at right angles by the two monochromators as shown in Figure 32. High and low pass filters were used to isolate the lower frequency of the two noise peaks (Figure 33) from the other frequencies present in the signal. The analyte aspirated in this case was a 1 ppm calcium solution and both monochromators monitored the CaII 393.3 nm emission signal. Signals from both channels were acquired simultaneously by the data acquisition system at a rate of 5 kHz, sufficient to oversample the characteristic frequency and provide accurate information about any relative phase shifts. The results shown in Figure 34 clearly indicate that the signal acquired at the second channel (B) is  $90^\circ$  out of phase (lagging behind) that acquired by the first channel (A). As a test, the signal arising from monochromator A was split at the output of the photomultiplier tube and fed simultaneously through both electronic channels. No phase shift could now be detected between the two acquired signals (Figure 35). Thus it is safe to conclude that the previously measured phase shift is real and not an artifact of the measurement electronics. If this measured phase shift is to confirm rotation not only should the two signals be shifted by  $90^\circ$  but the direction of the shift should be consistent with that of



**Figure 32.** Optical configuration for simultaneous dual channel measurement of plasma emission signals.



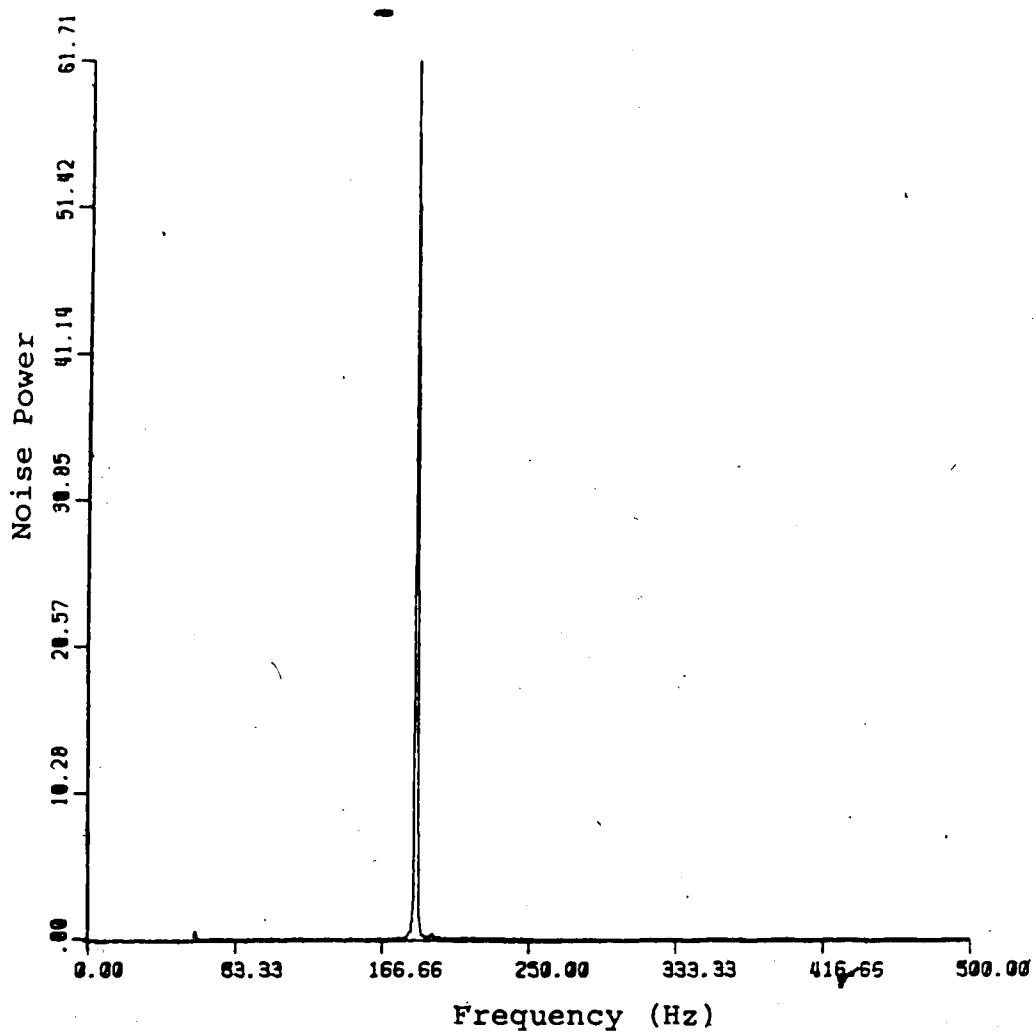


Figure 33. Noise peak. Isolated by means of electronic high and low pass filters.

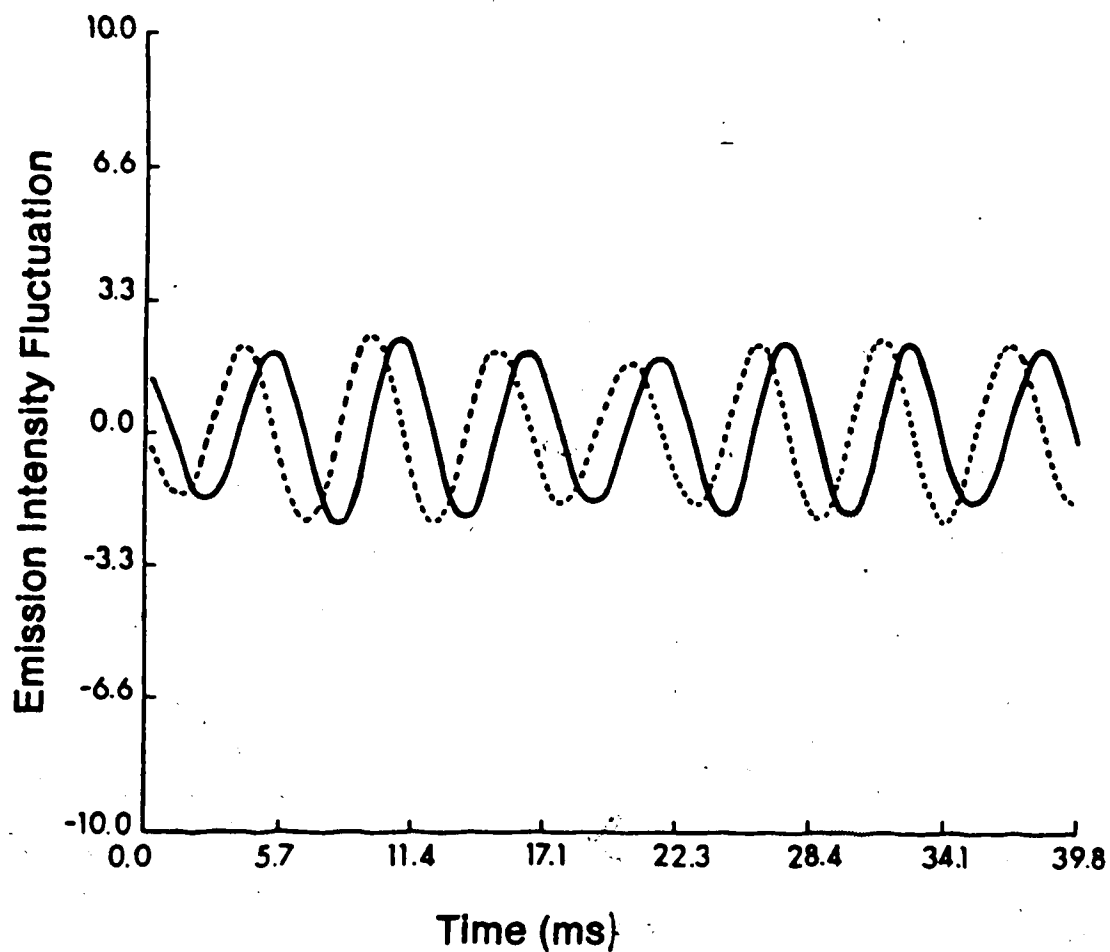


Figure 34. Simultaneously digitised noise signal for CaII 393.3 nm from monochromator A (solid line) and monochromator B (dashed line), showing  $90^\circ$  phase shift.

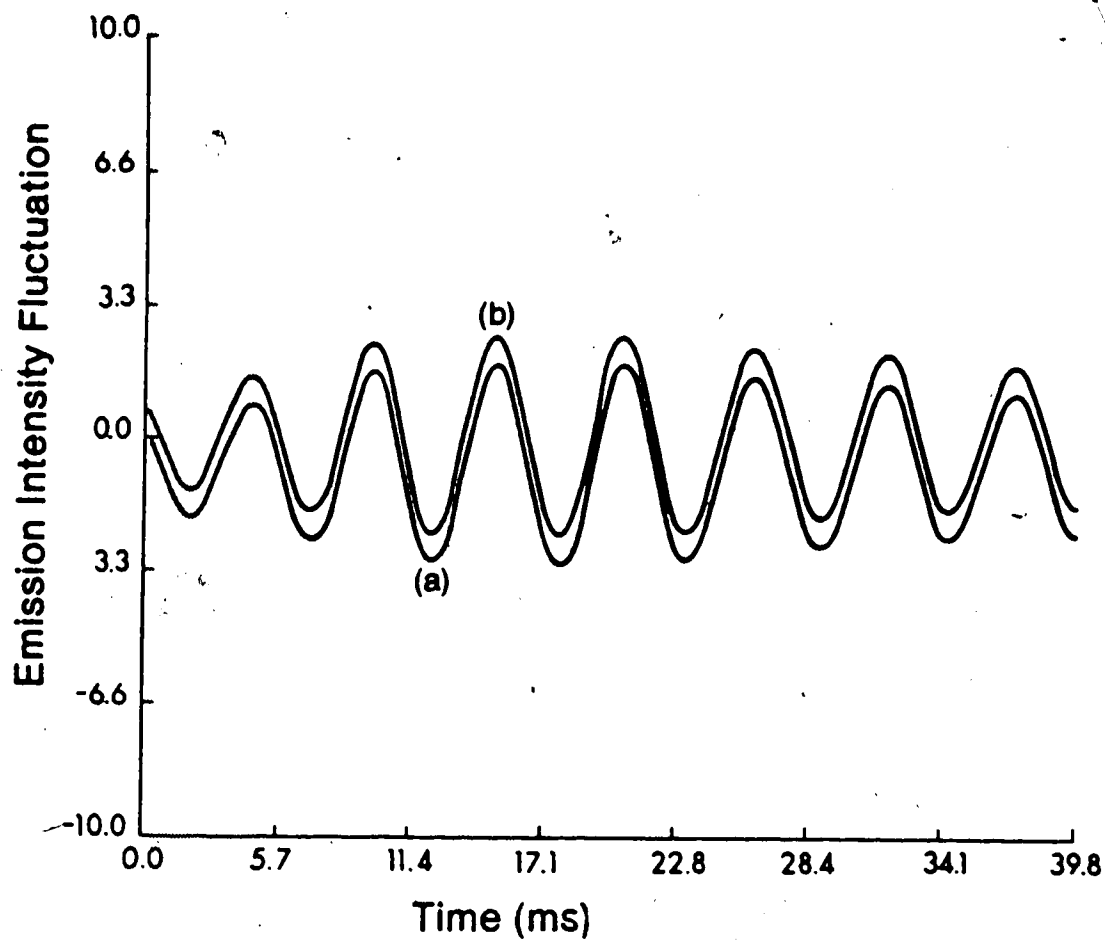


Figure 35. Simultaneous digitised noise signal for CaII 393.3 nm from monochromator (A) split and fed through electronic channels (A) and (B). Showing no measurement phase shift.

the expected direction of rotation. Signal A precedes signal B (Figure 34), which indicates an anticlockwise direction of rotation that is consistent with the direction of rotation, caused by the tangential introduction of plasma gas (Figure 32).

#### G. Conclusions

The measurement of noise power spectra of ICP emission signals has allowed the clarification of several aspects of the noise properties of ICP systems. In the 0 to 5 Hz region noise power spectra are highly characteristic and diagnostically useful with respect to nebulizer performance and design. They reveal clearly that analyte flicker is the dominant source of noise.

In the 0-500 Hz region a peak in the noise power spectrum occurs that appears to result from rotation of the plasma discharge at a frequency ranging from 200 to 400 Hz depending on the exact experimental conditions. This feature of the plasma discharge is interesting in its own right and is important, from a practical point of view, when measurements are carried out on ICP systems with bandwidth responses in this region. A knowledge of the frequencies where these peaks occur is also important when source modulation frequencies must be chosen

for atomic absorption and fluorescence measurements,  
using the plasma as the atom or ion cell.

## CHAPTER V

### CORRELATION OF SPRAY CHAMBER PRESSURE FLUCTUATIONS WITH NOISE IN THE EMISSION SIGNAL

#### A. Introduction

In dealing with source flicker noise one is faced with a major problem if it is necessary to improve the precision of an analysis. Because of the  $1/f$  nature of the flicker noise power spectrum, it is not possible to improve the result by the use of extended integration periods. Likewise, modulation techniques are of little use when the limiting noise is source flicker (37). Two alternatives remain:

1. Identify the causes of source flicker and either eliminate or reduce their effects. This may be brought about by careful redesign of the experiment or simply improvement in the operation of one component.
2. Utilize the internal standard principle. This requires the location of another parameter whose behaviour mimics as closely as possible fluctuations of the emission signal. By ratioing the emission intensity with this other parameter the multiplicative effects of source flicker noise may be partially or totally removed. Traditionally the other parameter used for

internal standardization has been the emission intensity of another element, however, there is no reason why any other physical parameter could not be used.

For instance it is common practice with laser vaporisation/excitation studies to ratio the emission intensity with the laser power output.

One of the parameters in an inductively coupled plasma system that may be correlatable to variations in the analyte emission intensity is the pressure in the nebulizer spray chamber (65). It is known that variations in the flow rates of the support gases of the ICP cause both intensity and spatial changes in the analyte emission intensity (66). It is also to be expected that changes in the support gas flow rate, especially the nebulizer gas will result in pressure changes in the spray chamber. It seems reasonable, bearing these facts in mind, that a correlation may exist between emission noise and spray chamber pressure fluctuations.

Preliminary to a study of such correlations, a study of the effects of the three gas flow rates and the incident rf power on the spray chamber pressure was carried out. To date few pressure measurements have been made associated with the ICP. The results are rather limited and mainly concern themselves with gas flow dynamics in the plasma itself (67-70).

## B. Experimental Measurement of Spray Chamber Pressure

Pressure measurements of the interior of the spray chamber were carried out using an electronic pressure transducer (model G-605-01-2-5, Gulton Industries, 1644 Whittier Ave., Costa Mesa, CA 92627). This pressure transducer was coupled to the spray chamber by a glass side arm and a short length of Tygon tubing (Figure 36a). Power for this transducer was provided by two 6 V batteries connected in series. The signal from the transducer was either measured directly using a digital voltmeter, or amplified prior to acquisition by the minicomputer system (Figure 36b). Prior to making these measurements the pressure transducer was calibrated against a simple water-filled manometer.

The nebulizer used for these experiments was the Meinhard concentric glass nebulizer. The Scott type spray chamber was used for the initial studies, though an improved spray chamber later evolved which will be discussed later in this chapter.

## C. The Effect of Plasma Operating Conditions on the Spray Chamber Pressure

The effects of nebulizer, auxiliary and coolant gas flow rates on the internal pressure of the spray chamber



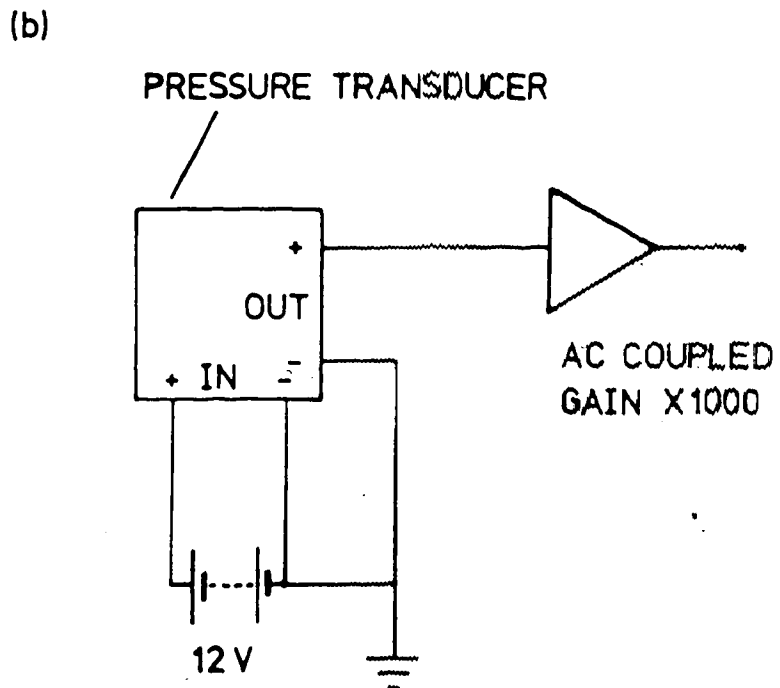
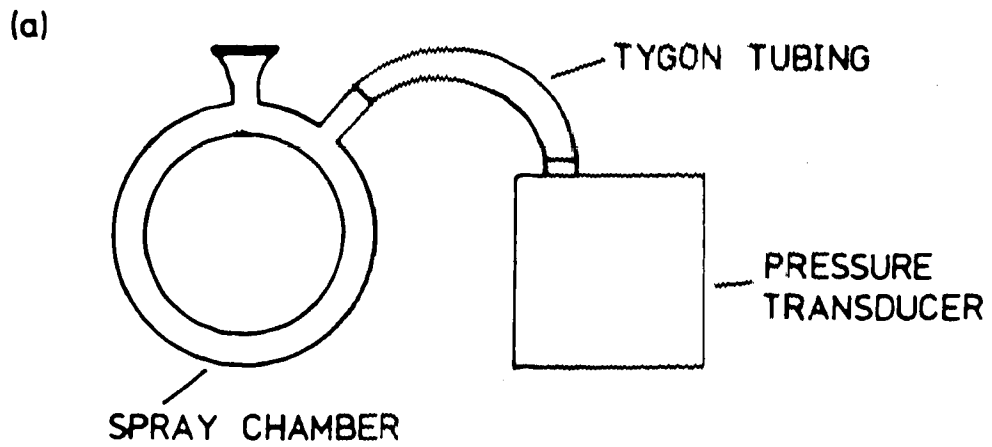


Figure 36. Pressure transducer for spray chamber pressure measurement (a) connection to spray chamber, (b) electrical connections.

are shown in Figures 37,38,39. The effect of incident power is shown in Figure 40. It should be noted that the pressure axis in Figure 37 is 2.5 times less sensitive than in the other figures.

When not a variable parameter, input power was kept constant at 1.5 kW, coolant gas flow rate was 16 l/min, auxiliary gas was 0.7 l/min and nebulizer gas flow rate was 1.1 l/min. All gas flows were argon. It should also be noted that the gas flow controls for the nebulizer gas were modified from the original Plasma-Therm arrangement, to provide a more accurate measurement of the nebulizer gas flow rate (see Chapter II, in particular Figure 5). The units on the pressure axes of the plots are PSI above atmospheric pressure.

As would be expected, the most important parameter is the nebuliser gas flow rate. An increase in the nebuliser gas flow rate increases the pressure in the spray chamber as shown in Figure 37. This measurement was made with and without the plasma lit. The back pressure created by the plasma is equal to the difference between the two curves. Thus there is a back pressure simply due to the passage of the nebulizer gas through the injector tube. An additional pressure is expected when the plasma is lit, created, perhaps by the rapidly heated nebulizer

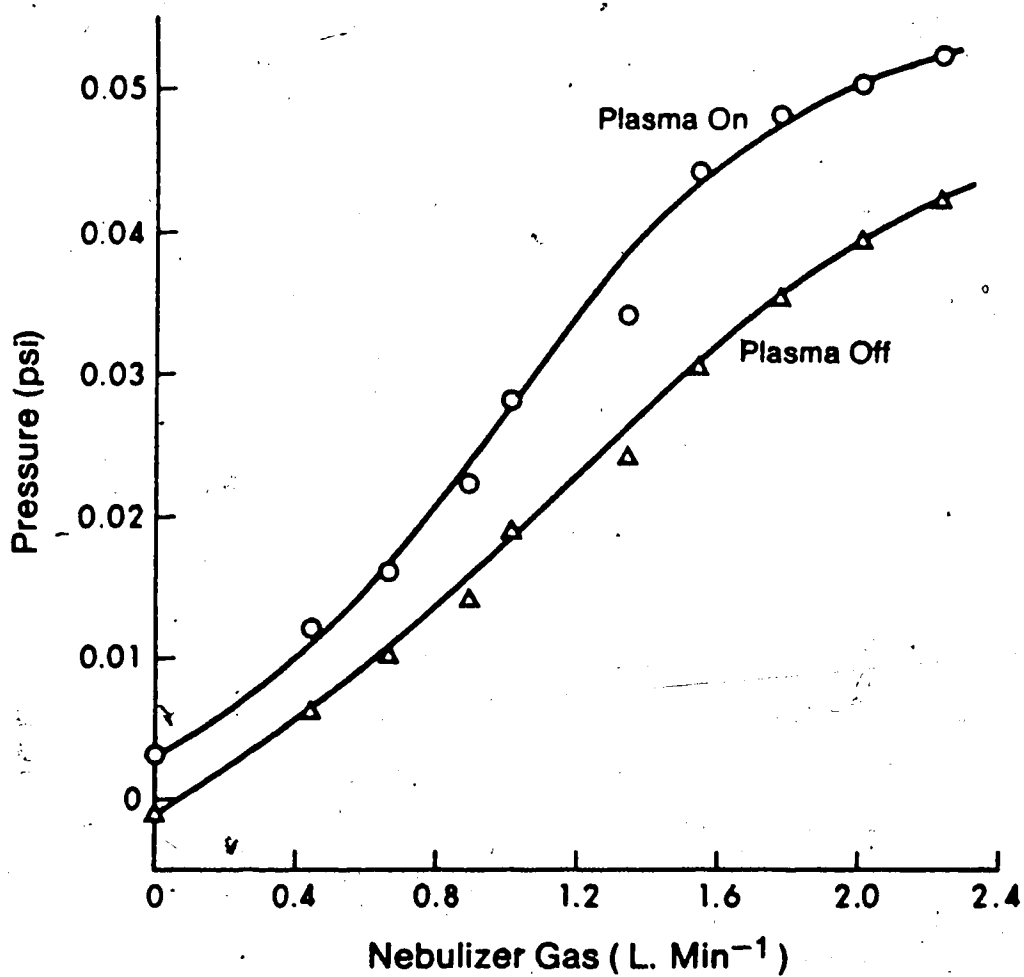


Figure 37. Plot of spray chamber pressure as a function of nebulizer gas flow rate.

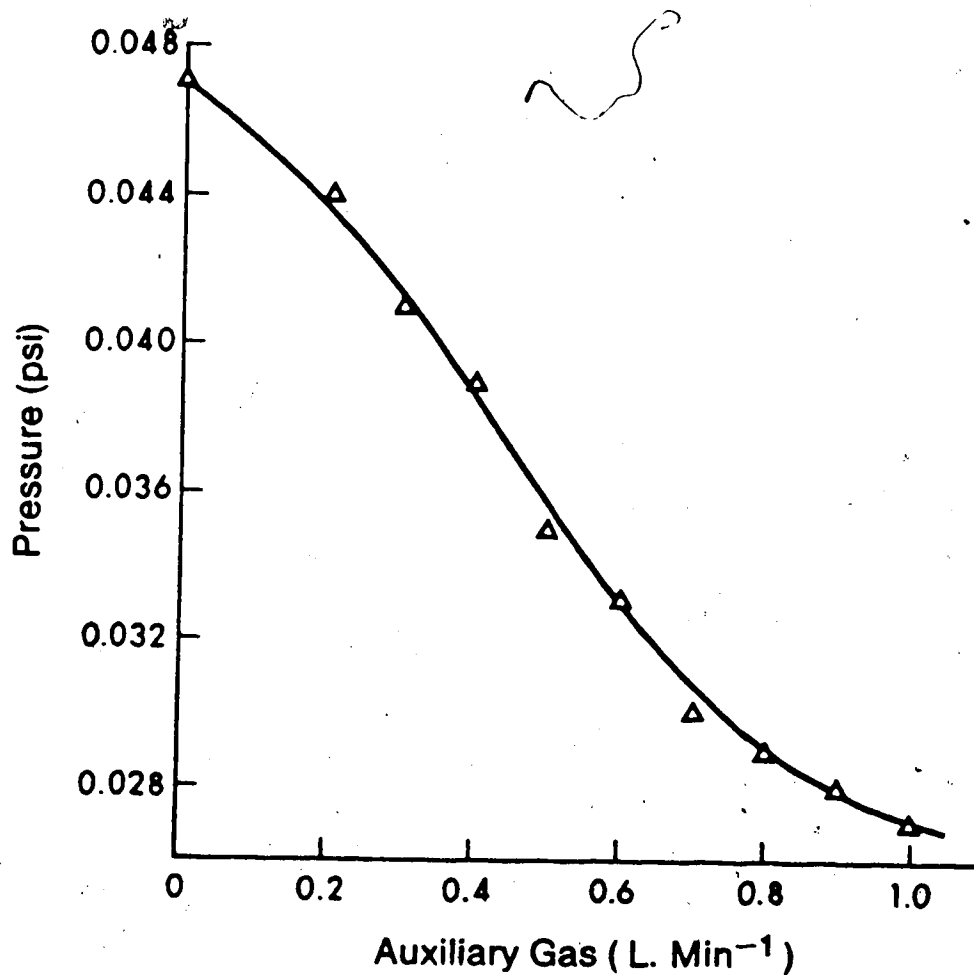


Figure 38. Plot of spray chamber pressure as a function of auxiliary gas flow rate.

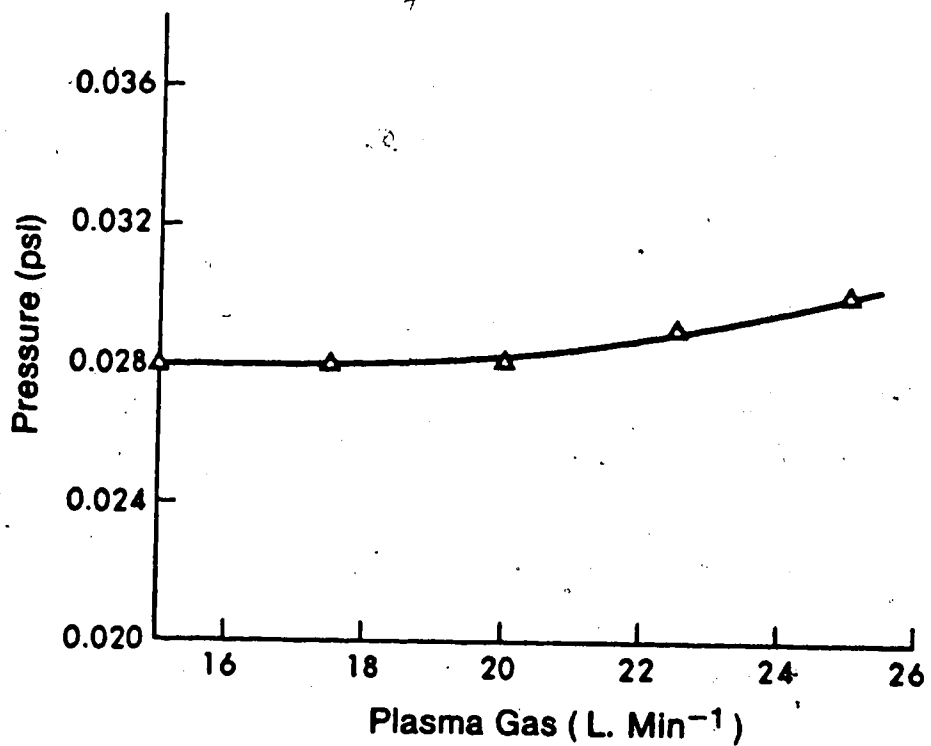


Figure 39. Plot of spray chamber pressure as a function of plasma gas flow rate.

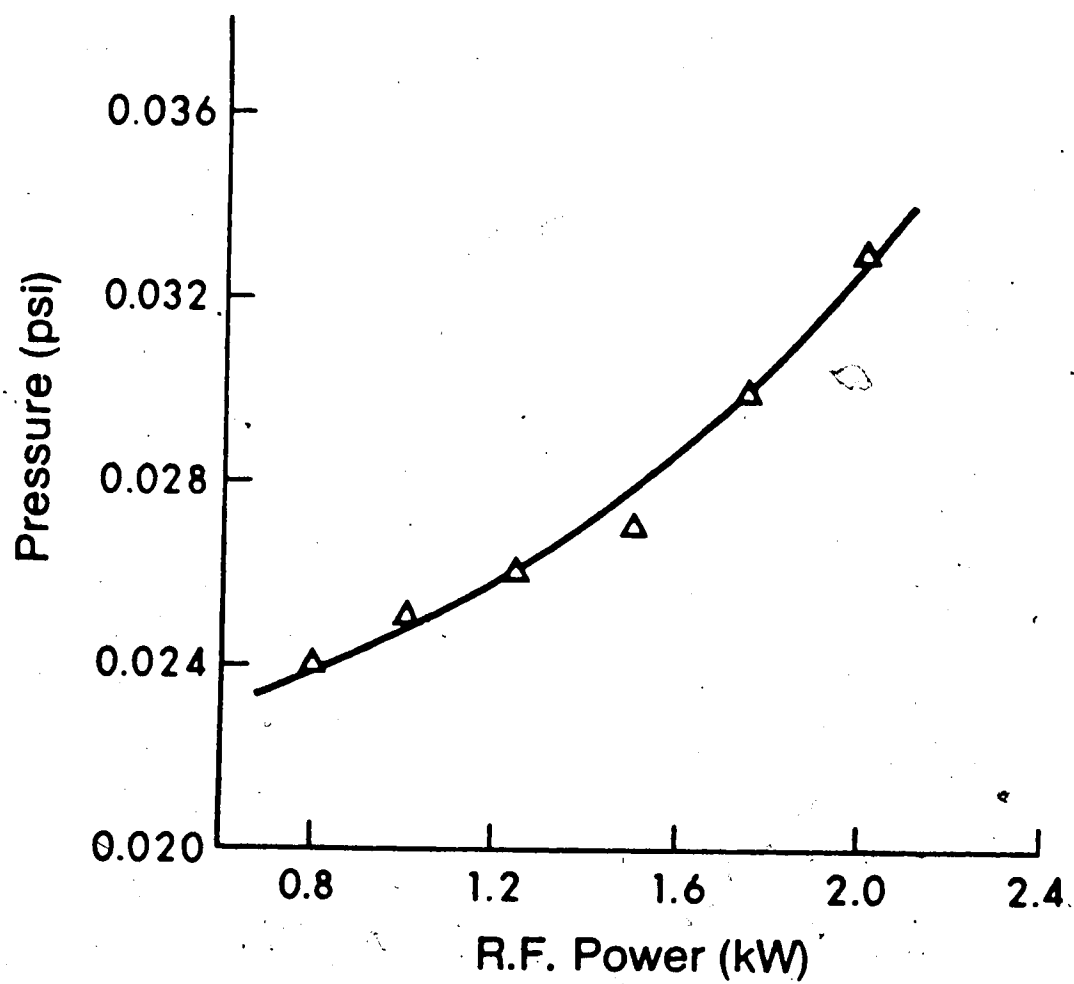


Figure 40. Plot of spray chamber pressure as a function of input rf power.

gas as it passes through the injector tube tip into the plasma toroid.

Calculations of the change in the injector tube orifice size as a function of temperature (0.033% increase for a 300°C rise) indicate that this effect on the back pressure is not important.

In contrast, increased flow of the auxiliary gas has the effect of decreasing the pressure (Figure 38). This makes intuitive sense as an increase in auxiliary gas flow rate raises the plasma body in the torch away from the injector tube. The heating of the injector tube tip is thereby lessened as is the inherent back pressure of the plasma.

Coolant (plasma) gas flow rate which does not substantially alter the plasma vertical position within the torch, has very little effect on the spray chamber pressure (Figure 39).

Finally, increasing the input power increases the spray chamber pressure (Figure 40). This would be expected as the plasma tends to increase in length (upwards and downwards) and in temperature with increasing power. This result is in keeping with those reported by Chase (68).

## D. Correlation Studies

### 1. Experimental

In order to investigate the correlation of pressure fluctuations in the spray chamber and noise in the emission signal, it is necessary to monitor simultaneously the two signals. To facilitate this the signal from the pressure transducer, after amplification and low pass filtering, was fed to channel 1 of the dual channel sample and hold amplifier (Figure 12). The signal from the photomultiplier tube, after amplification and low pass filtering, was fed to channel 0. Both signals could then be simultaneously acquired by the sample and hold amplifier and then sequentially digitised by the PDP 11/10 computer data acquisition system.

The bandwidth of both channels was limited by the Krohn-Hite low pass filters (-48 dB/octave) whose -3 dB points were set at 2.5 Hz. Data acquisition was at a rate of 5 Hz. This sampling rate was appropriate for observing the noise characteristics that are important in determining the precision of analysis with most low bandwidth measurement systems.

### 2. Calculation of the Cross-Correlation Function

In order to supplement the visual comparison of the



two signals the computer was used to calculate their cross-correlation function. Mathematically the cross-correlation function  $C_{ab}(n\Delta t)$  of two digitized signals (a and b) is given by the summation:

$$C_{ab}(n\Delta t) = \sum_t a(t) b(t \pm n\Delta t) \quad (24)$$

where  $\Delta t$  is the sampling interval and  $n\Delta t$  represents the relative displacement (71). The process of calculating this function directly is slow in the computer, due to the large number of multiplications required. Instead use is made of the relationship (71):

$$\begin{array}{ccc} a(t) & * & b(t) & = & C_{ab}(\tau) \\ \text{Fourier Transform} & \downarrow & & & \uparrow \\ a(f) & \times & a(t) & = & C_{ab}(f) \\ & & & & \text{Inverse Fourier Transform} \end{array} \quad (25)$$

It is quicker to Fourier transform both digitised signals, using the FFT algorithm, multiply the transforms together and then carry out an inverse Fourier transform to obtain the cross-correlation function. The scheme used to do this cross-correlation was that described by Ng and Horlick (72). A listing of the computer programs necessary to accomplish this are provided in reference (73).

### 3. Results from the Scott Spray Chamber

Figures 41 and 42 show the emission signals for CdII 214.4 nm (50 ppm) and ArI 415.9 nm, fluctuations in the spray chamber pressure and the cross-correlation functions. In this instance the axis for pressure fluctuations has not been calibrated with respect to the units of pressure.

Figures 41 and 42 clearly show a prominent noise spike, occurring at intervals of approximately 30 seconds in the emission signals. It is also clear that a similar, but somewhat different in shape, feature occurs at the same time in the signal from the pressure transducer. While it is obvious that these features are related the cross-correlation function is of little extra help in determining the relationship.

The cause of the noise spikes soon became apparent. A long drain hose (1 m) from the spray chamber to a reservoir bottle was being used. Droplets of water, from the spray chamber, running down this drain hose hit the surface of the liquid in the reservoir bottle, and caused the liquid level to oscillate slightly. These oscillations are then responsible for the rapid pressure fluctuations which in turn are responsible for the noise spikes in the emission signal. By changing the length and angle of the drain tube it was possible to reduce these effects or alter

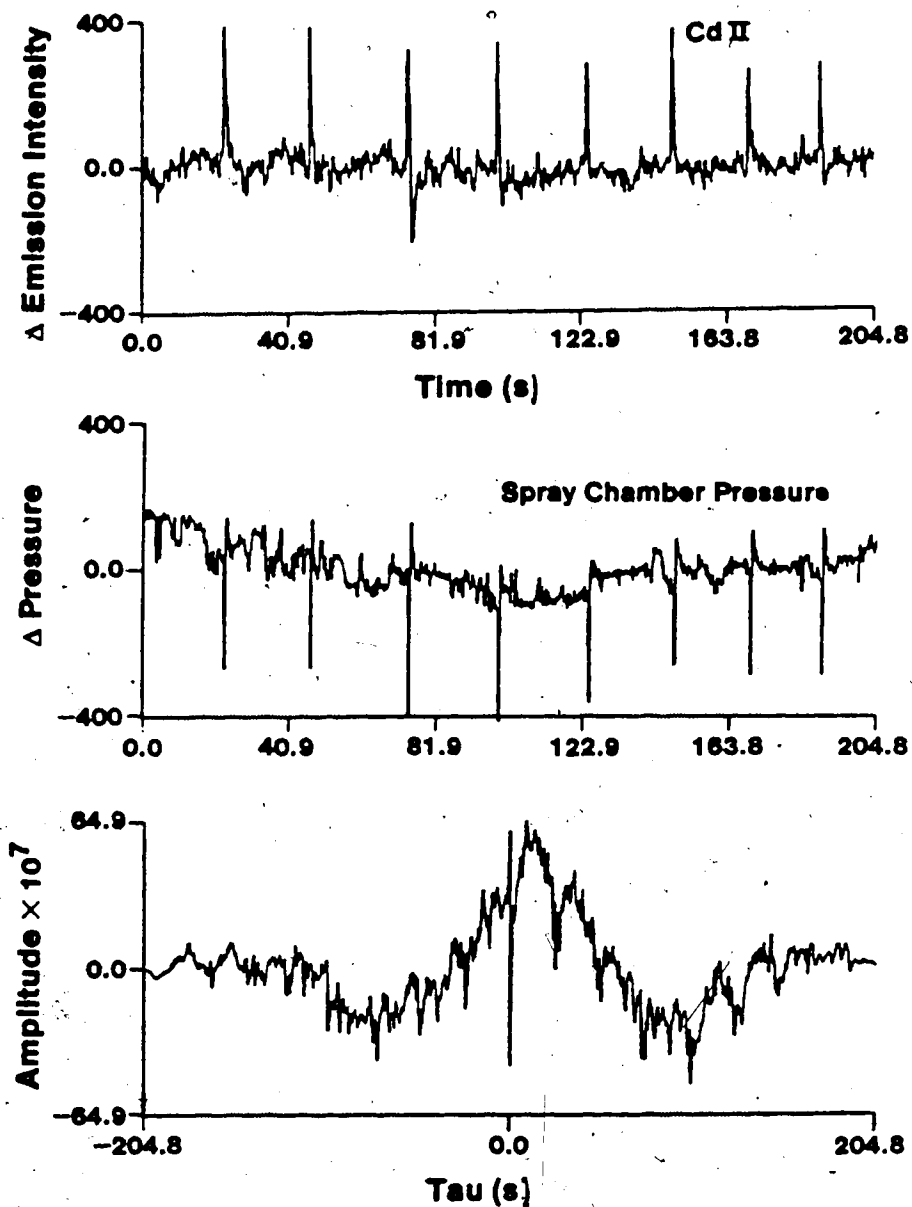
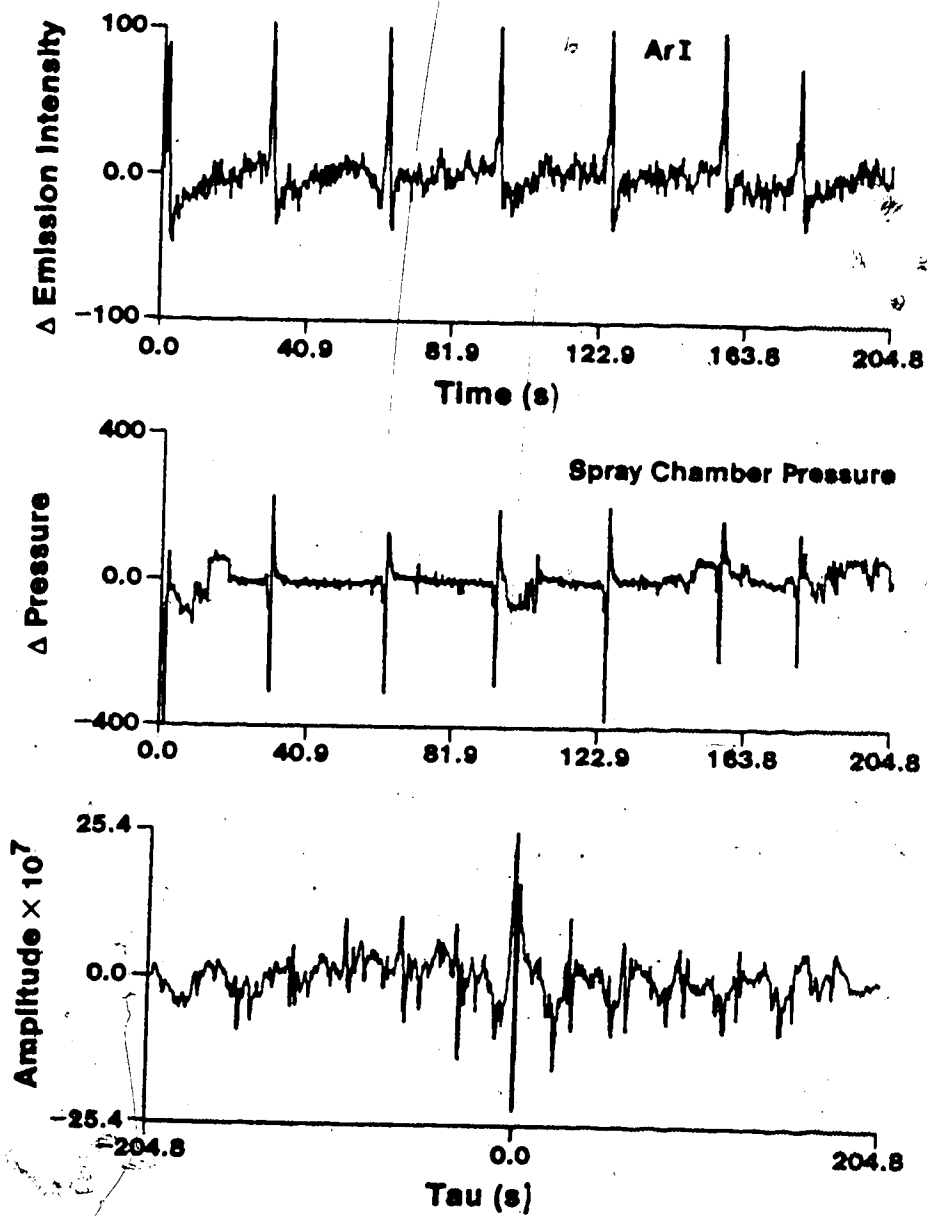


Figure 41. Correlation of CdII 214.4 nm (50 ppm) emission with spray chamber pressure fluctuations. Scott spray chamber.



**Figure 42.** Correlation of ArI 415.9 nm emission with spray chamber pressure fluctuations. Scott spray chamber.

the repetition rate. It was not possible, however, to eliminate them entirely. A number of drain traps were also tried but with somewhat limited success. Finally an improved spray chamber design which eliminated this problem was used.

#### 4. "Soak Away" Spray Chamber

To combat the fluctuations in spray chamber pressure caused by drain tube drips, a spray chamber with an improved drain system was constructed (Figure 43). In this design the Scott type spray chamber was modified so that it operated in a vertically upright position. The conventional drain tube was replaced by a bed of fine washed sea sand supported by a scintered glass frit. The layer of sand rapidly becomes saturated with analyte providing a barrier to the escape of nebulizer gas but allowing liquid to drain rapidly away.

#### 5. Results from the "Soak Away" Spray Chamber

When the "regular" Scott spray chamber was replaced with the soak-away system the pressure fluctuations disappeared (Figures 44,45). The signal-to-noise ratio for the measurement of the CdII 214.4 nm (50 ppm) signal improved (for a 1 second integration time) from 73.2 to 97.9, an im-

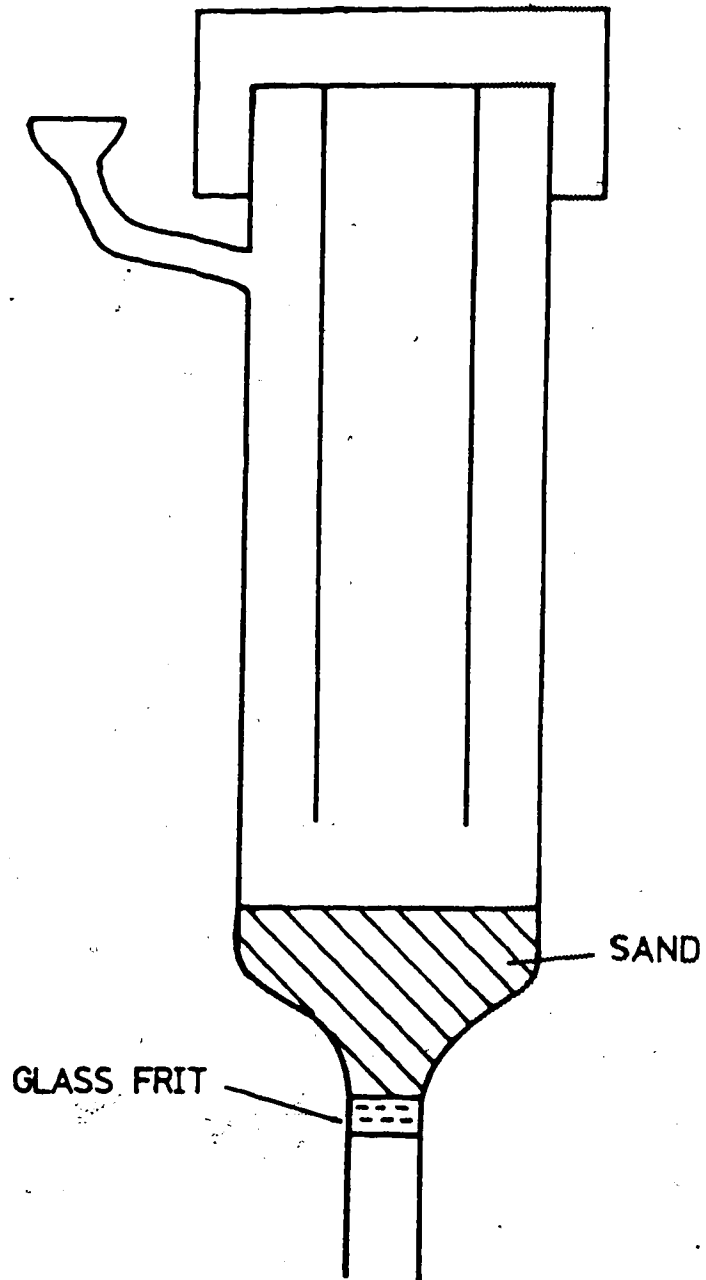


Figure 43. "Soak-away" spray chamber.

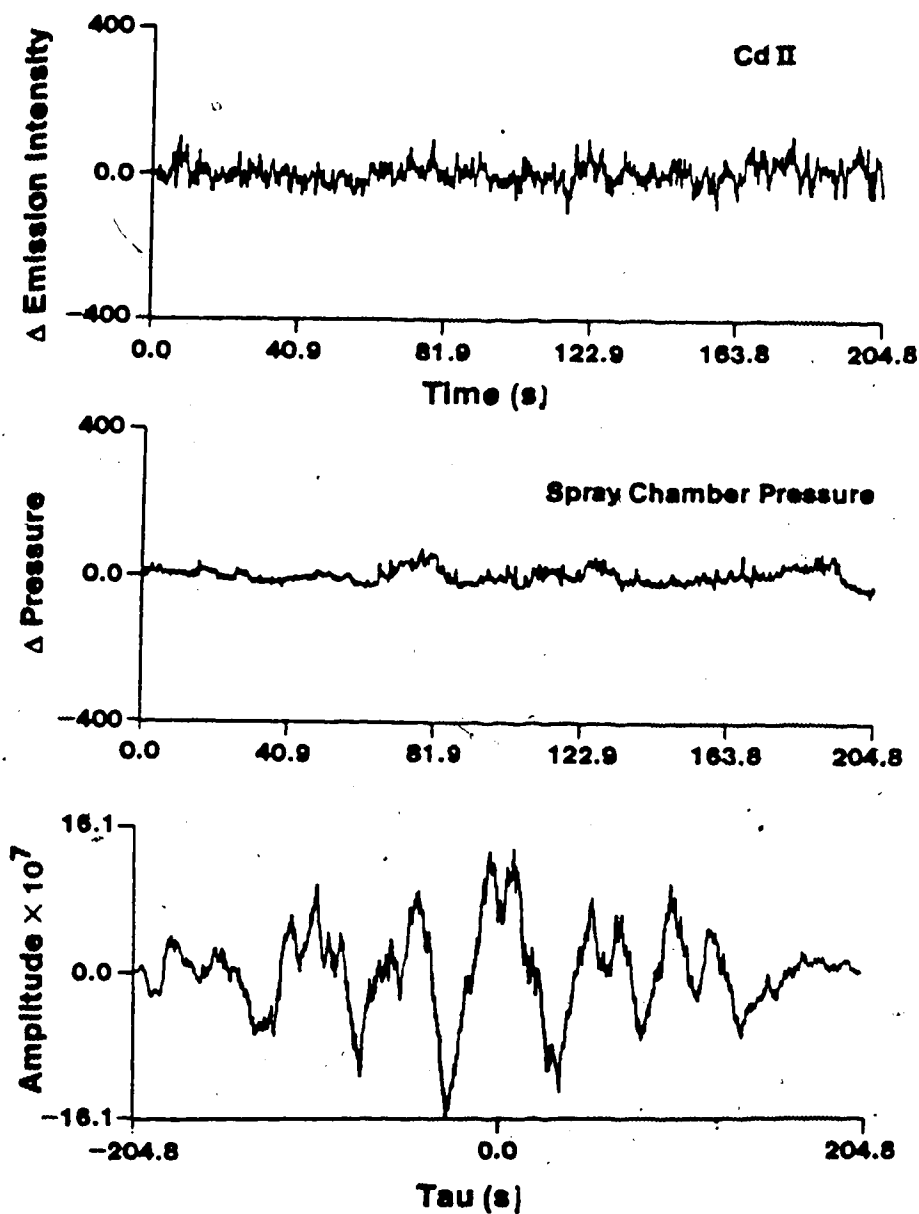


Figure 44. Correlation of CdII 214.4 nm (50 ppm) emission with spray chamber pressure fluctuations. Soak-away spray chamber.

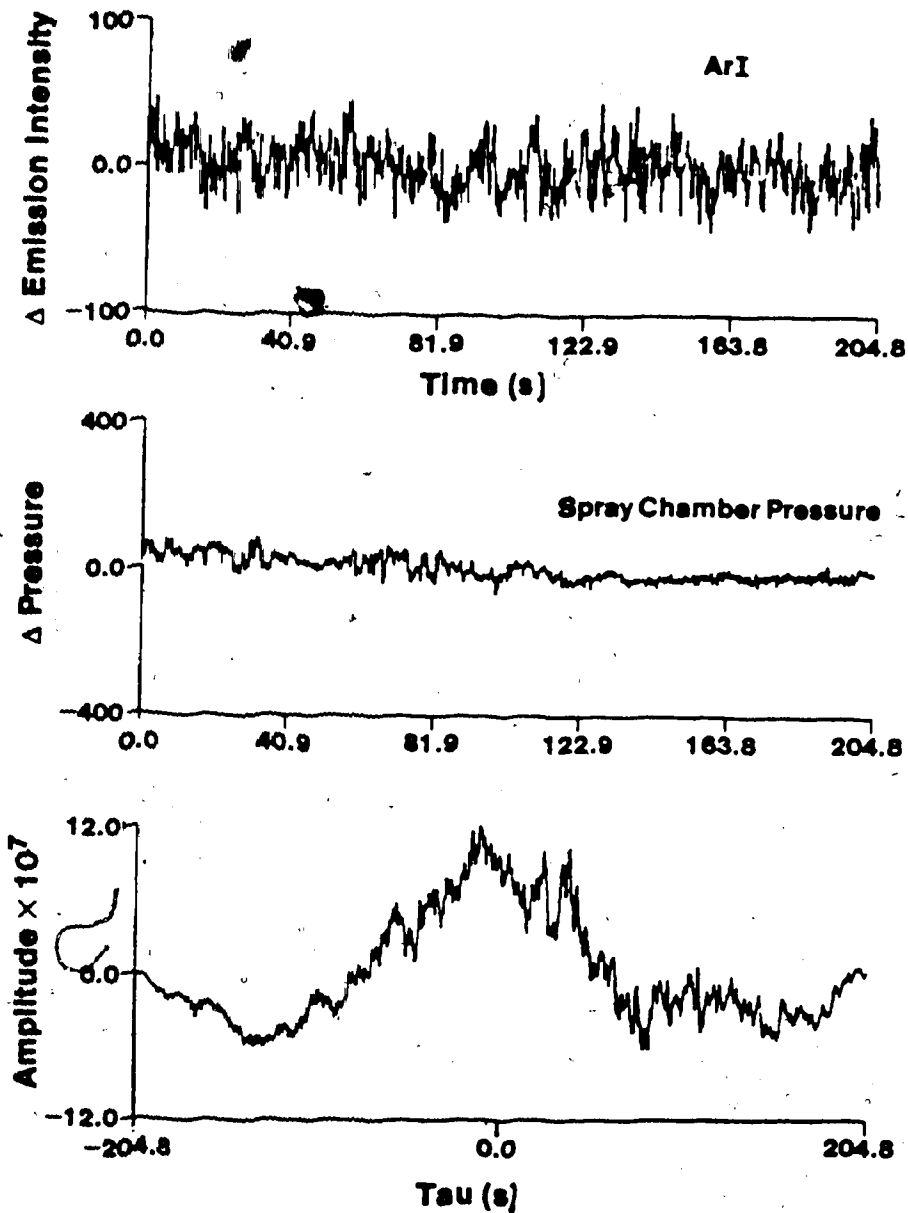


Figure 45. Correlation of ArI 415.9 nm emission with spray chamber pressure fluctuations. Soak-away spray chamber.



provement of approximately 34% over the original precision.

It should be noted now that no correlation could be detected when this spray chamber was used between noise in the emission signals and the spray chamber pressure. This was true for both the emission signals of CdII, (Figure 44) and ArI (Figure 45).

#### E. Conclusions from Spray Chamber Pressure Measurement

The data presented in Figures 37-40 indicate that three main plasma parameters nebulizer gas flow rate, auxiliary gas flow rate and power, significantly effect the pressure in the spray chamber. The other parameter studied, coolant gas flow rate, had a much lesser effect.

The measurement and correlation of spray chamber pressure and emission intensity fluctuations have been useful in pinpointing a problem associated with the drain hose arrangement. This led in turn to the development of an improved spray chamber design that eliminated the need for a drain hose.

When the effect of droplets running down the drain hose was removed no measurable correlation could then be detected between spray chamber pressure fluctuations and noise in the emission signals.

## CHAPTER VI

### CORRELATION OF NOISE IN THE INCIDENT AND REFLECTED POWER CIRCUITS WITH NOISE IN THE EMISSION SIGNAL

#### A. Introduction

A parameter of critical importance in influencing the precision of ICP analysis is the stability of the rf power supply. Kniseley et al. (74) reported severe modulation of emission line intensities caused by the use of an inadequately filtered power supply. Ohls (75) suggested that the feed back of ArI emission intensity may be used to stabilise the rf power output of the generator.

In addition to variations in the incident power, small changes in reflected power levels can often be observed. One cause of these small changes appears to be variations in the rate of introduction of analyte into the plasma.

It was decided to monitor fluctuations in both the incident and reflected power levels and to correlate, if possible, these fluctuations with those in the emission intensity.

#### B. Experimental Monitoring of Incident and Reflected Power Levels

The incident and reflected power levels were monitored

by the use of the circuit illustrated in Figure 46. The inputs of the incident or reflected power meters on the front panel of the matching and tuning network were disconnected. These meters are current meters directly connected to the power coupling system and provide a current path to ground. Any attempt to block this path to ground adversely effects the impedance matching characteristics of the system. Therefore an operational amplifier (model 25, Princeton Applied Research Corp., Princeton, N.J.) was used in the low impedance current amplifier mode to convert this current to a voltage signal. This voltage produced was proportional to the square root of the power. An analog multiplier (model 230, Princeton Applied Research Corp.) was then used to square this signal.

Signals from the analog multiplier were then low pass filtered and acquired by the minicomputer data acquisition system.

Cross-correlation studies (as described in Chapter V) were carried out between fluctuations in both the incident and reflected power circuits and in the emission signal. In addition the noise power spectra of both the incident and reflected power signals were obtained.

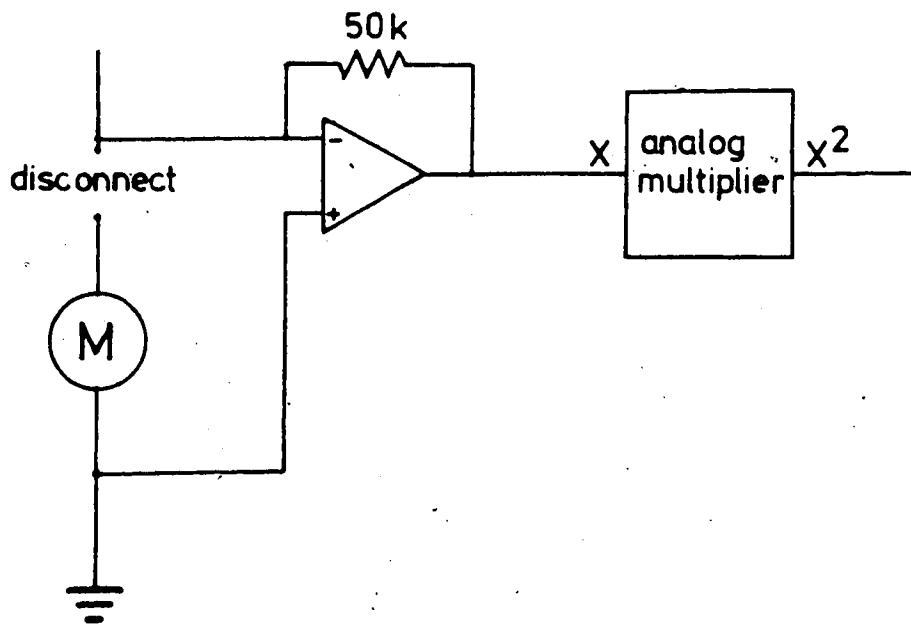


Figure 46. Circuit for monitoring incident and reflected power fluctuations.

### C. Discussion of Results

The noise power spectra of noise in the incident and reflected power circuits are shown in Figures 47 and 48. Simultaneously acquired signals from CaII (393.3 nm, 1 ppm) and ArI (415.9 nm) emission and the incident and reflected power circuits together with their corresponding correlation functions are shown in Figures 49-52. The presence of 60 Hz envelope ripple on the 27 MHz output of the generator is clearly shown in Figure 47. Also several of the higher harmonics of 60 Hz, which are occasionally visible in emission noise power spectra, are present. These features are also observed in the reflected power noise power spectrum. It seems reasonable to explain the presence of the 60 Hz peak present in the emission noise power spectrum as resulting from the 60 Hz modulation of the plasma by the RF generator. It is also worthwhile to note that none of the other distinct features noted in the emission noise power spectrum are seen in either the incident or reflected power noise spectra.

The cross-correlation studies show that no correlation (in the 0 - 2.5 Hz range) exists between emission noise and incident power fluctuations for either CaII (Figure 49) or ArI (Figure 50). Correlation is also absent between emission intensity of CaII (Figure 51), ArI (Figure 52)

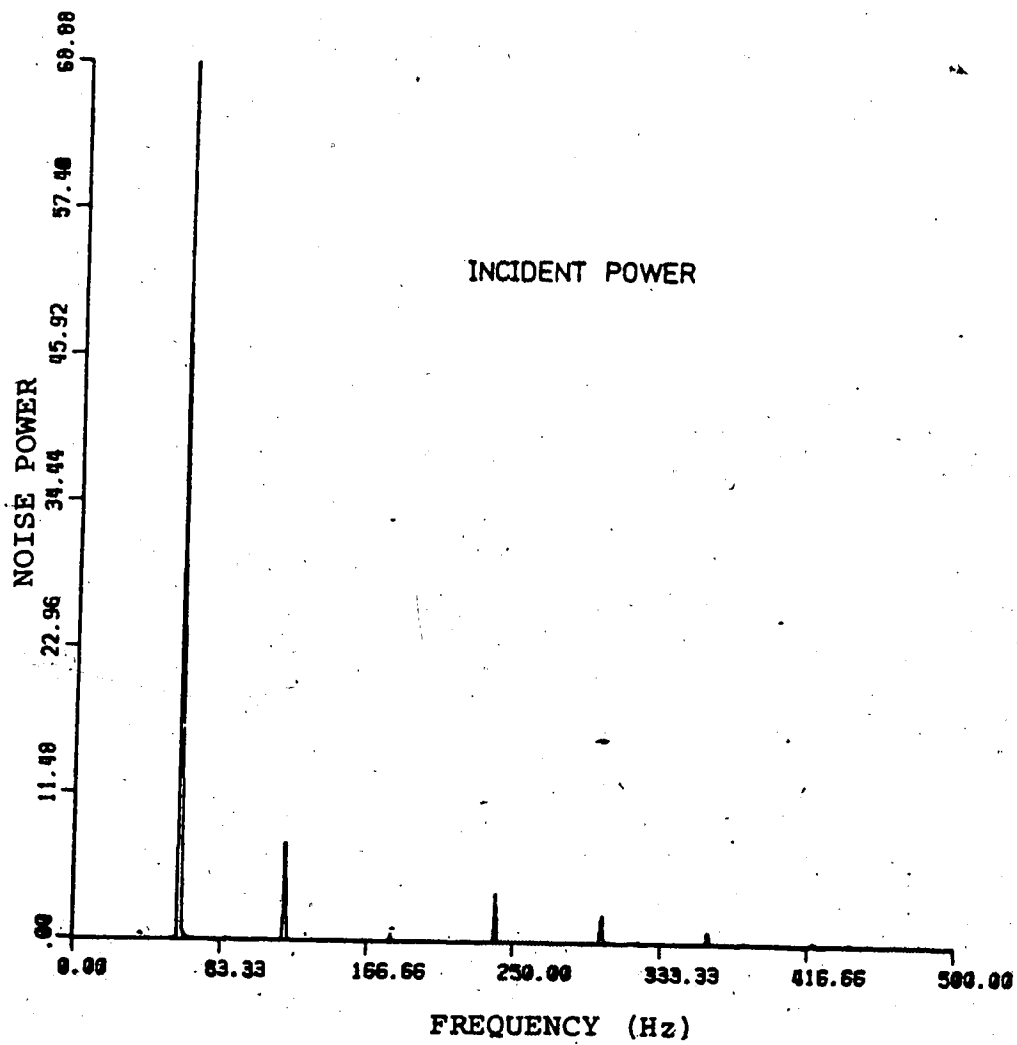


Figure 47. Noise power spectrum of incident rf power.

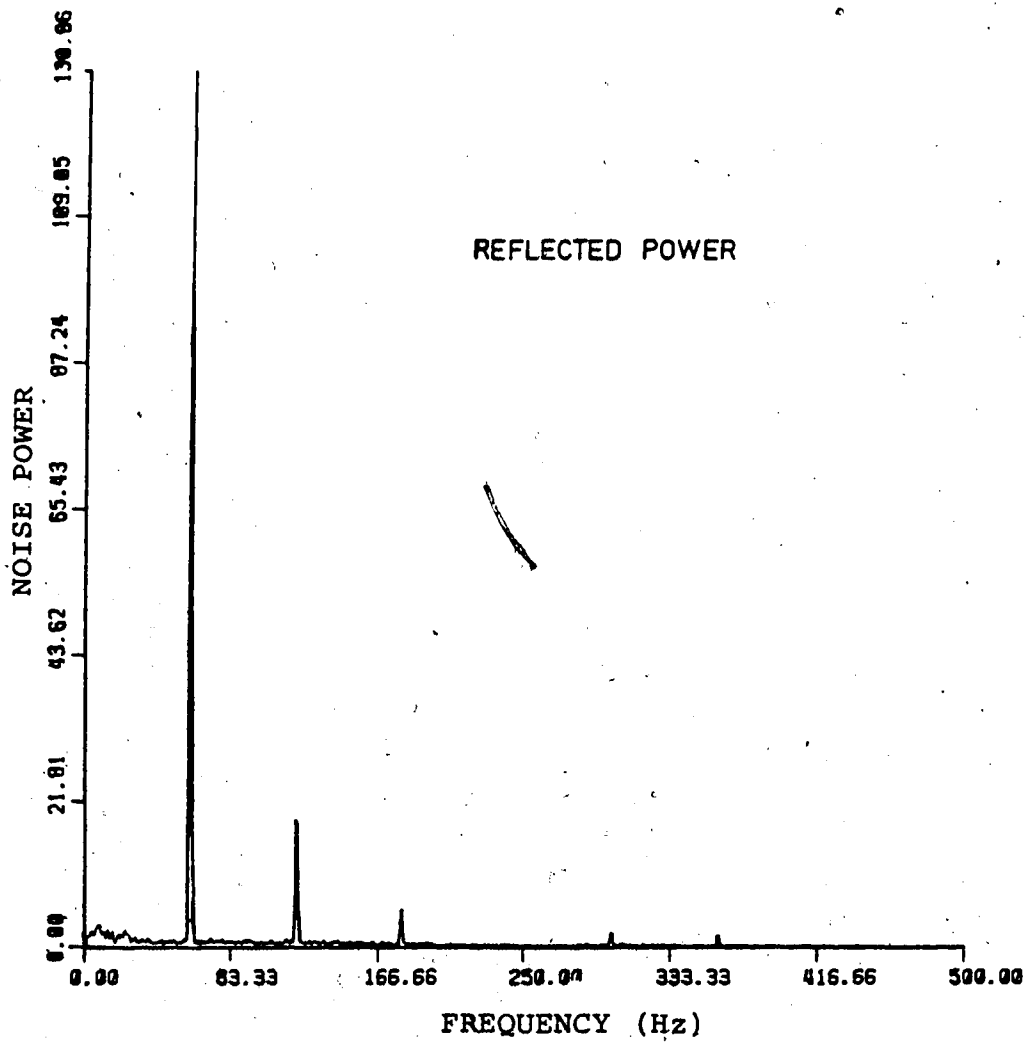


Figure 48. Noise power spectrum of reflected rf power.

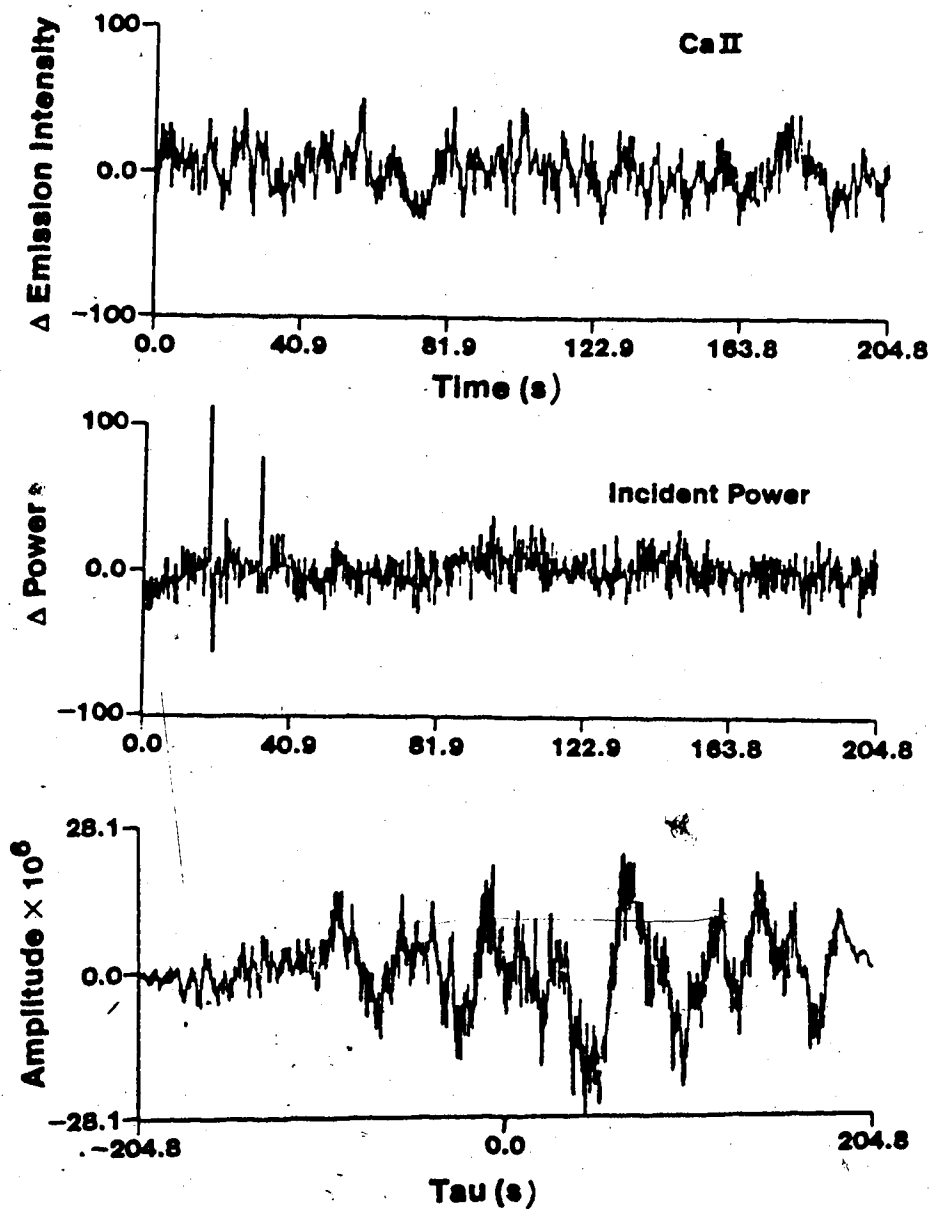


Figure 49. Correlation of CaII emission signal with incident power.



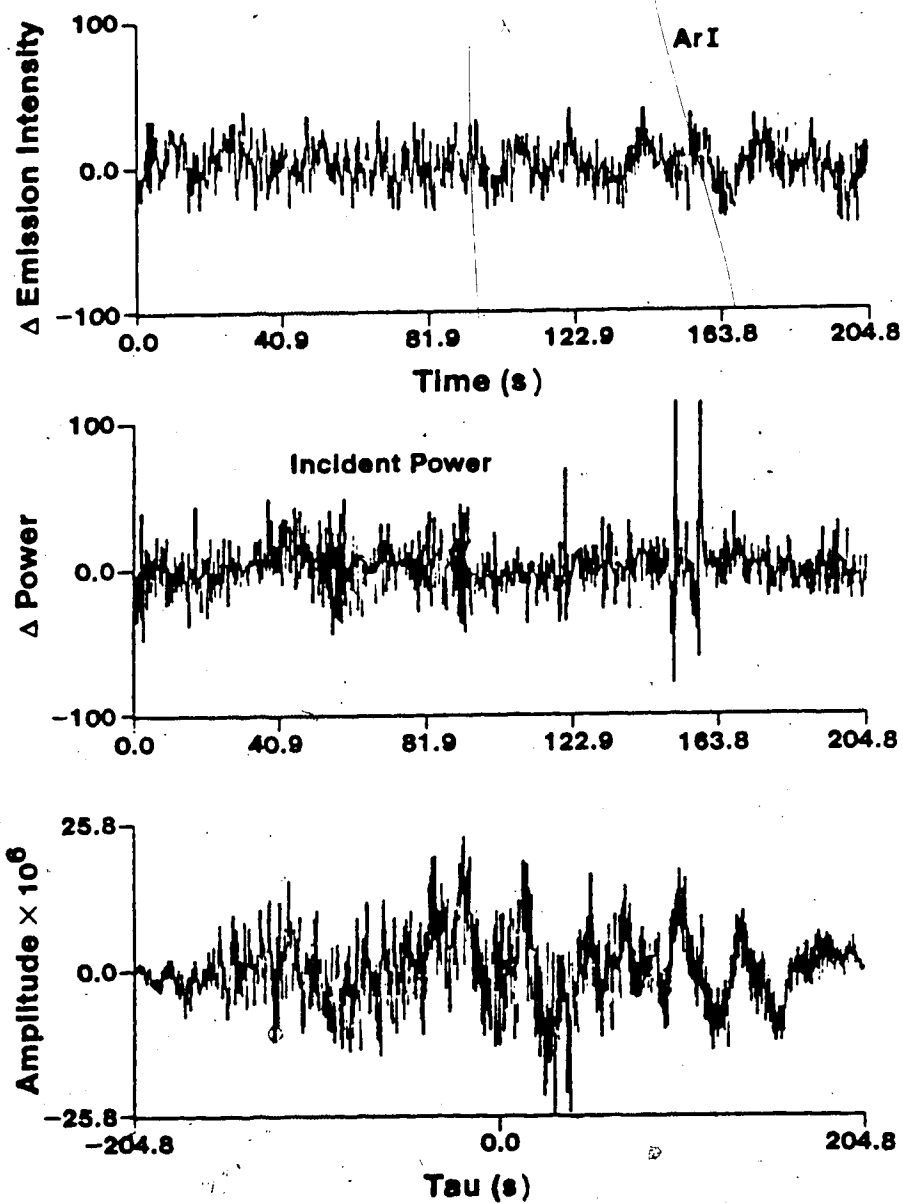


Figure 50. Correlation of ArI emission signal with incident power.

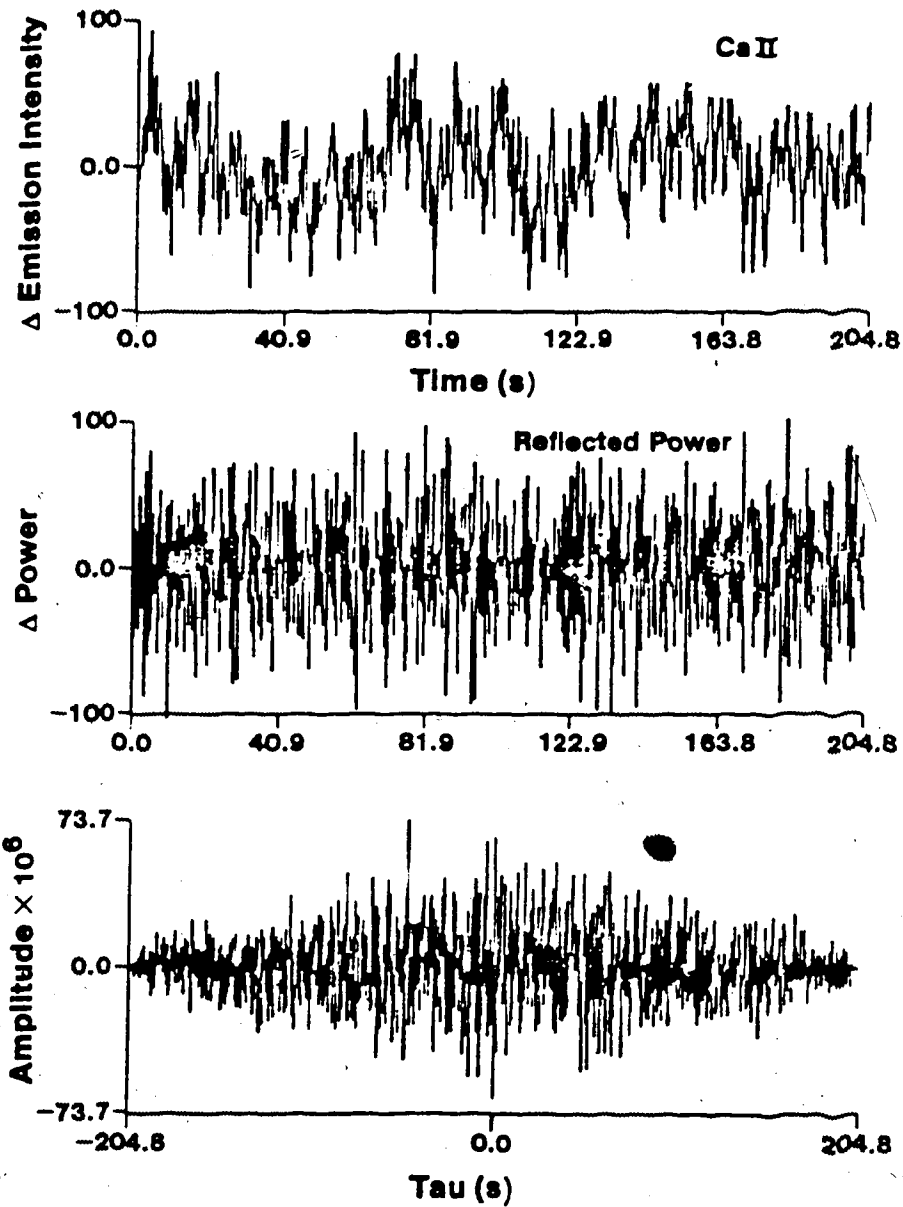


Figure 51. Correlation of CaII emission signal with reflected power.

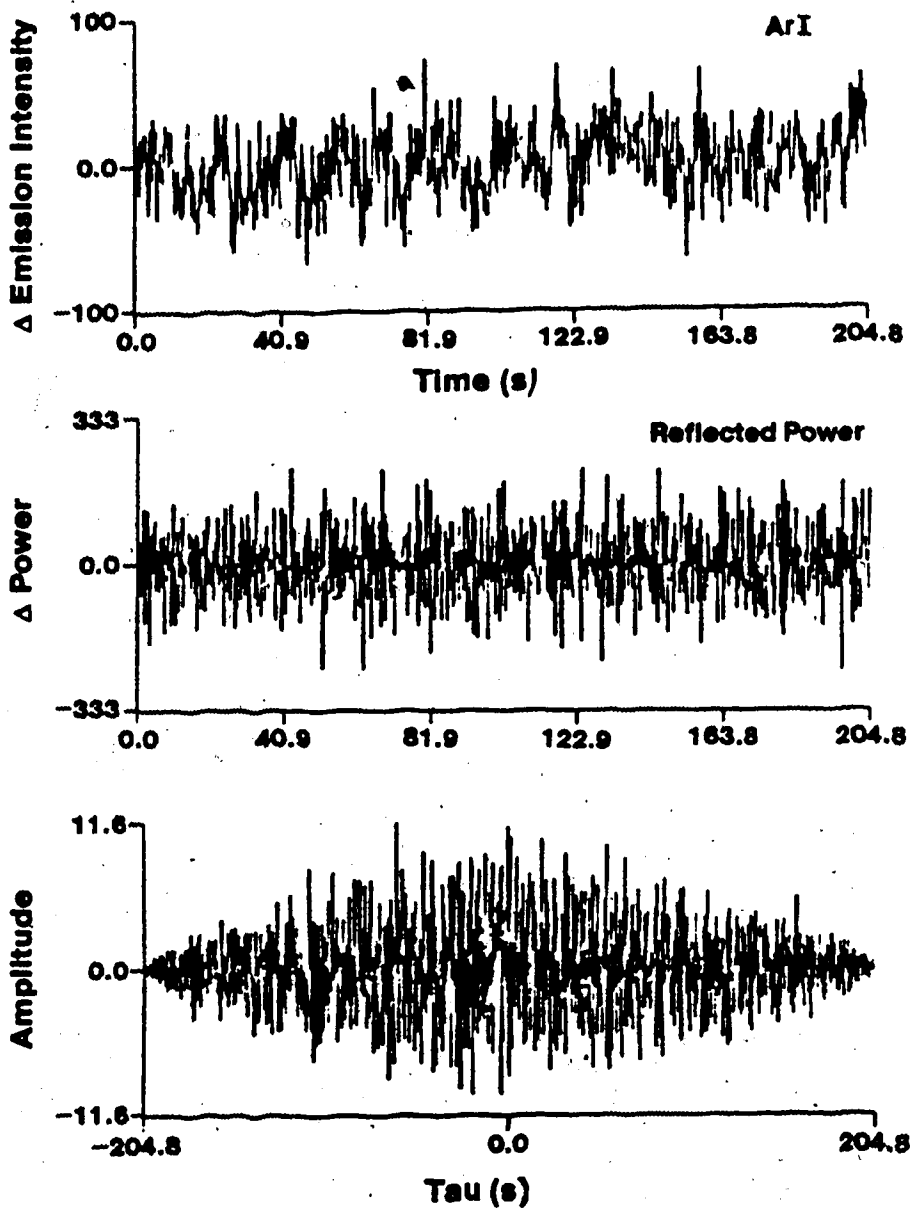


Figure 52. Correlation of ArI emission signal with reflected power.

and reflected power fluctuations.

From this study it can be clearly seen that stability of this RF generator would not be a problem with most low bandwidth measurement systems. With high bandwidth measurement systems (as discussed in Chapter III) the presence of 60 Hz and its harmonics may cause a decrease in precision.

Due to the lack of any detectable (low bandwidth) correlation between either the incident or reflected power fluctuations and emission intensity noise no use could be made of either of these parameters as an internal standard.

## CHAPTER VII

### THE USE OF INTERNAL STANDARDS WITH THE ICP

#### A. The Internal Standard Principle

The internal standard principle was introduced in 1925 by Gerlach (76). The technique involves ratioing the emission intensity of the analyte to that of another element which is present in a fixed or known concentration. This procedure of using the ratio instead of the actual emission intensity to calculate the concentration has a number of potential advantages. Fluctuations of the excitation conditions within the source, ideally, should be compensated for by proportional fluctuations both in the analyte and internal standard emission intensity. The internal standard also compensates for variations in the quantity of sample being presented for analysis or for variations in the rate of sample introduction to the source.

In order to ensure a similar behaviour between the analyte and the internal standard a number of rules have been built up over the years for the choice of a good internal standard element. Ahrens and Taylor (77) summarise these rules, which for convenience are reproduced here.

1. If the internal standard is to be added to the sample,

- its original concentration should be negligibly low.
2. If added to the sample, the internal standard should be in a high state of purity with respect to the elements being determined.
  3. The rates at which internal standard and analysis element volatilize should be very similar.
  4. The atomic weights of the internal standard and the analysis element should not differ greatly if either is a light element.
  5. The ionization energies of the internal standard and analysis elements should be roughly the same.
  6. Both the internal standard and analysis lines should have the same excitation energies.
  7. Both lines should be free of self absorption.
  8. When photographic recording methods are used both lines should be approximately the same wavelength.
  9. The internal standard line should if possible behave in such a way that the intensity ratio of the analysis pair is comparatively insensitive to changes of matrix and composition.

Barnett, Fassel and Kniseley (78) discussed quantitatively the importance of matching some of these factors. In addition they also include the partition function, which is temperature dependent and should be considered when

trying to match the internal standard to the analyte. These rules, however, have been built up around the classical techniques of emission analysis such as the dc arc or the ac spark. When the ICP is used for excitation it may be possible to relax some of these criteria. Self absorption is rarely a problem with the ICP and photographic recording is now seldom used for quantitative purposes. Also, because it is apparent that the major source of ICP flicker noise is the nebulization step it may be possible to relax the rules for matching ionization energies, excitation energies, partition functions and atomic weights.

Internal Standards have met with some success when used with the ICP. Benton-Jones (79) used molybdenum as an internal standard in the analysis of plant tissue ash. He stated that the choice of molybdenum was more for convenience than by design. Watters and Norris (80) observed that the emission intensity variation of the ICP of 1 or 2% relative standard deviation could be reduced to 0.5%, by concurrent ratioing of the intensities to the proper internal standard element. Salin and Horlick (34) investigated the use of SrII and ArI emission as internal standards for calcium. They found that the signal-to-noise ratio improved by a factor of approximately two when

strontium was used but decreased by a factor of two when the argon line was used. Meddings et al. (38) used scandium (1 ppm) as an internal standard for the analysis of twenty five elements. They reported an improvement in the relative standard deviation of their analysis from about 1.1% to 0.5% when a variable tip cross-flow nebulizer was used. However, internal standardization brought about only an improvement from 0.3% RSD to 0.2% RSD when their fixed tip cross-flow nebulizer was used. Uchida et al. (81) used yttrium as an internal standard with a micro-sampling technique to compensate for changes in the amount of sample fed to the plasma.

#### B. Some Statistics Associated with the Use of an Internal Standard

When an internal standard is used, the calculation of concentration ( $c$ ) is based on the ratio of the emission intensity of the analyte ( $x$ ) to that of the internal standard ( $y$ ) and a constant of proportionality ( $k$ ) (78).

$$c = kx/y \quad (26)$$

The noise in the ratio of the emission signals ( $\sigma_{x/y}$ ) is related to the noise in the analyte and internal standard signals ( $\sigma_x$ ) and ( $\sigma_y$ ), the average intensity of the signals



and the correlation coefficient between the signals  
(r) (33).

$$\left(\frac{\sigma_{x/y}}{\sigma_{x/y}}\right)^2 = \left(\frac{\sigma_x}{\sigma_x}\right)^2 + \left(\frac{\sigma_y}{\sigma_y}\right)^2 - 2r \frac{\sigma_x \sigma_y}{\sigma_{xy}} \quad (27)$$

The correlation coefficient expresses a measure of the linear relationship between fluctuations in the analyte and internal standard signals. The value of the correlation coefficient lies in the interval -1 to +1. A value of +1 for the correlation coefficient would indicate a perfect match of noise in the internal standard signal with noise in the analyte signal; under these conditions the right hand side of Equation (27) reduces to zero, which indicates that the internal standard has successfully eliminated the noise.

The correlation coefficient may be calculated from the covariance of the two signals ( $v_{xy}$ ) and their two standard deviations (33).

$$r = \frac{v_{xy}}{\sigma_x \sigma_y} \quad (28)$$

The covariance is calculated:

$$v_{xy} = \frac{\sum xy - \frac{(\sum x)(\sum y)}{n}}{n-1} \quad (29)$$

By making the assumption  $\sigma_{x/x} = \sigma_{y/y}$  (not too unreasonable in the case of the ICP) Equation (27) then becomes:

$$\left(\frac{\sigma_{x/y}}{x/y}\right)^2 = 2\left(\frac{\sigma_x}{x}\right)^2 - 2r\left(\frac{\sigma_x}{x}\right)^2 \quad (30)$$

$$= 2\left(\frac{\sigma_x}{x}\right)^2 (1 - r) \quad (31)$$

If an internal standard brings about an improvement in the precision of an analysis then:

$$\frac{\sigma_{x/y}}{x/y} < \frac{\sigma_x}{x} \quad (32)$$

If this criterion is substituted into Equation (31):

$$\left(\frac{\sigma_x}{x}\right)^2 > 2\left(\frac{\sigma_x}{x}\right)^2 (1 - r) \quad (33)$$

then

$$r > 0.5 \quad (34)$$

This shows that the correlation coefficient between the analyte and internal standard signals must be greater than 0.5 before the internal standard brings about any improvement in precision. If the correlation coefficient is

less than 0.5 then the use of the internal standard will result in a decrease in the precision.

Equation (27) is also useful in predicting the effect of shot noise on the precision when an internal standard is being used. At best, the internal standard can only be expected to remove the effects of flicker noise. There may be a high degree of correlation between the flicker noise present in the analyte and internal standard channels but other noises such as shot noise are of necessity, independent and therefore uncorrelated. Thus, in conditions where flicker noise is dominant the signals may be well correlated ( $r \rightarrow 1$ ) and the internal standard will be very effective in improving the precision. However, as other noises (such as shot noise) become dominant the correlation coefficient decreases in value, until it is less than 0.5 when the use of the internal standard will degrade the precision.

The other case where the internal standard will be of little use is under conditions of low signal-to-background ratio (discussed in Chapter I). Under these conditions fluctuations in the background emission intensity will have an additive effect on either the analyte or internal standard signals. These additive fluctuations will result in an apparent decrease in the correlation coefficient

between the two signals. For this reason it is important when using internal standards to ensure high signal-to-background ratios for both the analyte and internal standard emission lines.

### C. Experimental

To carry out the investigation into the use of internal standards the dual monochromator arrangement (Chapter IV) was utilised. In this system two identical monochromators were mounted at  $90^\circ$  to one another, to view independently the same region of the plasma (Figure 32). This arrangement allowed complete flexibility in the choice of the analyte and internal standard lines that were to be observed. Data from both monochromators were then acquired simultaneously using the dual channel measurement system illustrated in Figure 31.

The data acquisition rate was 5 Hz with the -3 dB point of the Krohn-Hite low pass filters (-48 dB/octave roll-off) set at 2.5 Hz. Normally 1024 data points were collected from which the cross-correlation function and the correlation coefficient were calculated. In addition signal-to-noise ratios were calculated for both the analyte emission signals and the ratio of the analyte emission intensity to that of the internal standard.

The emission lines picked for this study were selected from the tables of both Boumans and Bosveld (40), and Winge, Peterson and Fassel (82). These lines were selected on the basis of their intensity and that no spectral overlap problems were likely. The lines used and the concentrations of the solutions used are listed in Table VII.

#### D. Results From the Use of an Internal Standard

The signals acquired simultaneously from a number of analyte and internal standard elements and the corresponding cross-correlation functions are shown in Figures 53-60. The correlation coefficient, the signal-to-noise ratio of the analyte emission ratioed to that of the internal standard and the improvement in the signal-to-noise ratio brought about by the use of the internal standard are listed in Table VIII.

When the same emission line is used for both the analyte and the internal standard the precision is seen to improve. The correlation coefficients for CaII/CaII (Figure 53), CaI/CaI (Figure 58) and MnII/MnII (not plotted) were 0.9241, 0.8351 and 0.8082. These were a little disappointing as a much higher degree of correlation was expected, considering the same emission line was being

TABLE VII

Spectral Lines and Concentrations Used for  
Internal Standard Study

	<u>nm</u>	<u>ppm</u>
CaII	393.36	1
CaI	422.67	100
MnII	257.61	100
ArI	415.85	-
SrII	407.77	2
InI	451.13	110
ScII	361.38	20

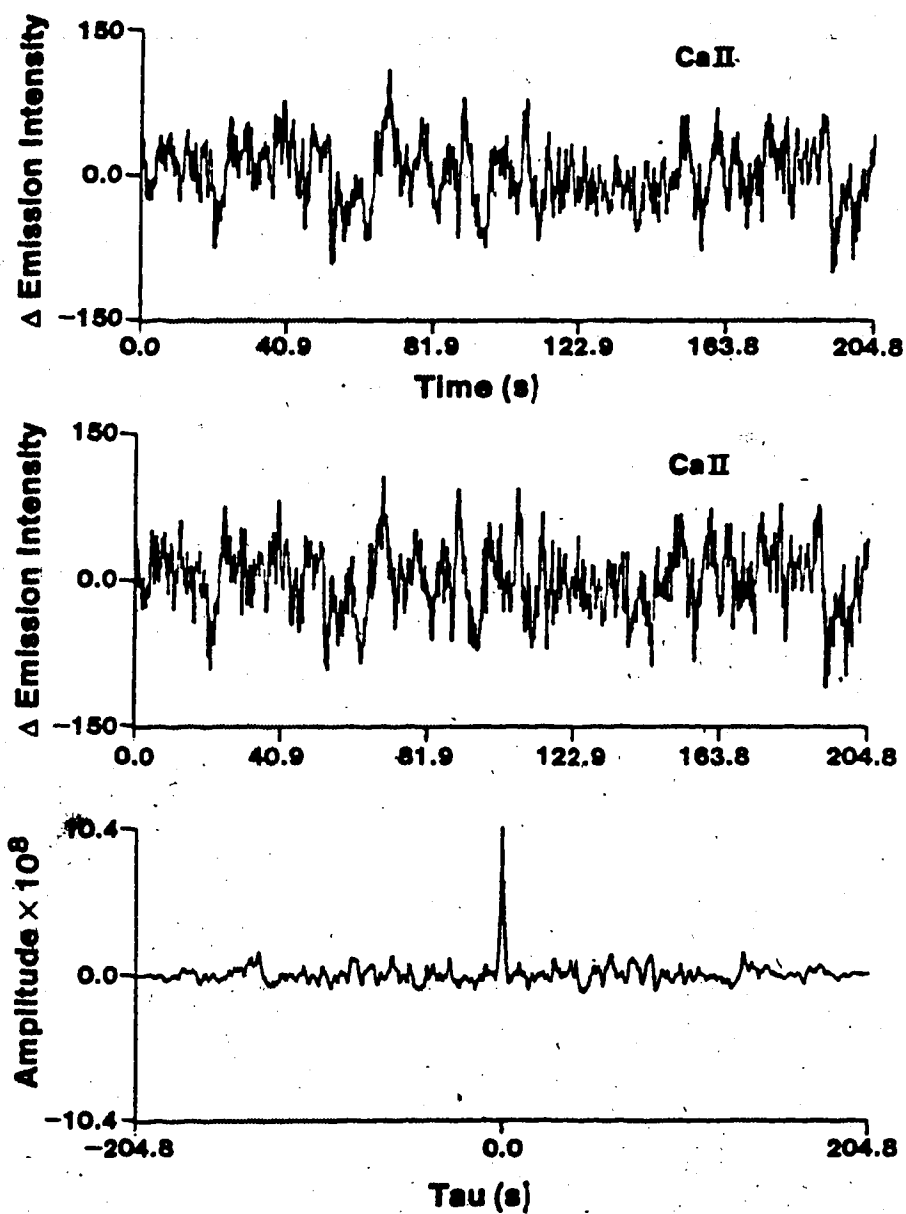


Figure 53. Correlation of CaII emission signals from dual monochromator system.

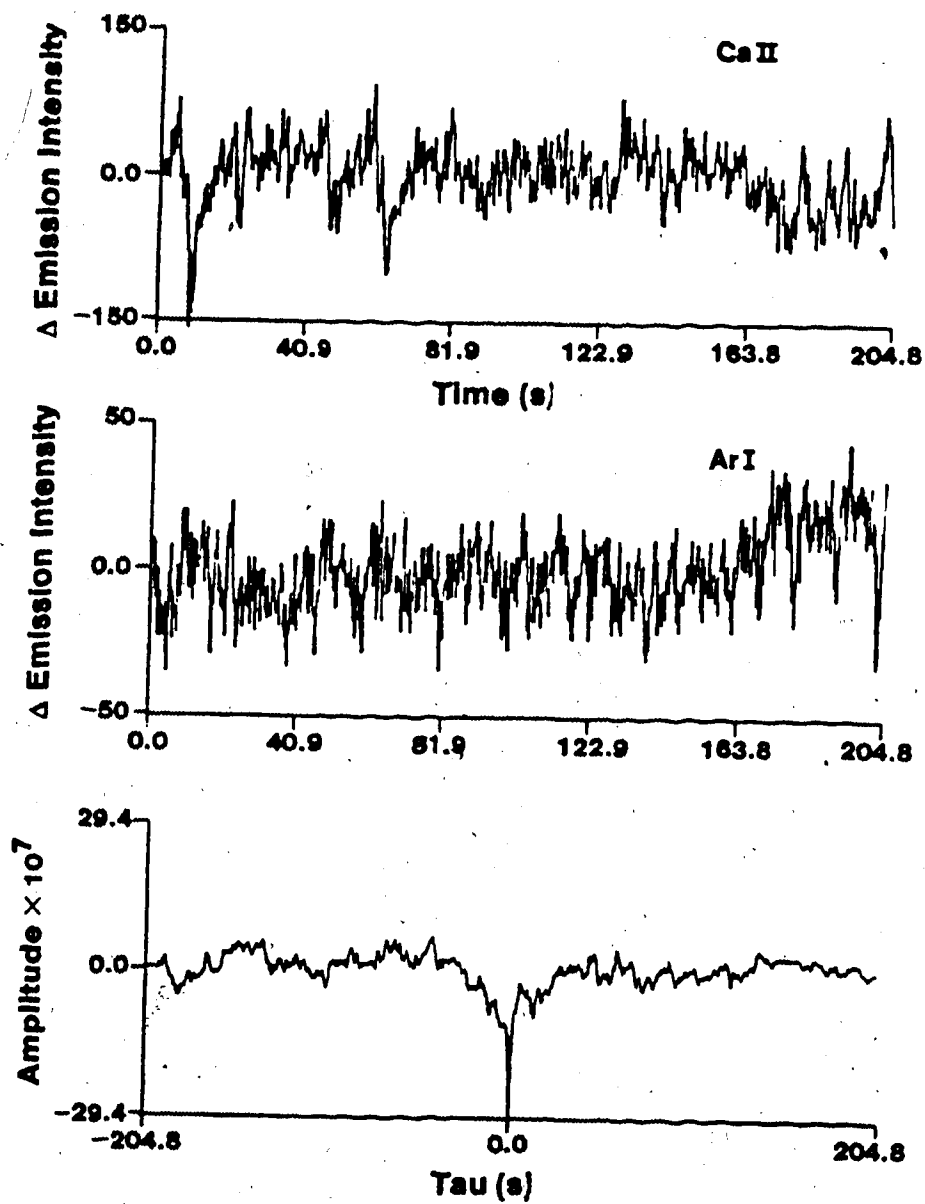


Figure 54. Correlation of CaII and ArI emission signals.



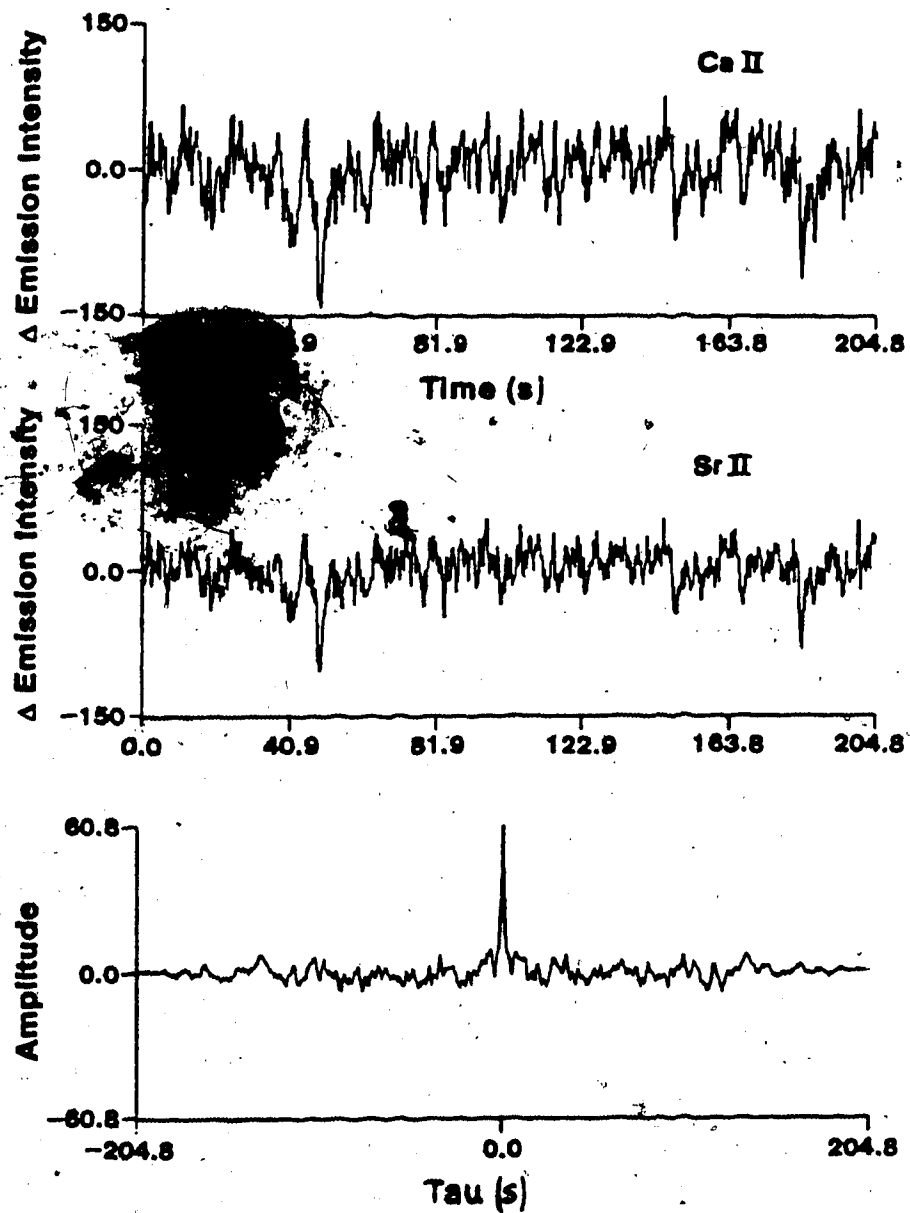


Figure 55. Correlation of CaII and SrII emission signals.

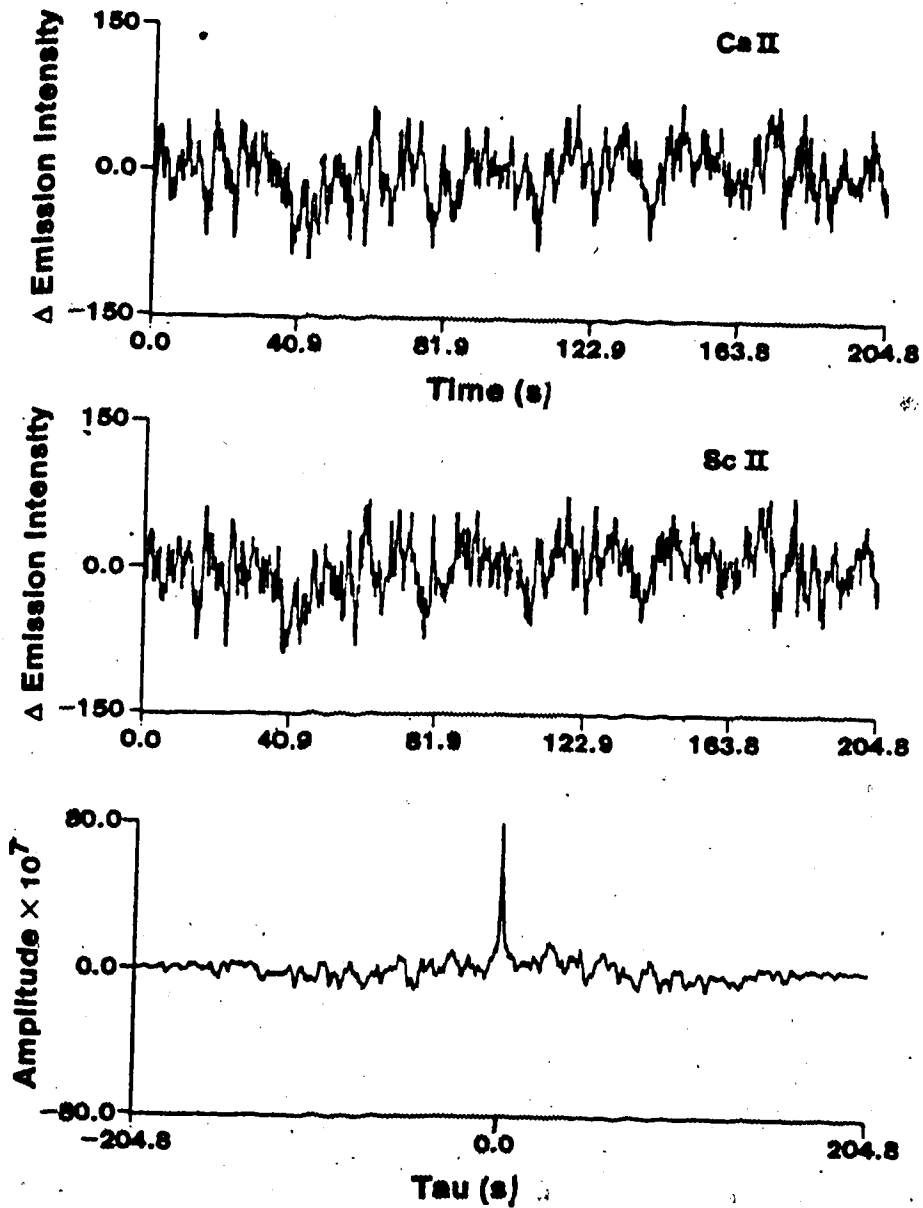


Figure 56. Correlation of CaII and ScII emission signals.

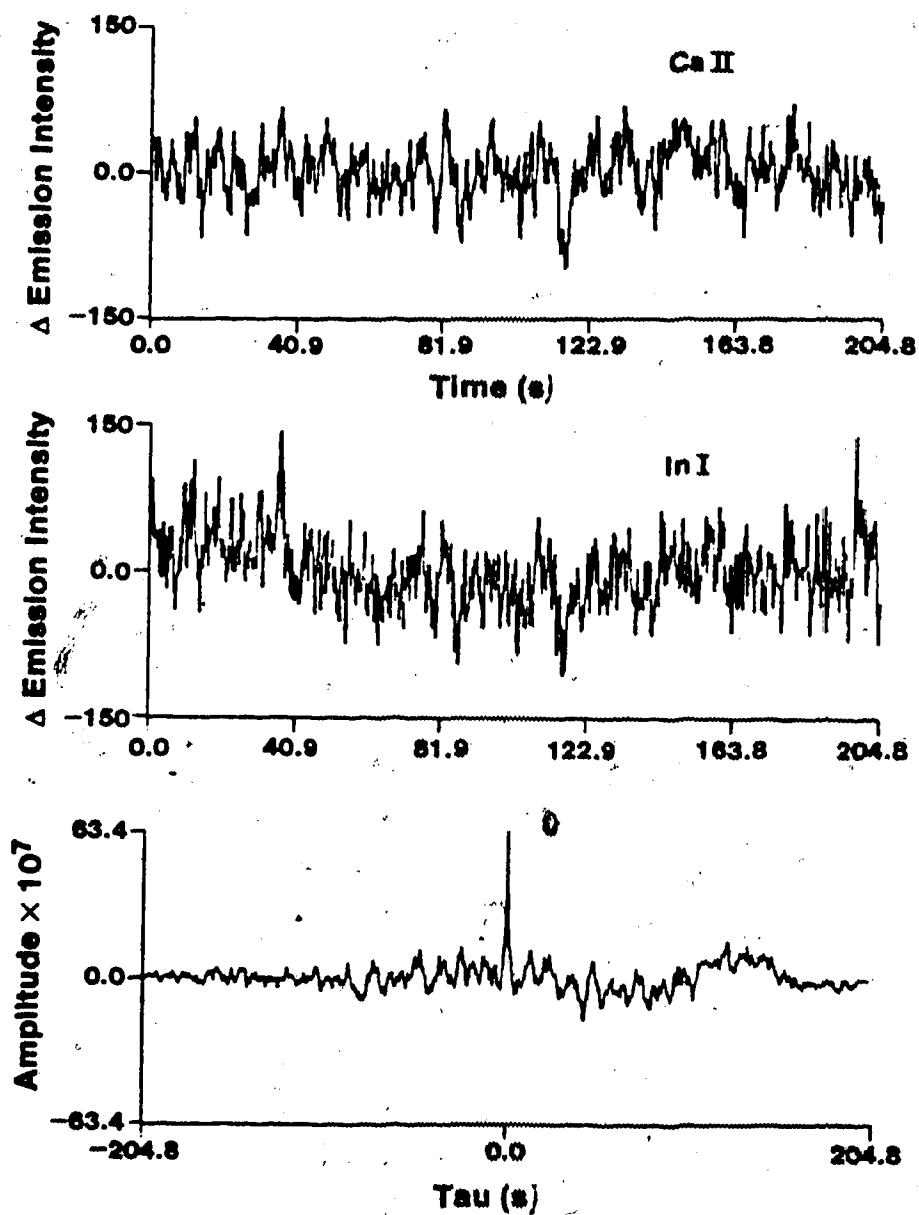


Figure 57. Correlation of CaII and InI emission signals.

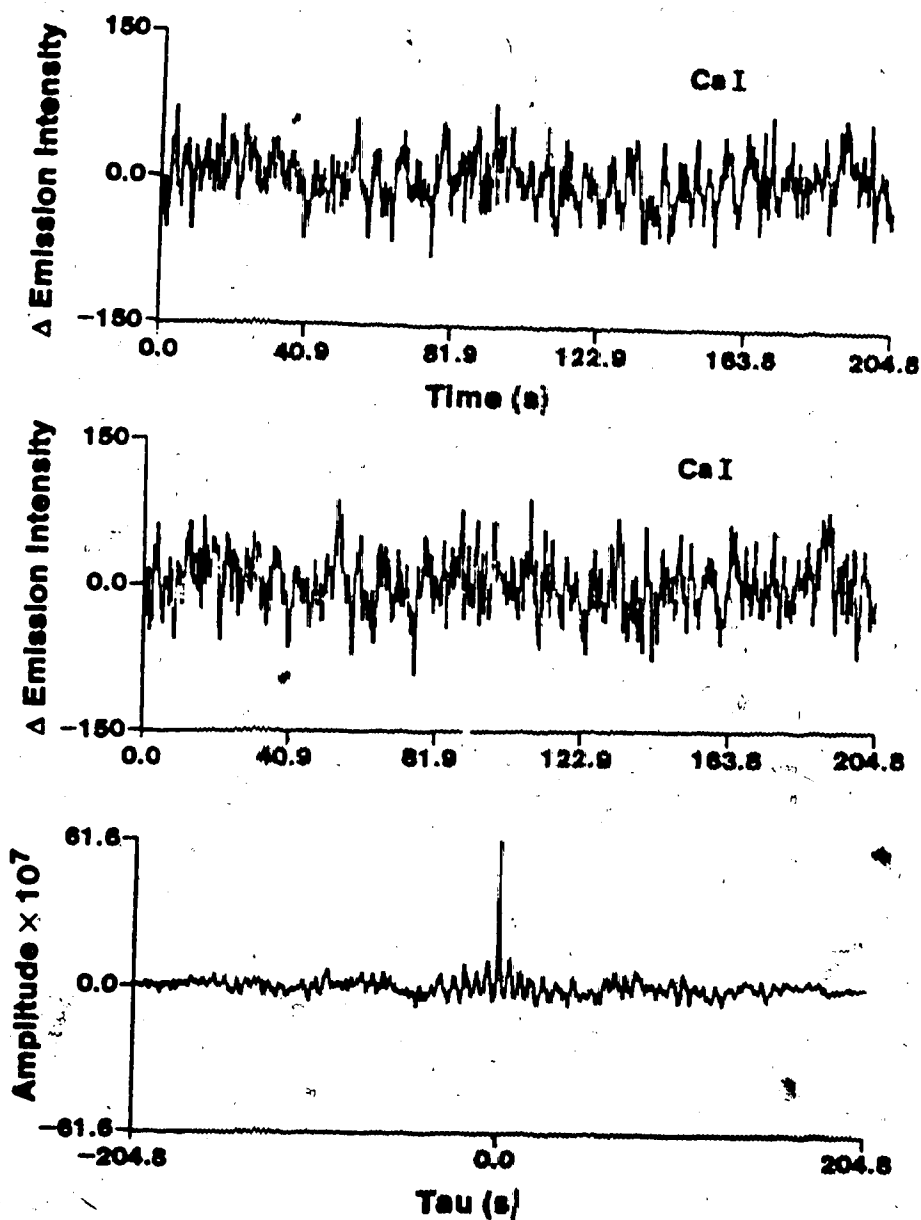


Figure 58. Correlation of CaI emission signals from dual monochromator systems.

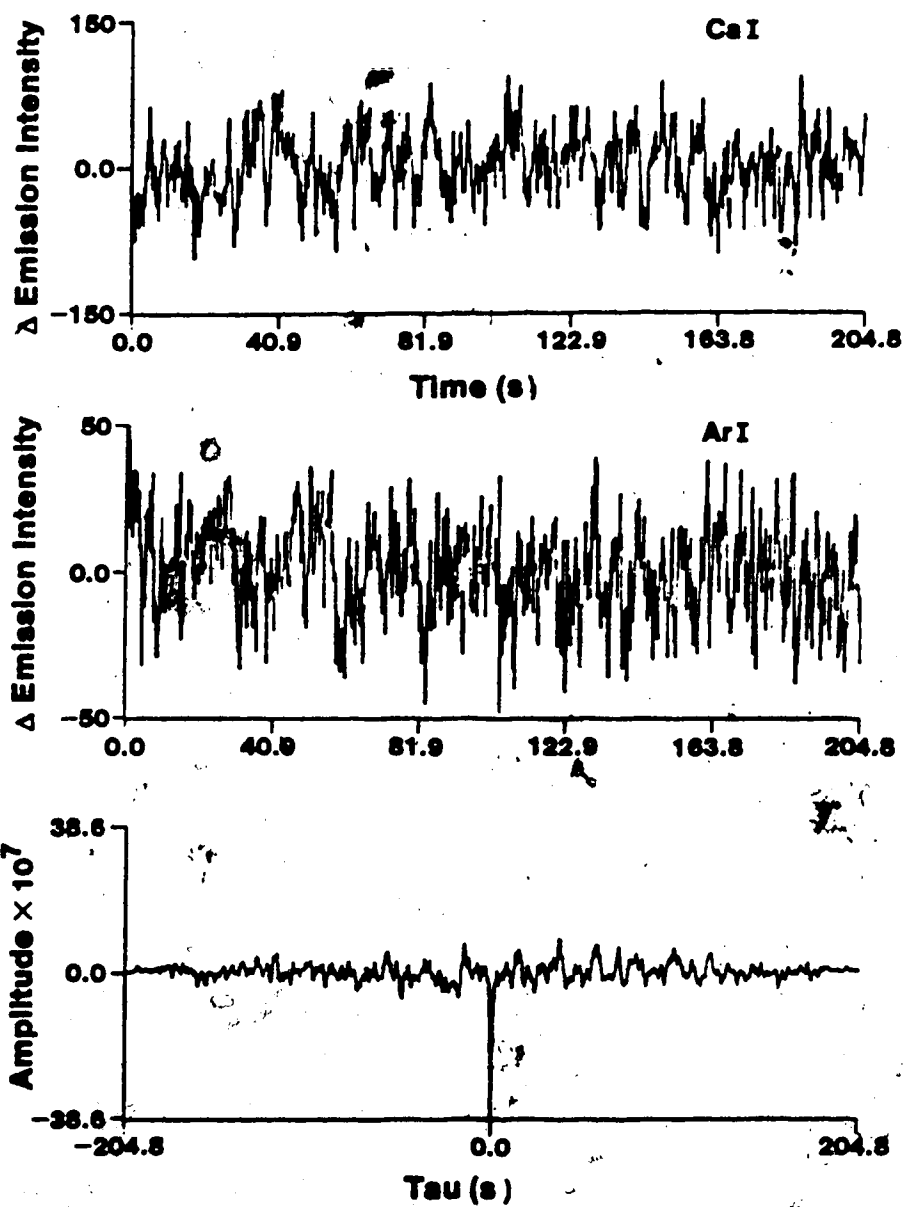


Figure 59. Correlation of CaI and ArI emission signals.

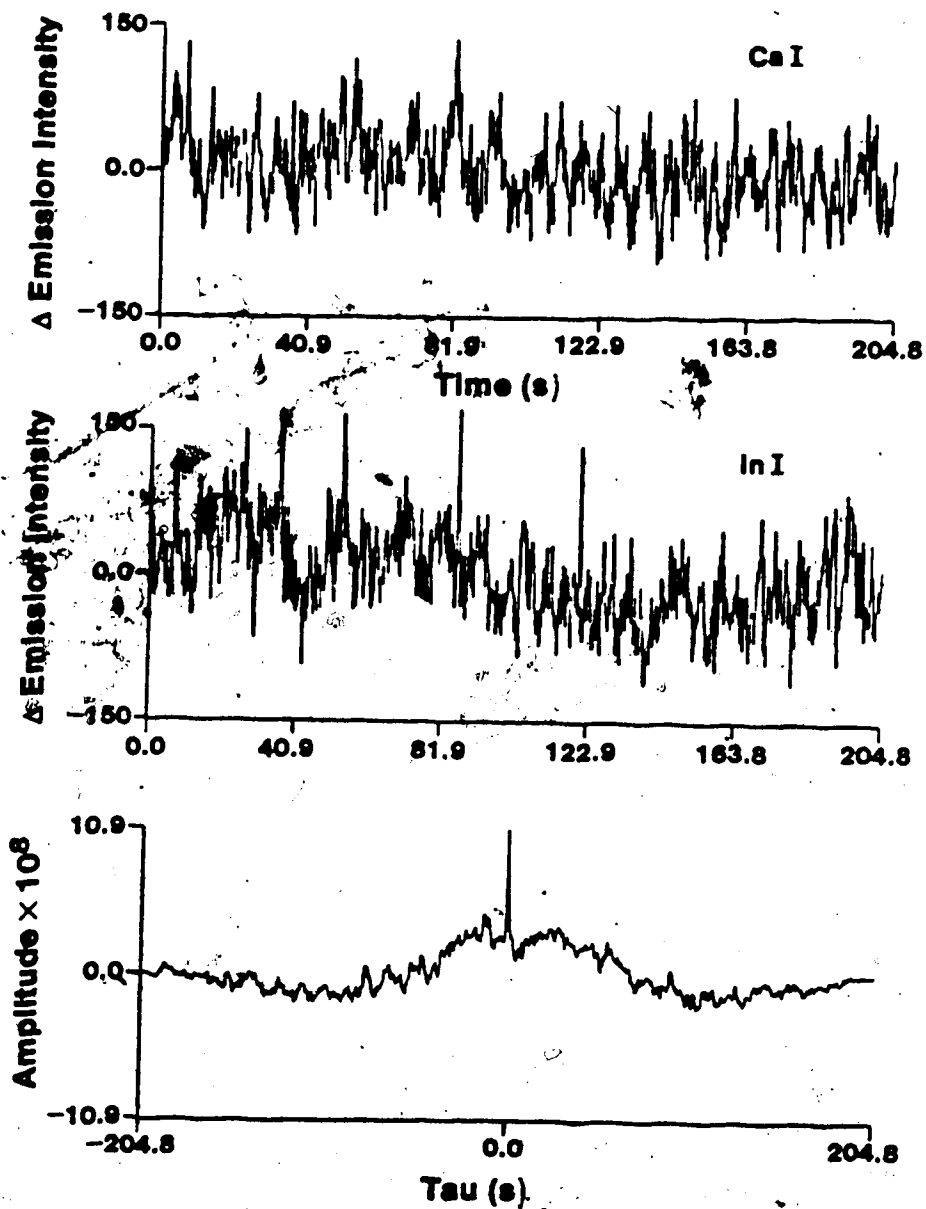


Figure 60. Correlation of CaI and InI emission signals.

TABLE VIII

## Internal Standard Study

Analyte	Internal Std.	r	S/N Analyte	S/N Ratio	Improvement
CaII	CaII	0.9241	103.8	265.8	2.56
CaII	ArI	-0.6063	75.5	49.3	0.65
CaII	SrII	0.9055	114.2	220.2	1.93
CaII	InI	0.6790	120.7	123.9	1.03
CaII	ScII	0.9165	115.8	348.3	3.0
CaI	CaI	0.8351	58.8	111.6	1.90
CaI	ArI	-0.6546	59.7	52.9	0.72
CaI	InI	0.5680	61.3	68.1	1.11
CaI	ScII	0.7043	58.2	85.9	1.48
MnII	MnII	0.8082	141.4	264.6	1.87
MnII	ArI	-0.6433	154.2	76.2	0.49
MnII	InI	0.5676	143.4	113.6	0.79
MnII	ScII	0.8818	141.2	165.8	1.17

monitored simultaneously by the two monochromators. The concentrations used were high enough that additive background noise should not be a problem nor should shot noise. The only remaining factor that is presently perceived as having an influence on these results may be the 90° viewing of the plasma. This, however, may not be the full story. Salin and Horlick (34) reported similar results from the study of two CaII lines (393.3 and 396.8 nm). In the ICP these lines behave almost identically. When the signal-to-noise ratio obtained from one of these lines was compared to that obtained from the ratioed intensities, only a factor of approximately two improvement was noted for the ratioed intensities. These results were obtained using a photodiode array spectrometer, which necessitates viewing the plasma from the same angle for both the analyte and the internal standard. Therefore, it seems likely that some other factor may have a part to play in limiting the ultimate performance of the internal standard.

Other elements when used as internal standards generally provided modest gains in the signal-to-noise ratio performance. Scandium and indium, two elements widely used as internal standards were compared. Strontium was also investigated as an internal standard for calcium



because CaII and SrII have remarkably similar spatial emission characteristics (66).

The cross-correlation functions reveal reasonable correlation of CaII emission signals with those of SrII, ScII and InI (Figures 55, 56 and 57). Correlation coefficients between these signals had values of 0.9055, 0.9165 and 0.6790. This led to modest improvements in the signal-to-noise ratio by a factor of 1.93 and 3.01 when SrII and ScII were used as internal standards. The relatively poorer correlation between CaII emission and InI emission led to only an improvement of factor of 1.03 (or essentially no change in the signal to noise ratio) when it was used as an internal standard. The poor performance of InI as an internal standard for CaII may be due to the quite different behaviour of neutral and ionic species in the plasma (66). However, a better correlation was observed between CaI emission noise and ScII noise than between CaI and InI (Figure 60). On a basis of the difference in behaviour between neutral and ionic species the reverse affect would be predicted. Scandium also proved to be a better internal standard for MnII emission than indium. The correlation coefficients of the MnII signal with ScII and InI signals were 0.8818 and 0.5676. This resulted in a slight improvement in the signal-to-noise ratio by a factor of 1.17 when scandium was used as

the internal standard but when indium was used the signal-to-noise ratio was degraded by about twenty percent.

The emission intensity of ArI was also monitored in an effort to assess its possible use as an internal standard. Also, there has been some interest in monitoring argon emission intensity and using feed back from this signal to control rf power input to the plasma (75). The simultaneously acquired CaII and ArI signals, and the CaI and ArI signals are shown in Figures 54 and 59. The sharp negative peaks present in both cross-correlation functions indicate a marked degree of inverse correlation between the analyte and the argon signals. Negative correlation coefficients were also calculated (see Table VIII). When argon emission intensity was ratioed with that of the analyte, as would be expected from the correlation coefficient, a decrease in precision was noted for CaII, CaI and MnII. These results are in keeping with those of Salin and Horlick (34) who also observed a degree of negative correlation between CaII and ArI emission noise. This negative correlation may result from variations in the nebuliser flow rate. As the rate increases more aerosol is transported to the plasma so that the analyte emission intensity increases. The other effect of the increased aerosol gas flow rate is to blow a larger "hole"

through the centre of the plasma which results in a decrease in the argon emission intensity. Thus it is possible to visualise a likely cause of the inverse correlation of noise in the analyte and argon emission signals.

#### E. Conclusions

From the results presented it is possible to eliminate some of the effects of source flicker noise by the use of a suitable internal standard. Generally, the gain in precision are modest (a factor of two being typical).

While it seems advisable to choose for ionic emission lines an ion line as an internal standard, other factors may have to be considered. The results presented here are limited to only a few elements and emission lines; internal standardisation does seem an area suitable for more extensive study.

## CHAPTER VIII

### SUMMARY

From the experimental results obtained, it is quite clear that the dominant emission noise of the ICP under normal operating conditions is source flicker. Experimentally a major source of this flicker noise was shown to be the nebulization step.

The effect of integration time on the precision of ICP analysis was investigated. No major change in precision was noted for an increase in integration time from 0.01 to 30 seconds. This was true for a number of nebulization systems and for an ultrasonic nebulizer the precision actually worsened with increasing integration time. These results are in keeping with the approximately  $1/f$  nature of the noise power spectrum associated with source flicker.

Noise power spectra were obtained from the ICP operating with a variety of nebulizers. While approximately a  $1/f$  noise power spectrum was observed for all the nebulizers the exact nature of the noise power spectrum in the 0-5 Hz region was dependent on the nebulizer used. In the 0-500 Hz noise power spectra sharp peaks are present at 60 Hz, caused by ripple in the rf generator output.

In addition rather broad but well defined peaks are located in the 200-400 Hz range. The exact frequency that these peaks occur at is dependent on the rf power and plasma gas flow rate. The origin of these peaks appears to be in the rotation of the plasma. This type of noise while not being a problem with low bandwidth integrating type measurement systems may be a problem with wider bandwidth systems. In techniques requiring source modulation such as atomic fluorescence and absorption, care should be taken to avoid choosing a modulation frequency close to these peaks. This high frequency noise is also a problem when dealing with high speed transient signals and when Fourier transform spectrometers are used.

Correlation studies between emission signals and incident and reflected power levels indicate that the rf generator (under normal conditions) is not a major source of ICP noise, apart from introducing some 60 Hz ripple. Reflected power level fluctuations do not bear a measurable correlation to noise in the emission signal.

Monitoring the spray chamber pressure revealed significant pressure fluctuations caused by improper design of the spray chamber drain arrangement. These pressure fluctuations correlated extremely well with similar fluctuations in the emission signals. A "soak-away"

drain arrangement is described which alleviates the spray chamber drain problem and increases the precision of analytical results.

The use of internal standards has been shown to give approximately two fold increases in precision. The use of an argon line as an internal standard proved ineffective and a measurable inverse correlation was observed between analyte and argon emission signals.

The use of internal standardisation appears to warrant further study. The construction of a system in which dual monochromators view the same segment of the plasma (by means of a beam splitter) may be useful, for more accurately comparing the performance of internal standards. A more complete investigation of various other elements and emission lines should reveal which excitation characteristics are important to match when using the internal standard principle with the inductively coupled plasma. Additionally, the effect of integration time and the noise power spectra of the ratioed signals would reveal the effectiveness of the internal standard in removing the  $1/f$  noise components. Indeed, if the use of an internal standard reduces the noise to where shot noise becomes limiting, then the use of long integration times will bring about further increase in the precision of ICP analysis.

## BIBLIOGRAPHY

1. S. Greenfield, I.L. Jones and C.T. Berry, *Analyst*, 89, 713 (1964).
2. R.H. Wendt and V.A. Fassel, *Anal. Chem.*, 37, 920 (1965).
3. T.B. Reed, *J. Appl. Phys.*, 32, 821 (1961).
4. T.B. Reed, *J. Appl. Phys.*, 32, 2534 (1961).
5. V.A. Fassel and R.N. Kniseley, *Anal. Chem.*, 46, 1155A (1974).
7. P.W.J.M. Boumans and F.J. de Boer, *Spectrochim. Acta*, 30B, 309 (1975).
8. S. Greenfield, H.McD. McGeachin and P.B. Smith, *Talanta*, 23, 1 (1976).
9. P.W.J.M. Boumans, L.C. Bastings, F.J. de Boer and L.W.J. van Kollenburg, *Fresenius Z. Anal. Chem.*, 291, 10 (1978).
10. P.W.J.M. Boumans, *Optica Pura y Aplicada.*, 11, 143 (1978).
11. V.A. Fassel, *Anal. Chem.*, 51, 1291A (1979).
12. P.W.J.M. Boumans, *Spectrochim. Acta*, 35B, 57 (1980).
13. H.V. Malmstadt, C.G. Enke, S.R. Crouch with G. Horlick, "Electronic Measurements for Scientists", W.A. Benjamin Inc. 1974.

14. G.L. Walden, J.N. Bower, S. Nikdel, D.L. Bolton and J.D. Windefordner, *Spectrochim. Acta*, 35B, 535 (1980).
15. R.J.J. Zijlstra and C. Th. J. Alkemade, *J. Appl. Phys.*, 27, 656 (1956).
16. G.V. Papayan and Yu.M. Rozanov, *Sov. J. Opt. Technol.*, 36, 97 (1969).
17. D. Wolf, "Noise in Physical Systems", Springer-Verlag, 1978.
18. A. van der Ziel, "Noise: Sources, Characterization, Measurements", Prentice Hall, 1970.
19. F.N.H. Robinson, "Noise and Fluctuations", Clarendon Press, 1974.
20. A. van der Ziel, "Noise in Measurements", John Wiley and Sons Inc., 1976.
21. A. van der Ziel, "Noise", Prentice-Hall Inc., 1954.
22. P.C. Kelly and G. Horlick, *Anal. Chem.*, 45, 518 (1973).
23. D.L. Fried, *Appl. Optics*, 4, 79 (1965).
24. J. Sharpe, "Photoelectric Cells and Photomultipliers", E.M.I. Electronics Ltd., 1961.
25. N.W. Bower and J.D. Ingle, Jr., *Spectrochim. Acta*, 34B, 275 (1979).



26. J.D. Winefordner, R. Avni, T.L. Chester, J.J. Fitzgerald, L.P. Hart, D.J. Johnson and F.W. Plankey, Spectrochim. Acta, 31B, 1 (1976).
27. C. Th.J. Alkemade, W. Snelleman, G.D. Boutilier, B.D. Pollard, J.D. Winefordner, T.L. Chester and N. Omenetto, Spectrochim. Acta, 33B, 383 (1978).
28. C.Th.J. Alkemade, H.P. Hooymayers, P.L. Lijnse and T.J.M.J. Vierbergen, Spectrochim. Acta, 27B, 149 (1972).
29. G.M. Hieftje and R.I. Bystrhoff, Spectrochim. Acta, 30B, 187 (1975).
30. A.G. Gaydon and H.G. Wolfhard, "Flames", Halstead Press, 1979.
31. R.M. Belchamber and G. Horlick, Spectrochim. Acta, (in press).
32. R. H. Hall, Ph.D. Thesis, University of Alberta, 1979.
33. H.H. Ku, J. Research of the Nat. Bureau of Standards-Engineering and Instrumentation, 70C, 263 (1966).
34. E.D. Salin and G. Horlick, Anal. Chem., 52, 1578 (1980).
35. C.Th.J. Alkemade, W. Snelleman, A.D. Boutilier and J.D. Winefordner, Spectrochim. Acta, 35B, 261 (1980).

36. S. Greenfield and D. Thorburn-Burns, Spectrochim. Acta, 34B, 423 (1979).
37. G.D. Boutilier, B.D. Pollard, J.D. Winefordner, T.L. Chester and N. Omenetto, Spectrochim. Acta, 33B, 401 (1978).
38. B. Meddings, H. Kaiser and H. Anderson, International Winter Conference on Developments in Atomic Spectrochemical Analysis, San Juan, 1980.
39. P.W.J.M. Boumans and F.J. de Boer, Spectrochim. Acta, 32B, 365 (1977).
40. P.W.J.M. Boumans and M. Bosveld, Spectrochim. Acta, 34B, 59 (1979).
41. P.W.J.M. Boumans, Spectrochim. Acta, 31B, 147 (1976).
42. P.W.J.M. Boumans, ICP Information Newsletter, 4, 230 (1978).
43. S. Greenfield, ICP Information Newsletter, 4, 199 (1978).
44. R.D. Ediger, W. Stelzer, T.J. Manson and A.R. Knott, Atomic Spectroscopy, ICP Application Study No. 8, 1980.
45. S. Greenfield, H.McD. McGeachin and P. Chambers, ICP Information Newsletter, 3, 117 (1977).
46. R.N. Kniseley, H. Amenson, C.C. Butler and V.A. Fassel, Appl. Spectrosc., 28, 285 (1974).

47. S.A. Myers, D.H. Tracy and R.D. Ediger, Pittsburgh Conference, Atlantic City, 1980, Paper No. 245.
48. H. Anderson, H. Kaiser and B. Meddings, "Development in Atomic Plasma Spectrochemical Analysis", R.M. Barnes, ed., Hayden, Philadelphia, 1981.
49. J.W. Novak, Jr., D.E. Lillie, P.W. Boorn and R.F. Browner, *Anal. Chem.*, 52, 576 (1980).
50. P. Schutyser and E. Janssens, *Spectrochim. Acta*, 34B, 443 (1979).
51. R.H. Scott, V.A. Fassel, R.N. Kniseley and D.E. Nixon, *Anal. Chem.*, 46, 75 (1974).
52. M.W. Blades, Ph.D. Thesis, University of Alberta, 1981.
53. Yu.I. Belyaev, L.M. Ivanstov, A.V. Kopyakin, Pham Hung Phi and V.V. Shemet, *J. Anal. Chem. USSR*, 23, 855 (1968).
54. Y. Talmi, R. Crossman and N.M. Larson, *Anal. Chem.*, 48, 326 (1976).
55. J.D. Ingle, Jr., *Anal. Chem.*, 49, 339 (1977).
56. C.Th.J. Alkemade, Tj. Hollander, K.E.J. Honings, M.A. Koenders and R.J.J. Zijlstra, *Spectrochim. Acta*, 34B, 85 (1979).
57. C.Th.J. Alkemade, Tj. Hollander, H. Snippe and R.J.J.

- Zijlstra, *Spectrochim. Acta*, 36B, 77 (1981).
58. W.K. Yuen, Ph.D. Thesis, University of Alberta, 1978.
59. E.D. Salin and G. Horlick, *Anal. Chem.*, 51, 2284 (1979).
60. J.W. Carr and G. Horlick, *Spectrochim. Acta*, Part B (submitted for publication).
61. R. Hull and G. Horlick, Pittsburgh Conference, Atlantic City, 1980, Paper No. 243.
62. G.L. Malden, Ph.D. Thesis, University of Florida, 1979 (University Microfilms International, Order No. 8016594).
63. D.R. Demers, Pittsburgh Conference, Atlantic City, 1981, Paper Nos. 122/123.
64. G. Horlick, R.H. Hall and W.K. Yuen in "Fourier Transform Infrared Spectroscopy", Vol. 3, J.R. Ferraro and L.J. Basile, Eds., Academic Press (in press).
65. D. Tracy, Perkin-Elmer Corporation. Personal communication, 1980.
66. T.E. Edmunds and G. Horlick, *Appl. Spectrosc.*, 31, 536 (1977).
67. J.D. Chase, *J. Appl. Phys.*, 40, 318 (1969).
68. J.D. Chase, *J. Appl. Phys.*, 42, 4870 (1971).
69. J.L. Genna, R.M. Barnes and C.D. Allemand, *Anal. Chem.*, 49, 1450 (1977).

70. S. Genna and R.M. Barnes, ICP Information Newsletter, 3, 187 (1977).
71. G. Horlick and G.M. Hieftje in "Contemporary Topics in Analytical and Clinical Chemistry", Vol. 3, D.M. Hercules, G.M. Hieftje, L.R. Snyder and M.A. Evanson, Eds., Plenum Publishing Corp., 1978.
72. R.C.L. Ng and G. Horlick, Spectrochim. Acta, Part B, (submitted for publication).
73. R.C.L. Ng, private communication.
74. R.N. Kniseley, G.E. Holland and C.C. Sobel, Pittsburgh Conference, Atlantic City, 1981, Paper No. 403.
75. K. Ohls, ICP Information Newsletter, 4, 83 (1978).
76. W. Gerlack, Z. Anorg. Allgem. Chem., 142, 383 (1925).
77. L.H. Ahrens and S.R. Taylor, "Spectrochemical Analysis", Addison-Wesley Inc., 1961.
78. W.B. Barnett, V.A. Fangel and R.N. Kniseley, Spectrochim. Acta, 23B, 649 (1968).
79. J. Benton-Jones in "Applications of Inductively Coupled Plasmas to Emission Spectroscopy", Ramon Barnes, Ed., Franklin Institute Press, 1977.
80. R.L. Watters, Jr. and J.A. Morris in "Applications of Inductively Coupled Plasmas to Emission Spectroscopy", R. Barnes, Ed., Franklin Press, 1977.

81. H. Uchida, Y. Nojiri, H. Haraguchi and K. Fuwa,  
Anal. Chim. Acta, 123, 57 (1981).
82. R.K. Winge, V.J. Peterson and V.A. Fassel, Appl.  
Spectrosc., 33, 206 (1979).

## APPENDIX A

### USE OF ADDED RANDOM NOISE TO IMPROVE BIT RESOLUTION IN DIGITAL SIGNAL AVERAGING

Digital signal averaging is one of the most common instrumental methods in use today to improve the signal-to-noise ratio of a measurement. It is important to keep in mind that for digital signal averaging to be effective a certain amount of noise *must* be present on the signal. In the absence of noise, an averaged signal will be distorted by quantization effects which result from the finite bit resolution of the analog-to-digital converter (ADC) associated with the digital signal averager, and no amount of averaging can remove these effects or improve measurement precision or accuracy. If a relatively small amount of random noise is present on the signal (standard deviation of the noise equal to about one half of the quantization-level, i.e. least significant bit, of the ADC) then the net effect of quantization is to increase the variance of the signal by  $q^2/12$  where  $q$  is the magnitude of the quantization level (A1-A3). Thus, if quantization effects are severe (i.e. the original signal is noise free

relative to the bit resolution of the ADC) it will be advantageous to add random noise to the signal before averaging the digitized values (A4-A6). In this appendix a simple practical equation is presented that can be used to estimate the effective bit resolution that can be achieved by signal averaging in the presence of added random noise.

As mentioned above, with sufficient noise on a signal the effect of quantization, under signal averaging, is to increase the variance of the signal by  $q^2/12$ . Thus total signal variance ( $V_T$ ) may be expressed as:

$$V_T = \frac{q^2}{12} + (qF)^2 \quad (A1)$$

where  $q$  is the magnitude of the quantization level and  $(qF)^2$  is the variance of the added noise on the signal expressed in units of the quantization level. Thus, in the situation in which the standard deviation (or root-mean-square value) of the added random noise is twice the magnitude of the quantization level, it would be 2. Signal averaging in the presence of random noise improves the signal-to-noise ratio [defined as (signal/standard deviation)] in proportion to the square root of the number



of signal repetitions averaged ( $N^{1/2}$ ), thus the final signal-to-noise ratio  $(\text{SNR})_F$  may be expressed as:

$$(\text{SNR})_F = \frac{S}{q \left( \frac{1}{12} + f_n^2 \right)^{1/2}} \cdot N^{1/2} \quad (\text{A2})$$

where  $S$  is the magnitude of the signal. It is instructive to express Equation (A2) in terms of effective bit resolution  $(\text{BR})_{\text{eff}}$  of the final signal-to-noise ratio, i.e.

$$\log_2 [(\text{SNR})_F]$$

$$(\text{BR})_{\text{eff}} = \log_2 \left( \frac{S}{q} \right) - \frac{1}{2} \log_2 \left( \frac{1}{12} + f_n^2 \right) + \frac{1}{2} \log_2 N \quad (\text{A3})$$

The first term of Equation (A3) represents the bit resolution of a single measurement. It is important to emphasize that this is not equal to the bit resolution of the ADC but is proportional to the relative magnitude of the signal to the quantization level of the ADC. The full bit resolution of an ADC is only utilized when the signal fills the dynamic range of the ADC. The second term represents the loss in bit resolution due to quantizing effects and the level of added noise. The third term represents the build-up of bit resolution that results from signal averaging when the least significant bit of the ADC is randomized.

A simple microprocessor controlled data logger (A7) was used to obtain data to test Equation (A3). This system is described in detail in Appendix B and was based on the Intel 8748. It contained an 8 bit successive approximation ADC with a dynamic range of 0-10 V and a quantization level of 39 mV. The ADC was front-ended by a sample-and-hold amplifier. Eight bit conversions could be acquired at a rate of 4.4 kHz and up to 65,536 successive conversions could be summed. The sum was accumulated with triple precision (i.e. 24 bits). Finally, 32 repeat measurements of the summed conversions were automatically acquired and logged to a teletype by this system.

Input dc and analog test signals were generated using a 16 bit digital-to-analog converter (Data Systems DAC-169). Using this DAC voltage levels over the range 0-10 V could be generated that could be continuously altered in steps as small as 0.153 mV. This DAC was used to provide a stable test signal to which various levels of random noise were added. A General Radio 1390B random noise generator was used as the noise source. The DAC and noise signals were summed together with an operational amplifier.

Test signals were generated consisting of a 5 volt dc

level upon which was superimposed 20 mV, 40 mV and 80 mV rms random noise (5 Hz to 20 kHz bandwidth). These noise levels correspond to  $f = 0.5, 1$  and  $2$ . The data logger was used to acquire 32 repeat measurements of one ADC conversion and 32 repeat measurements of 10, 100, 1000, 10,000 and 65,536 summed ADC conversions. Based on the 32 repeat measurements the standard deviation ( $\sigma$ ) of the acquired signal in each case could be calculated and the signal-to-noise ratio ( $\bar{S}/\sigma$ ) evaluated. The resulting values expressed in terms of bit resolution ( $\log_2(\bar{S}/\sigma)$ ) are presented in Table AI along with those calculated from Equation (A3). The agreement is quite good. Thus, if the measurement situation is amenable to signal averaging, the effective bit resolution of an ADC can be significantly improved if averaging is carried out in the presence of sufficient random noise. Equation (A3) is useful in estimating the benefit to be gained.

This improvement in bit resolution is further illustrated in Figure A1. The DAC was again used to provide a test signal, but this time the output of the DAC was set at 2.500 V and then incremented in 2.5 mV intervals to 2.550 V. The data logger was used to measure 1000 summed conversions at each incremental value, with and without added random noise (20 mV rms  $\equiv f = 0.5$ ). Without

TABLE A1

## Bit Resolution of ADC Measurements

Conversions Summed	Effective Precision of ADC (BITS)	
	<u>EXPERIMENTAL</u>	<u>EQUATION A3</u>
<u>f=0.5</u>		
1	7.6	6.8
10	8.5	8.5
100	9.9	10.1
1000	12.1	11.8
10000	13.8	13.4
65536	14.4	14.8
<u>f=1.0</u>		
1	6.1	5.9
10	7.6	7.6
100	9.1	9.2
1000	11.1	10.9
10000	12.5	12.6
65536	13.6	13.9
<u>f=2.0</u>		
1	4.5	5.0
10	6.7	6.7
100	8.6	8.3
1000	10.1	10.0
10000	11.5	11.6
65536	12.7	13.0

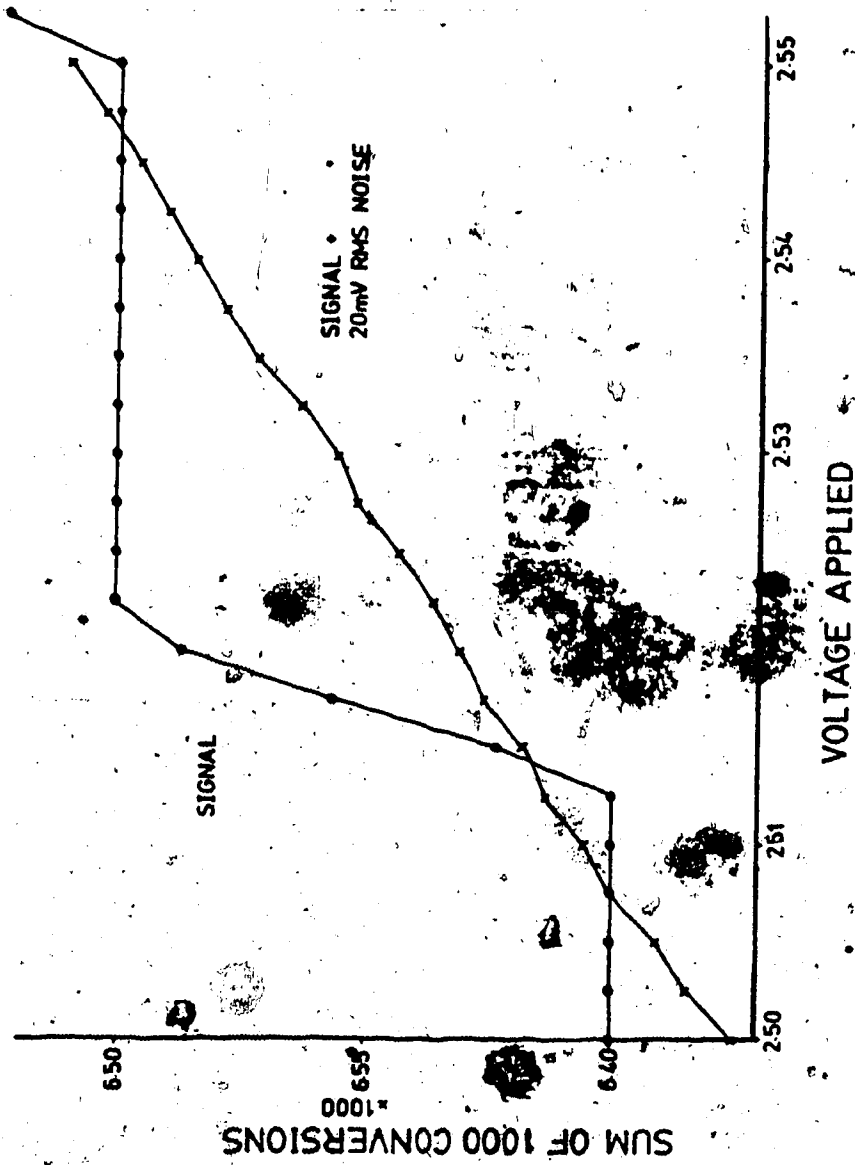


Figure A1. Bit resolution improvement of 8 bit ADC to 12 bits by signal averaging and added random noise.

added random noise the 8-bit ADC of the data logger can clearly only resolve signal changes of at least 39 mV (i.e. the value of the least significant bit) even if digitized values are summed. From Table AI, with 20 mV rms added random noise and 1000 summed conversions the effective bit resolution should improve to about 12-bits, making the least significant bit equivalent to about 2.5 mV. It can be seen in Figure A1 that 12-bit resolution is achieved because 2.5 mV incremental changes in DAC output are accurately measured when averaging is carried out in the presence of this level of added random noise.

The examples presented were based on an 8-bit ADC because this is the most convenient word length to manipulate in the interface to 8-bit microprocessors. In addition some manufacturers have developed microprocessors with self-contained 8-bit ADC's and DAC's. Examples are the Intel 8022 and 2920. With the considerations discussed here one need not think of these systems as limited to 8-bit precision or resolution when used for data acquisition. All considerations presented are, of course, equally applicable to higher resolution conversions. In fact the incremental cost in moving from a 12-bit converter to a 16-bit converter is quite high. Thus, if data acquisition time allows, signal averaging can be used to

achieve the desired higher bit resolution. Finally, the considerations presented in this appendix lead to some interesting conclusions about lower resolution converters. If the signal is noisy enough one should be able to relax the bit resolution specification of the ADC. In fact with very noisy signals it is possible to relax your specifications all the way to a one bit converter, i.e. a comparator or threshold detector. This measurement approach has recently been discussed in the literature (A8) and such one bit converters have been successfully utilized to facilitate the digital data acquisition of repetitive noisy signals at very high sampling rates (A9).

## BIBLIOGRAPHY - APPENDIX A

- A1. B. Widrow, Trans. Amer. Inst. Elec. Eng., 77, pt II, 555 (1961).
- A2. P.C. Kelly and Gary Horlick, Anal. Chem., 45, 518 (1973).
- A3. L.M. Schwartz, Anal. Chem., 52, 1141 (1980).
- A4. I. Coleman, J. Opt. Soc. Amer., 56/8, IV (1966).
- A5. J. Butterworth, P.E. MacLaughlin and B.C. Moss, J. Sci. Instrum. 44, 1029 (1967).
- A6. G. Horlick, Anal. Chem., 47, 352 (1975).
- A7. R. Delchamber and G. Horlick, Talanta (submitted for publication).
- A8. Z.L. Kovacs, IEEE Trans. Instrum. Meas., IM-28, 152 (1979).
- A9. T.G. Schmalz and W.H. Flygare, "Coherent Transient Microwave Spectroscopy" in "Laser and Coherence Spectroscopy", edited by J.I. Steinfeld, Plenum Press, N.Y., 1978, p. 136.



## APPENDIX B

### DATA LOGGING SYSTEM BASED ON THE INTEL 8748

#### SINGLE CHIP MICROCOMPUTER

One of the most common data logging tasks in the laboratory is the acquisition of repeat measurements of an averaged or integrated signal. A versatile way to integrate a signal is through the summation of a large number of rapidly acquired digitized signal values (B1). For example, if a measurement system is capable of acquiring digitized signal values at a rate of 1000 conversions per second, it is simply necessary to sum 10, 100, 1000, or 10,000 conversions to obtain precise signal integration periods ranging from 10 msec to 10 sec. A simple microprocessor based system was developed to acquire integrated values in this fashion.

The microprocessor chosen for this application was the Intel 8748. This is a so called single chip microcomputer in that it contains, in one integrated circuit, all the main functional units of a complete computer (B2), i.e. a central processing unit (CPU), input/output (I/O) ports, a timer/event counter, random access memory (RAM) and read only memory (ROM). The specific features of the 8748 are summarized in Table BI and a block diagram of

## TABLE BI

## Summary of 8748 Features

1. Full 8-bit central processing unit
2. Data memory (RAM) - 64 words × 8 bits
3. Program memory (EPROM) - 1024 × 8 bits
4. Input/Output Ports
  - (a) Ports 1 and 2
    - each 8 bits wide
    - all pins independently programmable as either input or output
    - outputs latched
    - inputs not latched
  - (b) Bus Port
    - 8 bit bidirectional port
    - all pins either input or output
    - outputs latched
    - inputs not latched
5. Input lines
  - 3 input lines T0, T1 and testable with the conditional jump instruction and INT an interrupt
6. Timer/Counter
  - 8 bit binary presettable counter

the chip is shown in Figure B1.

The 8748 is one chip in the "8048" family of single component 8-bit microcomputers (B3). A summary of the "8048" family of microcomputers is presented in Table BII. The 8748 is the development chip for the 8048. The difference between the two chips is that the 8748 has erasable programmable read only memory (EPROM) while the 8048 is strictly ROM based, i.e. it must be factory programmed. In general, the 8048 family was developed for high volume control applications and once a user has developed a set program using the 8748 or the 8035 or 8039 with off chip RAM or EPROM, factory mask programmed 8048's or 8049's can be manufactured. Within this family the 8022 (see Table BII) seems almost ideal for laboratory data acquisition as it contains an on chip analog-to-digital converter (ADC). However, this chip is again ROM based limiting its usefulness to quantity users. Thus, the 8748 is the only single chip microcomputer in this family that can be effectively utilized by unit quantity users. However, as outlined in Table BI, it has excellent features and capabilities that should allow the development of a very compact intelligent data acquisition system with a minimal number of integrated circuits.

The Intel Prompt 48 unit was used for system develop-

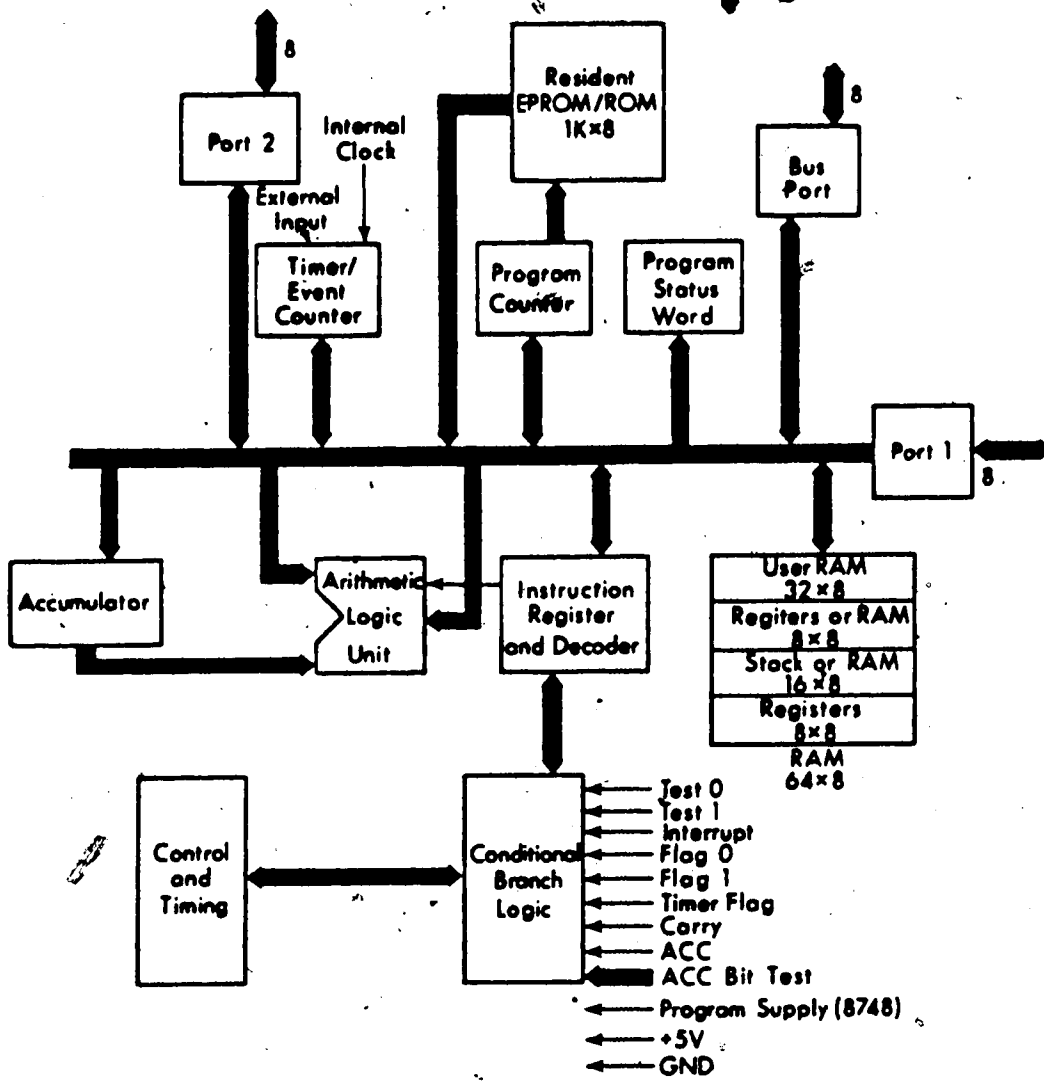


Figure B1. Block diagram 8748.

TABLE BII

## "8048" Family-Single Component Microcomputers

- 8048 - 1k×8 ROM, 64×8 RAM, 27 I/O lines, 8-bit timer/counter, full CPU
- 8748 - EPROM version of 8048
- 8035 - 8048 without on-chip ROM
- 8049 - 2k×8 ROM, 128×8 RAM, version of 8048
- 8039 - 8049 without on-chip ROM
- 8021 - 1k×8 ROM, 64×8 RAM, 21 I/O lines, 8-bit timer/counter, full CPU
- 8022 - 2k×8 ROM, 64×8 RAM, 28 I/O lines, on-chip 8 bit ADC with sample-and-hold and two multiplexed input channels

ment, program debugging, and EPROM programming. It should be noted that the 8048 family has its own language that is not compatible with 8080/85's.

A schematic diagram of the data acquisition system is shown in Figure B2. It consists of a sample-and-hold amplifier, an analog-to-digital converter and the 8748 microprocessor. The teletype interface for the 8748 is shown in Figure B3. These circuits were breadboarded using a Model ADD-8000 analog-digital designer available from E & L Instruments. This unit provides SK-10 breadboard cards for circuit construction which fit into a mainframe containing power supplies, logic level switches and indicators, a voltage reference source and a function generator.

The sample-and-hold amplifier (AD582) and the analog-to-digital converter (AD571) were obtained from Analog Devices. The sample-and-hold amplifier has a combined aperture and settling time (to 0.01%) of about 0.6  $\mu$ sec and an acquisition time of about 6  $\mu$ sec. The AD571 is a 10 bit successive approximation ADC with a conversion time of 25  $\mu$ sec. Only the eight most significant bits were used in this application. This significantly simplified both the hardware aspects of data acquisition and software complexity which was particularly important as programming

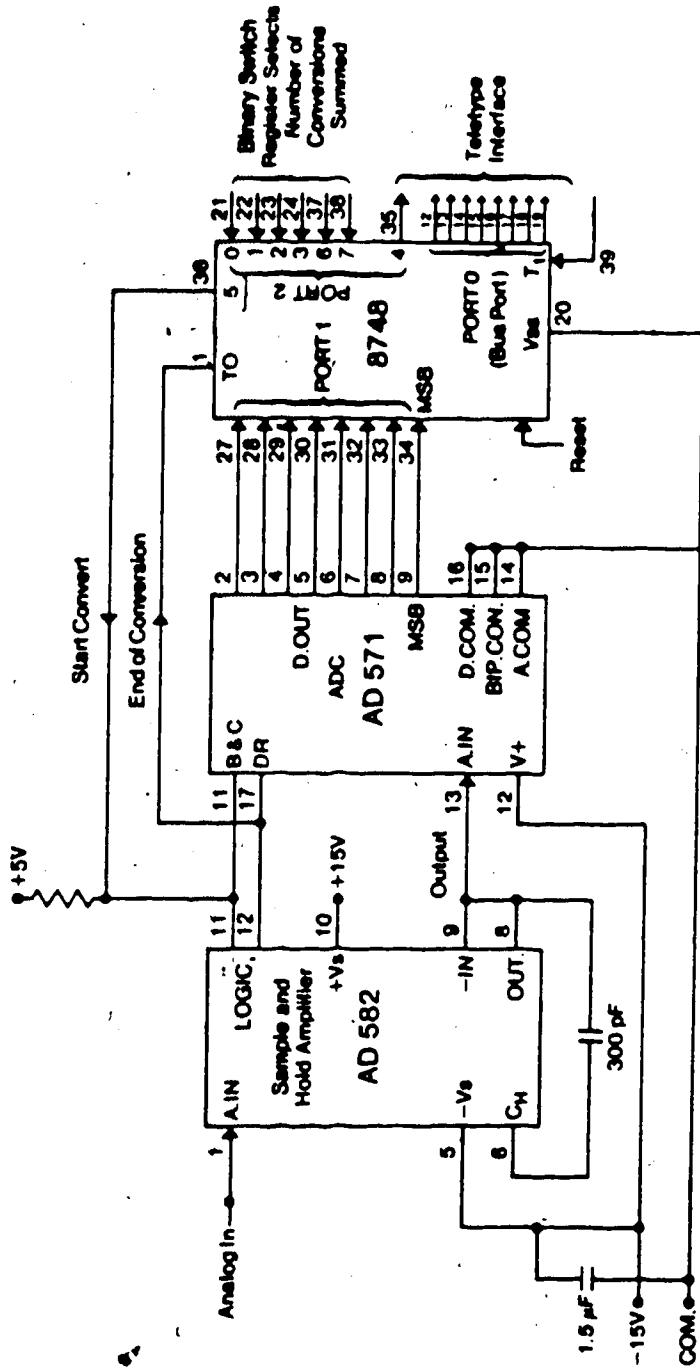


Figure B2. Schematic diagram of data acquisition system.

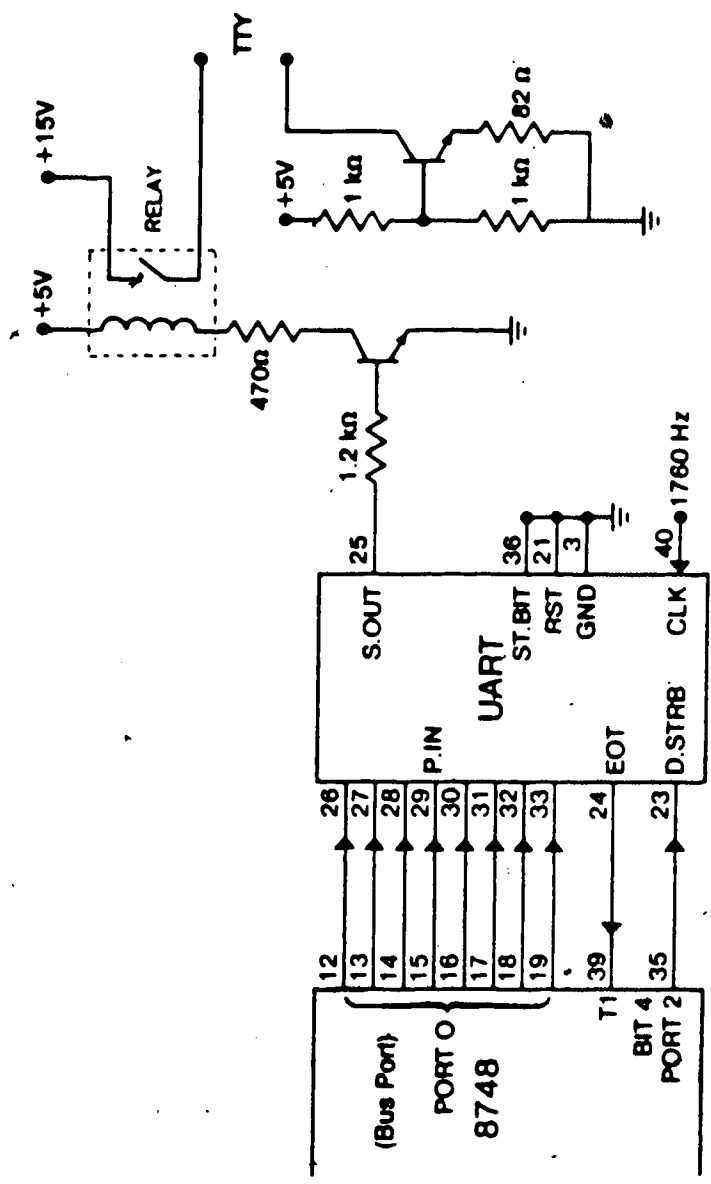


Figure B3. Schematic diagram of 8748-teletype interface.



space was at a premium. An 8-bit conversion provides adequate resolution when a large number of conversions are summed to provide an integrated signal value. This point is discussed and illustrated in Appendix A and reference (B4). The dynamic range of the ADC was set at 0-10 V resulting in a quantization limit of 39 mV. The eight digital lines from the ADC were interfaced to the 8748 through Port 1.

The sample-and-hold amplifier and the analog-to-digital converter were interconnected as recommended in literature supplied by Analog Devices (B5). A conversion is initiated by a positive pulse generated at bit 5 of Port 2. This puts the sample-and-hold amplifier in the hold mode and triggers the ADC. The amplifier is held in the hold mode by the  $\overline{DR}$  (NOT data ready) line of the ADC which remains high during conversion. The return of the  $\overline{DR}$  to the low state at the end of conversion is sensed at the TO input line of the 8748 and the 8-bit value is read into the 8748. At the same time the sample-and-hold amplifier returns to the track mode.

Inside the 8748 the new 8-bit value is added to the sum of the previous conversions. The addition is carried out in triple precision (24 bits). This allows a maximum of 65,536 full scale 8-bit ADC conversions to be ac-

cumulated. After the addition, the program checks to see if the requested number of conversions have been summed, and if not, initiates another conversion. The number of conversions to be summed in order to achieve the desired signal integration period is hardware set at pins of Port 2 which are read at the start of the data acquisition program. Application of a positive logic level at the appropriate pin selects 1, 10, 100, 1000, 10000 or 65,536 conversions to be summed. When the selected number of conversions has been summed the 24-bit binary sum is converted to an 8-digit BCD number and output to the teletype. The basic data rate for conversion was 4.4 kHz, thus a summation of 65,536 conversion represents an integration period of about 15 sec. Also the acquisition of replicate integrated measurements was programmed into the software. For our applications 32 replicate integrated measurements were automatically sequenced and logged to the teletype. This enabled the reliable calculation of statistical quantities of the measured values such as standard deviation and signal-to-noise ratios. Unfortunately, this simple 8748 system was not large enough to do such calculations directly.

The 8748 was interfaced to the teletype by means of a universal asynchronous receiver transmitter (UART) (B6)

via the bus port, Port 0. See Figure B3. The output routine converts the BCD digits to 7-bit ASCII code which the UART then transmits in a serial manner to the teletype. The transmission of a character is initiated by application of a positive pulse to the data strobe input of the UART from bit 4 of Port 2 on the 8749. The UART must be externally clocked at a rate appropriate for the device to which data is being sent. Teletypes operate at 110 baud (110 bits/sec). The clock frequency, provided by the function generator on the ADD-8000 breadboard system, was set at 1760 Hz. This is the correct input frequency in order to allow the UART to transmit data at 110 baud. When transmission of a single character is complete the end of transmission (EOT) line of the UART is sensed at the T1 input line of the 8748 and the next character is output. The rest of the circuitry in Figure B3 provides the 20 ma current loop used to interface the UART to the teletype (B6).

In this application the teletype was used as a passive printer and information could not be transmitted to the 8748 from the teletype. One practical reason was the fact that the unexpanded 8748 did not contain sufficient programming space to accommodate the necessary programs. On the other hand, this was also in keeping with the basic

philosophy of keeping the system small. We did not want a system that required inputs from an expensive device such as a teletype in order to function. That is also why, in fact, a simple switch register was used to select the integration period.

In conclusion, the 8748 single chip microcomputer can be used to develop simple intelligent data logging systems. The system discussed and illustrated here consists of only four integrated circuits, the sample-and-hold amplifier, the analog-to-digital converter, the 8748 and the UART. It is capable of acquiring digitized signal values with a resolution of 8-bits at rates up to 4.4 kHz. Pre-selected numbers of conversion can be summed to obtain integrated signal measurements. Summation is carried out in triple precision (24 bits) and up to 32 replicate measurements can be sequentially acquired and logged, in BCD format, to a serial terminal such as a teletype.

## BIBLIOGRAPHY - APPENDIX B

- B1. M.W. Blades and G. Horlick, Talanta (submitted for publication).
- B2. G. Horlick, Talanta (submitted for publication).
- B3. MCS-48 Microcomputer Users Manual, Intel Corporation, 3065 Bowers Ave., Santa Clara, CA 95051.
- B4. R.M. Belchamber and G. Horlick, Talanta (submitted for publication).
- B5. Analog Devices, Route 1, Industrial Park, P.O. Box, 280, Norwood, Mass. 02062. AD571 Product Information.
- B6. D.G. Larsen and P.R. Rony, "Bugbook IIA, Using the Universal Asynchronous Receiver/Transmitter", E & L Instruments, Inc., Derby, Conn. 06418, 1975.

## APPENDIX C

### SOFTWARE DEVELOPED FOR DATA ACQUISITION AND PROCESSING

The software for data acquisition and processing listed here are written in Fortran IV and Macro assembly language; for implementation on PDP 11/10 minicomputers. While the majority of the programs can be run on computers with 16 k bytes core, the Fourier transform routine requires a 32 k bytes core.

The programs are documented. Program RMBINT allows background subtracted signals to be acquired from a photomultiplier tube and integrated for specified periods. This program uses sub-routine RBPROG written in assembly language to actually acquire and integrate the signal.

The program RMBPMT is part of the noise power spectra package. It allows time series data to be collected from a photomultiplier tube. A specified number of scans may be collected so that signal averaging may be carried out after the Fourier transformation step. Sub-routine AQUIRE written in assembly language is used for the actual data acquisition step. This sub-routine was written for simultaneous dual channel data acquisition using external sample-and-hold amplifiers. However, in this particular application only one channel is utilised.

After acquisition by program RMBPMT data is d.c. level subtracted, apodised and Fourier transformed by program RBFFTP. This program also provides signal averaging ability, after the Fourier transformation.

Noise power spectra are finally plotted using the plotting routine RBPLOT.

Dual channel data acquisition for correlation studies was achieved by the use of program CORPMT and sub-routine AQUIRE. CORPMT not only allows dual channel data to be acquired simultaneously but also calculates the correlation coefficient between the two sets of data.

```

C      RMBINT
C      .PMT SIGNAL INTEGRATION ROUTINE
C
C      FILES REQUIRED
C      1) RBPROG
C      2) 131 BLOCK FORTRAN LIBRARY (FORLIN)
C
C      DIMENSION SIGN(100),BSR(100),STDEV(100),SNR(100)
C      DOUBLE PRECISION ARRAY(100),RRPTS,SUM,SMSQ
C      COMMON /RON/JINT,IBL,IBH
C      MNEX=0
1000   MNEX=MNEX+1
C      WRITE(7,14)
14     FORMAT(' ', 'INPUT INTEGRATION TIME.')
C      READ(5,16)TIME
16     FORMAT(F6.2)
C      WRITE(7,18)
18     FORMAT(' ', 'DO YOU REQUIRE BACKGRND SUBTRACTION Y=1 N=0 .')
C      READ(5,20)IBACK
20     FORMAT(I1)
C      WRITE(7,22)
22     FORMAT(' ', 'INPUT NUMBER OF REPEATS.')
C      READ(5,24)MRPTS
24     FORMAT(I3)
C      IF (IBACK.EQ.0) GO TO 1006
1005   WRITE(7,26)
26     FORMAT(' ', 'ENTER 0 FOR BACKGROUND 1 FOR SAMPLE.')
C      READ(5,20)ISOB
1006   JINT=IFIX(TIME*1000.0)
C      NRPTS=MRPTS
C
C      CALLS MACRO DATA ACQUISITION ROUTINE
C
C      WRITE(7,28)
28     FORMAT(' ', 'ENTER CR TO START AQUISITION.')
C      READ(5,20)ISTR
1015   CALL RBCONV
C
C      (CONVERTS TWO WORD INTEGER DATA TO FLOATING POINT
C
C      ARRAY(NRPTS)=DBLE(FLOAT(IBL))+DBLE(FLOAT(IBH))*32768.0
C
C      OUTPUTS DATA AS IT ARRIVES
C
C      N=NRPTS-NRPTS+1
C      WRITE(7,66)N,ARRAY(NRPTS)
66     FORMAT(I5,5X,E16.7)
C      NRPTS=NRPTS-1
C      IF (NRPTS.NE.0) GO TO 1015
C
C      THIS SECTION CALCULATES MEAN AND STD.DEV. OF ARRAY
C
C      SUM=0.0
C      DO 100 NRPTS=1,MRPTS
C      SUM=SUM+ARRAY(NRPTS)
100    CONTINUE
C      SMSQ=0.0

```



```

DO 200 NRPTS=1,MRPTS
SMSQ=SMSQ+ARRAY(NRPTS)**2
200 CONTINUE
RRPTS=DBLE(FLOAT(MRPTS))
AURG=SNGL(SUM/RRPTS)
STDEV(MNEX)=SNGL(DSQRT((SMSQ-SUM**2/RRPTS)/(RRPTS-1.0)))
C
C THIS SECTION SORTS OUT SIGNAL OR BACKGROUND DATA
C
IF(IRACK.EQ.0) GO TO 1020
IF(ISOB.EQ.1) GO TO 1025
WRITE(7,30)AURG,STDEV(MNEX)
30 FORMAT(' ',10H BACKGRND=,E10.4,12H STD-DEV=,E10.4)
BAKVAL=AURG
GO TO 1005
1020 BAKVAL=0.0
1025 SIGN(MNEX)=AURG
BSR(MNEX)=SIGN(MNEX)-BAKVAL
SNR(MNEX)=BSR(MNEX)/STDEV(MNEX)
WRITE(7,32)MNEX,BSR(MNEX),STDEV(MNEX),SNR(MNEX)
32 FORMAT(' ',I3,1X,'SIGNAL=',E10.4,4X,'STD-DEV=',E10.4,4X,'SNR=',
1 E10.4)
1027 WRITE(7,34)
34 FORMAT(' ',TYPE 1 TO EXIT ,2 TO RUN PROGRAM AGAIN ,3 TO LIST')
READ(5,20)IRUN
GO TO (1040,1000,1300) IRUN
1030 WRITE(7,36)
36 FORMAT(' ',
SIGNAL BSSIGNAL STD-DEV SNR//)
DO 700 NEX=1,MNEX
WRITE(7,38)NEX,SIGN(NEX),BSR(NEX),STDEV(NEX),SNR(NEX)
38 FORMAT(' ',I3,3X,E10.4,3X,E10.4,3X,E9.3,3X,E9.3)
700 CONTINUE
GO TO 1027
1040 STOP
END

```

```

.TITLE RBPROG
.MCALL ..V2...REGDEF
..V2..
.REODEF
.GLOBAL RBCONV

ADSR=170400
ADBF=170402
CKSR=170404
CKPR=170406

;
;
RBCONV: MOV      JINT,R0          ;SET CONVERSION COUNTER
;
;
MOV      #176027,CKPR          ;RATE TO CLK PRESET REGISTER
MOV      #000403,CKSR          ;SET CLK STATUS REGISTER
MOV      #000000,R2            ;CLEAR REGISTER 2
MOV      #000000,R3            ;CLEAR REGISTER 3
LP2:    MOV      #000040,ADSR    ;START CONVERSION CHO
LP1:    TSTR     ADSR            ;CHECK FOR EOC
;
;
BPL      LP1                    ;LOOP
MOV      ADBF,R4                ;MOVE DATA TO REGISTER 4
ADD      R4,R2                  ;PERFORM INTEGRATION
ADC      R3                      ;TAKE CARE OF OVER FLOW
DEC      R0                      ;DECREMENT CONVERSION COUNTER
BNE      LP2                    ;LOOP FOR NEXT CONVERSION IF REQD
;
;
ASL      R3                      ;CONVERTS DATA TO FORTRAN I FORMAT
ROL      R2
ADC      R3
CLC
ROR      R2
MOV      R2,IBL
MOV      R3,IBH
;
;
.EVEN
.CSECT  RON
JINT:   .WORD  0
IBL:   .WORD  0
IBH:   .WORD  0
.CSECT
.EVEN
END:   .END  RBCONV
*

```

```

C      RMBPMT.FOR
C      DATA ACQUISITION
C
C      SUBROUTINES NEEDED:
C      (1)AQUIRE
C      (2)SYSLIB
C      (3)FORLIN
C
C
C      DIMENSION TITLE(3),DAT(3)
C      COMMON /RON/ JNP,JSR,JCR,IA(1032) /RMR/ IR(1032)
C
C      INPUT ACQUISITION PARAMETERS
C
C      20      CALL DATE(DAT)
C              WRITE(7,5010)
C      5010      FORMAT(' ', ' ENTER NUMBER OF DATA SETS REQUIRED')
C              READ(5,5020) NFILE
C      5020      FORMAT(I4)
C              WRITE(7,5030)
C      5030      FORMAT(' ', ' INPUT SAMPLE NAME')
C              READ(5,5040) TITLE
C      5040      FORMAT(3A4)
C              WRITE(7,5050)
C      5050      FORMAT(' ', ' INPUT NUMBER OF POINTS')
C              READ(5,5020) JNP
C              WRITE(7,5060)
C      5060      FORMAT(' ', ' INPUT CLOCK RATE', //, ' 2=1 MHZ', //, ' 4=100 KHZ', //,
C      1' 6=10 KHZ', //, ' 8=1 KHZ', //, ' 10=100 HZ', //, ' 14=60 HZ' //)
C              READ(5,5020) IMCR
C              WRITE(7,5070)
C      5070      FORMAT(' ', ' INPUT NUMBER OF CLOCK PULSES BETWEEN SAMPLES')
C              READ(5,5020) JSR
C
C      SET UP LPS CLOCK STATUS REGISTER PARAMETERS
C
C      JCR=(IMCR+257)
C
C      CALCULATE ACQUISITION FREQUENCY
C
C      IF (IMCR.EQ.2) FREQ=1000000.0/FLOAT(JSR)
C      IF (IMCR.EQ.4) FREQ=100000.0/FLOAT(JSR)
C      IF (IMCR.EQ.6) FREQ=10000.0/FLOAT(JSR)
C      IF (IMCR.EQ.8) FREQ=1000.0/FLOAT(JSR)
C      IF (IMCR.EQ.10) FREQ=100.0/FLOAT(JSR)
C      IF (IMCR.EQ.14) FREQ=60.0/FLOAT(JSR)
C      IFREQ=IFIX(FREQ)
C
C      ACQUIRE DATA WITH SUBROUTINE AQUIRE
C
C      5080      WRITE(7,5080)
C              FORMAT(' ', ' CR TO START ACQUISITION')
C              READ(5,5020) I
C              DO 500 IFILE=1,NFILE
C              CALL AQUIRE
C
C      FORMS TEMPORARY DATA FILE ON DISC

```

```

JFILE=IFILE+20
IA(JNP+1)=JNP
IA(JNP+2)=IFREQ
IA(JNP+3)=IA(1)
IA(JNP+4)=1
IA(JNP+5)=IA(1)
IA(JNP+6)=1
CALL ASSIGN(JFILE)
WRITE(JFILE)(IA(I),I=1,JNP)
ENDFILE JFILE
CALL CLOSE(JFILE)
500 CONTINUE
C
C PROGRAM CONTROL
C
90 WRITE(7,5090)
5090 FORMAT(' ',///' STORE DATA =1. PFRUN =2. EXIT =3')
READ(5,5020) J
GO TO (10,20,30) J
C
C COMPOUNDS DATA FILES & FORMS PERMANENT DATA FILE ON DISC
C
10 WRITE(7,6000)
6000 FORMAT(' ', ' ENTER DE:FILE.DAT FOR STORAGE'//)
CALL ASSIGN(2,'DK:FTN2.DAT',-1,'NEW','NC'-1)
WRITE(2) NFILE
WRITE(2) JNP
WRITE(2) IFREQ
WRITE(2)(DAT(I),I=1,3)
WRITE(2)(TITLE(I),I=1,3)
DO 600 JFILE=21*NFILE+20
CALL ASSIGN(JFILE)
READ(JFILE)(IA(I),I=1,JNP)
WRITE(2)(IA(I),I=1,JNP)
ENDFILE JFILE
CALL CLOSE(JFILE)
600 CONTINUE
ENDFILE 2
CALL CLOSE(2)
GO TO 90
30 STOP
END
*
```

```

.TITLE TWO CHANNEL ADC
.MCALL ..V2...REODEF
..V2..
.REODEF
.GLOBL AQUIRE

```

```

ADSR=170400
ADBF=170402
CKSR=170404
CKPR=170406
DBUF=170414
DBSR=170410

```

```

AQUIRE: MOV     JNP,R0           #NUMBER OF POINTS TO R0
          CLR     DBSR           #CLEAR DIGITAL BUFFER STATUS REGISTER
          MOV     #177777,DBUF   #CAUSE ANALOG DATA TRACK
          NEG     JSR           #TWO'S COMPLEMENT
          MOV     JSR,CKPR       #RATE TO CLOCK PRESET
          MOV     JCR,CKSR       #SET CLOCK STATUS REGISTER
          MOV     #IA,R2         #SET ADDRESS ARRAY IA
          MOV     #IB,R3         #SET ADDRESS ARRAY IB

LP3:     TSTB    CKSR           #CHECK CLOCK
          BPL     LP3           #LOOP
          MOV     JCR,CKSR       #RESET MODE FLAG

          MOV     #177776,DBUF   #CAUSE ANALOG DATA HOLD
          CLR     ADRF           #CLEAR A/D BUFFER
          MOV     #000001,ADSR   #SELECT CHANNEL 0
LP1:     TSTB    ADSR           #CHECK FOR ADC
          BPL     LP1           #LOOP
          MOV     ADRF,(R2)+     #STORE DATA ARRAY IA

          CLR     ADRF           #CLEAR A/D BUFFER
          MOV     #000401,ADSR   #SELECT CHANNEL 1
LP2:     TSTB    ADSR           #CHECK FOR ADC
          BPL     LP2           #LOOP
          MOV     ADRF,(R3)+     #STORE DATA ARRAY IB
          MOV     #177777,DBUF   #CAUSE ANALOG DATA TRACK

          DEC     R0             #DECREMENT POINT COUNTER
          BNE     LP3           #LOOP IF NOT ZERO
          NEG     JSR           #TWO'S COMPLEMENT

          .EVEN
          .CSECT RDN
JNP:     .WORD   0
JSR:     .WORD   0
JCR:     .WORD   0

```

```
IA:  .BLKW  1032
      .CSECT RMB
IB:  .BLKW  1032
      .CSECT
      .EVEN
END: .END  ACQUIRE
*
```

```

C      RFFFTP.FOR
C      FLOATING POINT FAST FOURIER TRANSFORM
C
C      FILES REQUIRED:
C      (1)SYSLIB
C      (2)FORLIB
C      (3)LPSLIB
C
C      DIMENSION X(1100),Y(1100),L(20)
C      DIMENSION DAT(3),TITLE(3),AU(20)
C      INTEGER ID(1100)
C      CALL DATE(DAT)
1200    WRITE(7,1200)(DAT(I),I=1,3)
C      FORMAT(' ',3A4)
C      WRITE(7,1000)
1000    FORMAT(' ','ENTER DE:FILE.DAT FOR STORAGE'/' ')
C      CALL ASSIGN(12,'DK:FTN12.DAT',-1,'NEW','NC',1)
C      WRITE(7,1100)
1100    FORMAT(' ','ENTER DE:FILE.DAT FOR DATA'/' ')
C      CALL ASSIGN(10,'DK:FTN10.DAT',-1,'OLD','NC',1)
C      WRITE(7,2000)
2000    FORMAT(' ','APODIZATION? 0 FOR NO, OTHERWISE FACTOR')
2100    READ(5,2100) IAPOD
C      FORMAT(I1)
C      READ(10) NF
C      READ(10) NP
C      READ(10) NS
C      READ(10)(DAT(I),I=1,3)
C      READ(10)(TITLE(I),I=1,3)
C      WRITE(12) NF
C      WRITE(12) NP
C      WRITE(12) NS
C      WRITE(12)(DAT(I),I=1,3)
C      WRITE(12)(TITLE(I),I=1,3)
1300    WRITE(7,1300)(DAT(I),I=1,3)
C      FORMAT(' ',DATE: ',3A4)
1400    WRITE(7,1400)(TITLE(I),I=1,3)
C      FORMAT(' ',TITLE: ',3A4)
C      WRITE(7,1600) NF
1600    FORMAT(' ',NUMBER OF SETS OF DATA: ',I4)
C      WRITE(7,1700) NP
1700    FORMAT(' ',NUMBER OF DATA PER SET: ',I4)
C      WRITE(7,1800) NS
1800    FORMAT(' ',SAMPLING FREQUENCY OF DATA ACQUISITION: ',I7,
*      HZ'/' ')
C      CALL ASSIGN(14,'DK:FTN14.DAT',12,'SCR','NC',1)
C      DO 1500 IF=1,NF
C      CALL LED(IF,'15')
C
C      DC LEVEL SUBTRACTION
C
C      READ(10)(ID(I),I=1,NP)
C      SUM=0.0
C      DO 100 I=1,NP
C      X(I)=FLOAT(ID(I))
C      SUM=SUM+X(I)
100    CONTINUE
C      SUM=SUM/FLOAT(NP)

```

```

DO 200 I=1,NP
X(I)=X(I)-SUM
200 CONTINUE
AV(IF)=SUM
C
C APODISATION
C
IF(IAPOD.EQ.0) GO TO 2600
FACTOR=FLOAT(IAPOD)
ZPD=512.0
DO 2500 I=1,NP
DDUM0=ABS(FLOAT(I)-ZPD)/(FLOAT(NP)-ZPD)
DDUM1=EXP(-FACTOR*DDUM0**2)
X(I)=X(I)*DDUM1
2500 CONTINUE
C
C DC LEVEL SUBTRACTION
C
SUM=0.0
DO 120 I=1,NP
SUM=SUM+X(I)
120 CONTINUE
SUM=SUM/FLOAT(NP)
DO 220 I=1,NP
X(I)=X(I)-SUM
220 CONTINUE
C
C FFT ALGORITHM
C
2600 NPT=NP/2
N=NP
DO 2 I=1,NPT
X(I)=X(I*2-1)
2 Y(I)=X(I*2)
DO 3 I=NPT+1,NP
Y(I)=0.0
3 X(I)=0.0
N2POW=10
NTHPOW=2**N2POW
N4POW=N2POW/2
IF(N4POW)60,63,60
60 DO 61 IPASS=1,N4POW
NXTLTH=2**(N2POW-2*IPASS)
LENGTH=4*NXTLTH
SCAL=6.2831853/FLOAT(LENGTH)
DO 61 J=1,NXTLTH
ARG=FLOAT(J-1)*SCAL
C1=COS(ARG)
S1=SIN(ARG)
C2=C1*C1-S1*S1
S2=C1*S1+C1*S1
C3=C1*C2-S1*S2
S3=C2*S1+S2*C1
DO 61 ISQLOC=LENGTH,NTHPOW,LENGTH
J1=ISQLOC-LENGTH+J
J2=J1+NXTLTH
J3=J2+NXTLTH
J4=J3+NXTLTH
R1=X(J1)+X(J3)
R2=X(J1)-X(J3)
R3=X(J2)+X(J4)
R4=X(J2)-X(J4)
FI1=Y(J1)+Y(J3)
FI2=Y(J1)-Y(J3)
FI3=Y(J2)+Y(J4)
FI4=Y(J2)-Y(J4)

```



```

X(J1)=R1+R3
Y(J1)=FI1+FI3
64 IF(J-1)64,62,64
X(J3)=C1*(R2+FI4)+S1*(FI2-R4)
Y(J3)=-S1*(R2+FI4)+C1*(FI2-R4)
X(J2)=C2*(R1-R3)+S2*(FI1-FI3)
Y(J2)=-S2*(R1-R3)+C2*(FI1-FI3)
X(J4)=C3*(R2-FI4)+S3*(R4+FI2)
Y(J4)=-S3*(R2-FI4)+C3*(R4+FI2)
62 GO TO 61
X(J3)=R2+FI4
Y(J3)=FI2-R4
X(J2)=R1-R3
Y(J2)=FI1-FI3
X(J4)=R2-FI4
Y(J4)=R4+FI2
61 CONTINUE
63 IF(N2POW-2*N4POW)65,66,65
65 DO 67 J=1,NTHPOW,2
R1=X(J)+X(J+1)
R2=X(J)-X(J+1)
FI1=Y(J)+Y(J+1)
FI2=Y(J)-Y(J+1)
X(J)=R1
Y(J)=FI1
X(J+1)=R2
67 Y(J+1)=FI2
66 DO 68 J=1,13
L(J)=1
69 IF(J-N2POW)69,69,68
68 L(J)=2*(N2POW+1-J)
CONTINUE
IJ=1
L1=L(13)
NTHPOW=L(12)
ISQLOC=L(11)
J=L(10)
N2P1=L(9)
N2=L(8)
NP2MJ=L(7)
L8=L(6)
N2POW=L(5)
N4POW=L(4)
LENGTH=L(3)
NXTLTH=L(2)
IPASS=L(1)
DO 601 J1=1,L1
DO 601 J2=J1,NTHPOW,L1
DO 601 J3=J2,ISQLOC,NTHPOW
DO 601 J4=J3,J,ISQLOC
DO 601 J5=J4,N2P1,J
DO 601 J6=J5,N2,N2P1
DO 601 J7=J6,NP2MJ,N2
DO 601 J8=J7,L8,NP2MJ
DO 601 J9=J8,N2POW,L8
DO 601 J10=J9,N4POW,N2POW
DO 601 J11=J10,LENGTH,N4POW
DO 601 J12=J11,NXTLTH,LENGTH
DO 601 JI=J12,IPASS,NXTLTH
IF(IJ-JI)610,610,601
610 R=X(IJ)
X(IJ)=X(JI)
X(JI)=R
FI=Y(IJ)
Y(IJ)=Y(JI)
Y(JI)=FI

```

```

401      IJ=IJ+1
        ARG=3.1415927/FLOAT(N)
        C1=COS(ARG)
        S1=-SIN(ARG)
        C1JX=1.
        S1JX=0.
        N2=N/2
        N2P1=N2+1
        DO 70 J=2,N2P1
          NP2MJ=N+2-J
          SORR1=X(J)+X(NP2MJ)
          SORI1=Y(J)-Y(NP2MJ)
          R=C1JX
          C1JX=C1JX*C1-S1JX*S1
          S1JX=R*S1+S1JX*C1
          SORR2=X(J)-X(NP2MJ)
          SORI2=Y(J)+Y(NP2MJ)
          SORR3=C1JX*SORR2-S1JX*SORI2
          SORI3=C1JX*SORI2+S1JX*SORR2
          Y(J)=0.5*(SORI1-SORR3)
          X(J)=0.5*(SORR1+SORI3)
          IF(J-N2P1)71,70,71
71      Y(NP2MJ)=0.5*(-SORI1-SORR3)
          X(NP2MJ)=0.5*(SORR1-SORI3)
70      CONTINUE
          X(1)=X(1)+Y(1)
          Y(1)=0.
          DO 501 I=1,1024
            X(I)=(X(I)*X(I)+Y(I)*Y(I))
501      CONTINUE
          WRITE(14)(X(I),I=1,NP)
1500     CONTINUE
C
C      DISC CONTROL
C
          ENDFILE 10
          CALL CLOSE(10)
          ENDFILE 14
          REWIND 14
C
C      SIGNAL AVERAGING FOURIER DOMAIN
C
          DO 3000 I=1,NP
            Y(I)=0.0
            DO 3100 I=1,NP
              READ(14)(X(J),J=1,NP)
              DO 3200 J=1,NP
                Y(J)=Y(J)+X(J)
            CONTINUE
            DO 4000 I=1,NP
              Y(I)=Y(I)/NF
            CONTINUE
            YAU=0.0
            DO 4001 I=1,NP
              YAU=YAU+Y(I)
            CONTINUE
            YAU=YAU/FLOAT(NF)
            ENDFILE 14
            CALL CLOSE(14)
3000
C
C      WRITE FT DATA ON DISC
C
          WRITE(12)(Y(I),I=1,NP)
          WRITE(12)(YAU)
          ENDFILE 12
          CALL CLOSE(12)
          STOP
          END

```

```

C      RBPLOT.FOR
C      ZETA PLOTTING FOR FOURIER TRANSFORMS
C
C      FILES REQUIRED:
C      (1)SYSLIB
C      (2)XYLIB
C      (3)FORLIB
C
      DIMENSION X(1100),Y(1100)
      DIMENSION DAT(3),TITLE(3)
      CALL DATE(DAT)
      WRITE(7,1200)(DAT(I),I=1,3)
1200    FORMAT(' ',3A4)
      WRITE(7,1100)
1100    FORMAT(' ', 'ENTER DE:FILE.DAT FOR DATA'//')
      CALL ASSIGN(10,'DK:FTN10.DAT',-1,'OLD','NC',1)
      WRITE(7,3500)
3500    FORMAT(' ', 'ENTER LENGTH FOR X-AXIS, INCH')
      READ(5,6000)IIXX
      WRITE(7,6100)
6100    FORMAT(' ', 'ENTER LENGTH FOR Y-AXIS, INCH')
      READ(5,6000)IIYY
6000    FORMAT(I2)
      XAXIS=FLOAT(IIXX)
      YAXIS=FLOAT(IIYY)
      READ(10) NF
      READ(10) NP
      READ(10) NS
      READ(10)(DAT(I),I=1,3)
      READ(10)(TITLE(I),I=1,3)
      READ(10)(Y(I),I=1,NP)
      READ(10) YAU
      WRITE(7,1300)(DAT(I),I=1,3)
1300    FORMAT(' ', 'DATE: ',3A4)
      WRITE(7,1400)(TITLE(I),I=1,3)
1400    FORMAT(' ', 'TITLE: ',3A4)
      WRITE(7,1600) NF
1600    FORMAT(' ', 'NUMBER OF SETS OF DATA: ',I4)
      WRITE(7,1700) NP
1700    FORMAT(' ', 'NUMBER OF DATA PER SET: ',I4)
      WRITE(7,1800) NS
1800    FORMAT(' ', 'SAMPLING FREQUENCY OF DATA ACQUISITION: ',I7,
      *  ' HZ'//')
      WRITE(7,1900) YAU
1900    FORMAT(' ', 'MEAN SIGNAL= ',E11.4)
      ENDFILE 10
      CALL CLOSE(10)
C
C      NORMALISES SPECTRUM IF REQUIRED
C
      WRITE(7,4000)
4000    FORMAT(' ', 'NORMALISED SPECTRUM =0, NON-NORMALISED =1')
      READ(5,9001)INORM
      IF (INORM.EQ.1) GO TO 700
      DO 400 I=1,NP
      Y(I)=Y(I)/YAU
400    CONTINUE

```

```

C      CORPMT.FOR
C
C      TWO CHANNEL DATA ACQUISITION FOR CORRELATION
C
C      SUBROUTINES NEEDED:
C      (1)AQUIRE
C      (2)SYSLIB
C      (3)FORLIN
C
C
C      DIMENSION TITLE(3),DAT(3),A(1200),B(1200)
C      DOUBLE PRECISION SUMA,SUMB,SUMA2,SUMB2,SUMAR,SA,SB,SAB,R
C      COMMON /RON/ JNP,JSR,JCR,IA(1024) /RMB/ IB(1024)
C
C      INPUT ACQUISITION PARAMETERS
C
C      CALL DATE(DAT)
5020  FORMAT(I4)
      WRITE(7,5030)
5030  FORMAT(' ',' INPUT SAMPLE NAME')
      READ(5,5040) TITLE
5040  FORMAT(3A4)
      WRITE(7,5050)
5050  FORMAT(' ',' INPUT NUMBER OF POINTS')
      READ(5,5020) JNP
      WRITE(7,5060)
5060  FORMAT(' ',' INPUT CLOCK RATE',/, ' 2=1 MHZ',/, ' 4=100 KHZ',/,
1' 6=10 KHZ',/, ' 8=1 KHZ',/, ' 10=100 HZ',/, ' 14=60 HZ')
      READ(5,5020) IMCR
      WRITE(7,5070)
5070  FORMAT(' ',' INPUT NUMBER OF CLOCK PULSES BETWEEN SAMPLES')
      READ(5,5020) JSR
      WRITE(7,5080)
5080  FORMAT(' ',' CORRELATION COEFF. CALCULATED? 0=NO, 1=YES')
      READ(5,5020) ICALC
C
C      SET UP LPS CLOCK STATUS REGISTER PARAMETERS
C
C      JCR=(IMCR+257)
C
C      CALCULATE ACQUISITION FREQUENCY
C
      IF (IMCR.EQ.2) FREQ=1000000.0/FLOAT(JSR)
      IF (IMCR.EQ.4) FREQ=100000.0/FLOAT(JSR)
      IF (IMCR.EQ.6) FREQ=10000.0/FLOAT(JSR)
      IF (IMCR.EQ.8) FREQ=1000.0/FLOAT(JSR)
      IF (IMCR.EQ.10) FREQ=100.0/FLOAT(JSR)
      IF (IMCR.EQ.14) FREQ=60.0/FLOAT(JSR)
      IFREQ=IFIX(FREQ)
C
C      ACQUIRE DATA WITH SUBROUTINE AQUIRE
C
      WRITE(7,5090)
5090  FORMAT(' ',' CR TO START ACQUISITION')
      READ(5,5020) I

```

```

CALL AQUIRE
C
C   CALCULATION OF MEANS & CORRELATION COEFFICIENT
C
RNP=FLOAT(JNP)
R=0.33333E+33
SUMA=0.0
SUMB=0.0
SUMA2=0.0
SUMB2=0.0
SUMAR=0.0
DO 50 I=1,JNP
SUMA=SUMA+FLOAT(IA(I))
SUMB=SUMB+FLOAT(IB(I))
50 CONTINUE
IF (ICALC.EQ.0) GO TO 80
DO 60 I=1,JNP
SUMA2=SUMA2+FLOAT(IA(I))**2
SUMB2=SUMB2+FLOAT(IB(I))**2
SUMAR=SUMAR+FLOAT(IA(I))*FLOAT(IB(I))
60 CONTINUE
SA=DSQRT((SUMA2-(SUMA**2/RNP))/(RNP-1.0))
SB=DSQRT((SUMB2-(SUMB**2/RNP))/(RNP-1.0))
SAB=(SUMAR-((SUMA*SUMB)/RNP))/(RNP-1.0)
SASB=SA*SB
IF (SASB.EQ.0.0) GO TO 70
R=SAB/SASB
70 IF (SASB.NE.0.0) GO TO 80
R=0.33333E+33
80 SUMA=SUMA/RNP
SUMB=SUMB/RNP
SUMAR=SUMAR/SUMB
C
C   OUTPUT DATA TO TERMINAL
C
WRITE(7,6000)
6000 FORMAT(' ', ' MEAN A      MEAN B      MEAN A/B      R'//)
WRITE(7,6020)SUMA,SUMB,SUMAR,R
6020 FORMAT(' ',E10.4,3X,E10.4,3X,E10.4,3X,E11.4)
90 WRITE(7,6040)
6040 FORMAT(' ', '////' STORE DATA =1, RERUN =2, EXIT =3')
READ(5,5020) J
GO TO (10,20,30) J
C
C   FORMS DATA FILE ON DISC
C
10 WRITE(7,6060)
6060 FORMAT(' ', ' ENTER DE:FILE.DAT FOR STORAGE'//)
CALL ASSIGN(2,'DK:FTN2.DAT',-1,'NEW','NC',1)
DO 200 I=1,JNP
A(I)=FLOAT(IA(I))
B(I)=FLOAT(IB(I))
200 CONTINUE
WRITE(2)(A(I),I=1,1024)
WRITE(2)(B(I),I=1,1024)
ENDFILE%2
CALL CLOSE(2)
30 GO TO 90
STOP
END

```

```

C
C   CALCULATES & DISPLAYS MAX AMPLITUDE
C
200  DO 500 I=1,NP
      IF (Y(I).GT.AMAX) AMAX=Y(I)
500  CONTINUE
      WRITE(7,8000)AMAX
8000  FORMAT(' ', 'MAX AMPLITUDE = ',E10.4)
C
C   COMPUTES SCALING FACTOR
C
      WRITE(7,6050)
6050  FORMAT(' ', 'DO YOU REQUIRE SCALED PLOT Y=1 N=0')
      READ(5,8100)M
8100  FORMAT(I1)
      IF(M.EQ.0) GO TO 5
      Y(NP+1)=0.0
      Y(NP+2)=AMAX/YAXIS
      GO TO 6
5     WRITE(7,6150)
6150  FORMAT(' ', 'INPUT MAX AMPLITUDE TO BE PLOTTED')
      READ(5,6200)PMAX
6200  FORMAT(E10.4)
      Y(NP+1)=0.0
      Y(NP+2)=PMAX/YAXIS
6     RSCAL=FLOAT(NS)/2.0
      RINC=RSCAL/FLOAT(NP)
      DO 6500 I=1,NP
        J=I-1
6500  X(I)=FLOAT(J)*RINC
C
C   TRUNCATES DATA TO FIT PLOT
C
      DO 600 I=1,NP
        IF(Y(I).GT.PMAX) Y(I)=PMAX
600  CONTINUE
C
C   XY PLOTTING ROUTINE
C
      CALL PLOTST(0.005, 'IN')
      CALL PLOT (0.2,0.5,-3)
      CALL SYMBOL(0.0,0.0,0.16,DAT,90.0,12)
      CALL SYMBOL(0.0,2.0,0.16,TITLE,90.0,12)
      CALL PLOT(0.8,0.0,-3)
      CALL AXIS(0.0,0.0,5HPOWER,+5,YAXIS,90.0,Y(NP+1),Y(NP+2))
      CALL SCALE(X,XAXIS,NP,1)
      CALL AXIS(0.0,0.0,9HFREQUENCY,-9,XAXIS,0.0,X(NP+1),X(NP+2))
      CALL LINE(X,Y,NP,1,0,0)
      CALL PLOT(XAXIS,0.0,-3)
      CALL PLOT(0.5,-0.5,-3)
      CALL PLOTND
      STOP
      END

```